The author(s) shown below used Federal funds provided by the U.S. Department of Justice and prepared the following final report:

Document Title: Improving Forensic Identification Using Bayesian Networks and Relatedness Estimation: Allowing for Population Substructure

Author: Amanda B. Hepler

Document No.: 231831

Date Received: September 2010

Award Number: 2004-DN-BX-K006

Abstract

Hepler, Amanda Barbara. Improving Forensic Identification Using Bayesian Networks and Relatedness Estimation: Allowing for Population Substructure (Under the direction of Bruce S. Weir.)

Population substructure refers to any population that does not randomly mate. In most species, this deviation from random mating is due to emergence of subpopulations. Members of these subpopulations mate within their subpopulation, leading to different genetic properties. In light of recent studies on the potential impacts of ignoring these differences, we examine how to account for population substructure in both Bayesian Networks and relatedness estimation.

Bayesian Networks are gaining popularity as a graphical tool to communicate complex probabilistic reasoning required in the evaluation of DNA evidence. This study extends the current use of Bayesian Networks by incorporating the potential effects of population substructure on paternity calculations. Features of HUGIN (a software package used to create Bayesian Networks) are demonstrated that have not, as yet, been explored. We consider three paternity examples; a simple case with two alleles, a simple case with multiple alleles, and a missing father case.

Population substructure also has an impact on pairwise relatedness estimation. The amount of relatedness between two individuals has been widely studied across many scientific disciplines. There are several cases where accurate estimates of relatedness are of forensic importance. Many estimators have been proposed over the years, however few appropriately account for population substructure. New maximum likelihood estimators of pairwise relatedness are presented. In addition, novel methods for relationship classification are derived. Simulation studies compare these estimators to those that do not account for population substructure. The final chapter provides real data examples demonstrating the advantages of these new methodologies.

Improving Forensic Identification Using Bayesian Networks and Relatedness Estimation: Allowing for Population Substructure

BY

Amanda B. Hepler

A DISSERTATION SUBMITTED TO THE GRADUATE FACULTY OF

NORTH CAROLINA STATE UNIVERSITY

IN PARTIAL FULFILLMENT OF THE

REQUIREMENTS FOR THE DEGREE OF

DOCTOR OF PHILOSOPHY

DEPARTMENT OF STATISTICS

RALEIGH

August 15, 2005

APPROVED BY:

<div style="display:flex">

Dr. Bruce Weir (Chair)   Dr. Jacqueline Hughes-Oliver

Dr. Maria Oliver-Hoyo   Dr. Jung-Ying Tzeng

</div>

Dedication

To Carol and Ernest Hepler.

Biography

Amanda Hepler was born on July 26, 1977, in Frankfurt, Germany. Because her father was a career Army officer she had an opportunity to travel extensively and live in many places including Germany, Texas, Virginia, Florida, and Maryland. During her vacations with her family she visited over fifteen European countries and developed a love for traveling.

In 1995, Amanda graduated from Fallston High School, in Fallston Maryland. She attended the University of Central Florida for her first year of undergraduate studies. Amanda returned to Maryland to continue her education at Towson University majoring in applied mathematics and computing. During her undergraduate program, Amanda was nominated by professors within the Mathematics Department for honorary membership in the Association for Women in Mathematics. She received the Mary Hudson Scarborough Honorable Mention for Excellence in Mathematics during her final year at Towson and graduated summa cum laude in 2001.

Amanda selected North Carolina State University for graduate school where she received her Masters in Statistics in 2003. During her masters' program she was nominated for membership in the Phi Kappa Phi Honor Society and Mu Sigma Rho, a National Statistics Honor Society. Amanda worked for two years as a research assistant for the Office of Assessment performing various statistical analyses under the direction of Dr. Marilee Bresciani. During her 2003 spring semester, she began researching Bayesian Networks under the direction of Bruce Weir. Amanda was formally accepted into the statistics doctoral program in the fall of 2003. Dr. Weir continued to guide her research during her doctoral studies. Amanda finished the requirements for her doctoral degree in August, 2005, and is currently working with Dr. Weir as a post-doctoral student.

Acknowledgements

Dr. Bruce Weir provided me with the tremendous opportunity of working with him during the past few years. His guidance has been invaluable and it is an honor to have been selected as one of his students. No doctoral student could have a better mentor and advisor. It has truly been a pleasure.

There have certainly been others who have influenced me during this long academic journey. I began as a struggling speech pathology student at Towson University. Dr. Diana Emanuel, a hearing science professor, was the first to suggest I take a few math courses. A former psychology professor, Dr. Arthur Mueller, provided a brilliant introduction to the world of statistics. His enthusiasm and passion for the field started me on this path. Dr. Bill Swallow, a statistics professor at NCSU encouraged me to explore forensic research opportunities with Dr. Weir. These professors marked my path at critical decision points and made it possible for me to be here today.

There have been long sleepless nights torturing over homework, much academic confusion, misery, and wishes for the end. Survival was due to the willingness of my closest friends to be tortured beside and by me. My eternal gratitude is given to Aarthi, Clay, Darryl, Donna, Eric, Frank, Harry, Joe, Jyotsna, Kirsten, Lavanya, Marti, Matt, Michael, Mike, Paul, Ray, and Theresa. Basketball games, Friday's at Mitch's, and

hours and hours of playing pool with the best of friends made this experience bearable...almost enjoyable. There are others who have who have encouraged and supported me through this experience. David, Lisa and Laura have given me endless love and support. My three loving grandparents have never been shy in saying how proud they are of me. Their faith and encouragement are a constant source of inspiration. I would also like to thank Joel, who has been by my side and endured all the emotional "ups and downs" of this last year. He has helped me stay focused and encouraged me every step of the way. I only hope I can do half the job he's done when it's my turn.

Last, and certainly not least, there is the profound influence of my parents, Carol and Ernie Hepler. Throughout my life, they provided an environment rich in support, guidance, patience and most importantly, love. I am in awe every day of the things they have both accomplished, and are continuing to strive towards. My father's vision, integrity, and ambition have inspired me all my life. In my eyes, my mother has attained excellence in every aspect of her career, all along keeping it in perfect balance with her family and friends. As I embark on my own career, I am blessed to have her example to follow. My parents have always been in my corner, believing in me, encouraging me to try things I never thought were possible. Their love (not to mention great genes) are the foundation for my success. Thank you both!

Table of Contents

List of Tables

ix

List of Figures

x

xii

CHAPTER 1

Bayesian Networks and Population Substructure

1.1 Introduction

Population Substructure Effects on Forensic Calculations

One method of evaluating a body of evidence is to calculate a likelihood ratio [4]. This is a ratio of two probabilities:

$$\text{LR} = \frac{\Pr(\text{Evidence given the prosecutor's hypothesis})}{\Pr(\text{Evidence given the defendant's hypotheses})}. \tag{1.1}$$

Generally, the defense's hypothesis is that the evidence profile reflects someone other than the defendant. The prosecution, in contrast, argues that the match between the evidence profile and the defendant's profile means that the defendant was the source of the evidence. The denominator of this likelihood ratio requires that a forensic scientist determine the probability of observing the same DNA profile twice, commonly referred to as the *match probability* [2]. The numerator is typically 1, as the prosecutor is proposing that the evidence points to the defendant. In this case, the likelihood ratio reduces to the inverse of the match probability. Likelihood ratios can take on values from 0 to ∞. If we obtain a value of 100 for our ratio, the common interpretation is "The evidence is 100 times more probable if the suspect left the evidence than if some unknown person left the evidence" [2].

When population substructure is ignored, the match probability is simply the relative frequency of the defendant's profile in the suspected population of the culprit [5]. Essentially, this treats each human population as large and randomly mating, ignoring

1

Chapter 1. Bayesian Networks and Population Substructure

possible subpopulations. People in these subpopulations could tend to mate within their subpopulation which would lead to different allelic frequencies than those estimated from the overall population. To estimate these possible differences, it is necessary to introduce a measure of background relatedness among the subpopulations under consideration. This term, typically denoted θ, is commonly referred to as the *inbreeding coefficient* [4]. In 1994, Balding and Nichols proposed a method for calculating match probabilities, which makes use of this inbreeding coefficient [6]. We use this methodology here, and it is further examined in Sections 1.2 and 1.3.

Bayesian Networks in Forensics

Likelihood ratios can be calculated rather simply using Bayesian Networks (also known as Probabilistic Expert Systems or Bayesian Belief Networks). A Bayesian Network (BN) is a graphical and numerical representation which enables us to reason about uncertainty. Contrary to the name, BNs are not dependent upon Bayesian reasoning. In fact, the methods and assumptions we use in this research are not Bayesian in nature, we appeal only to Bayes Theorem and probability calculus. BNs are simply a tool to make the implications of complex probability calculations clear to the layperson, without requiring an understanding of the complexity involved [7]. They provide an automated way to calculate likelihood ratios in cases where the calculations are quite laborious to perform analytically.

The use of BNs for forensic calculations has been gaining popularity over the past decade due to the development of several software packages available which make the construction of these networks relatively simple. These packages include HUGIN[1] (which is used in this study), XBAIES[2], Genie[3], WINBUGS[4], and most recently FINEX[5] [8]. A detailed discussion of BNs and their applications can be found in [9],

---

[1] Free evaluation version available at http://www.hugin.dk
[2] Free to the public, available at http://www.staff.city.ac.uk/~rgc
[3] Available at http://www2.sis.pitt.edu/~genie
[4] Free to the public, available at http://www.mrc-bsu.cam.ac.uk/bugs/winbugs/contents.shtml
[5] Not yet available to the public, for updates see http://www.staff.city.ac.uk/~rgc

however a brief introduction is presented in Appendix A.

In this study extensive use is made of a table generating feature of HUGIN Version 6.3. This feature allows the use of general formulas for probability tables and avoids the need to enter each probability by hand. The use of this feature should significantly reduce data entry time which historically has been one of the major complaints in using BN software.

1.2   Review of Relevant Literature

The examination of DNA evidence has become important to legal systems throughout the world. Because of this, considerable research has focused on the validity and reliability of current methods used to evaluate DNA. Two aspects of this research are reviewed. First, the current state of forensic research concerning DNA calculations, when accounting for population substructure, is summarized. It is also important to critically examine the contributions of research using Bayesian Networks to answer relevant questions in this forensic area.

Effects of Population Substructure

Incorporating population substructure in the evaluation of DNA profile evidence is relatively recent. Several researchers, including Balding and Nichols [6, 5] and Weir et al. [10, 11, 4], have pioneered examining the impact of population substructure on DNA evidence evaluation. In 1995, Balding and Nichols conclude ignoring population substructure "would unfairly overstate the strength of the evidence against the defendant and the error could be crucial in some cases, such as those involving partial profiles or large numbers of possible culprits, many of whom share the defendant's ethnic background" [5]. In this review, we demonstrate the detrimental effects of ignoring population substructure when evaluating DNA evidence. Balding and Nichols' approach for accounting for population substructure is also reviewed.

Chapter 1. Bayesian Networks and Population Substructure

In 1994, Weir calculated estimates of the inbreeding coefficient, θ, using data obtained from the Arizona Department of Public Safety on Native American, Hispanic, African American, and Caucasian populations [11]. Weir showed a tenfold increase in θ values for the Native American sample, relative to the other samples considered. These estimates for θ ranged from 0.001 up to 0.097. Weir also demonstrated the potential impacts of using a subpopulation with a high background relatedness factor. For example, when assuming $\theta = 0$, and an allele frequency of 0.05, the likelihood ratio obtained is 200. However, if the true value of θ was actually 0.05, the likelihood ratio obtained is 58. According to Evett and Weir [2], these two values could be communicated as "moderate support" (LR=58) versus "strong support." These two interpretations could have quite a large impact when presented to a jury, and Weir's study demonstrates that the effects of population substructure need to be taken into account when evaluating DNA evidence.

A relatively simple method of taking population substructure into account while investigating DNA evidence was proposed by Balding and Nichols in 1994. This method is being used in some UK courts and has been endorsed by several researchers [4, 12, 13]. As mentioned earlier, to calculate a likelihood ratio in a DNA evidence case one needs to determine the match probability. Balding and Nichols proposed that these calculations need to take into account all other observed alleles, whether taken from the suspect or not. For example, suppose we are considering a paternity case in which we have the genotypes for the mother, child, putative (alleged) father, as well as both of the mother's parents. In this case, Balding and Nichols propose that the probability the putative father's genotype matches the true father's varies based on the observed genotypes of all others involved. The actual formula used is presented in Section 1.3. Their derivation of this formula depends upon the assumptions that they have a "randomly-mating subpopulation partially isolated from a large population, in which migration and mutation events occur independently and at constant rates." They provide both a genetical derivation and a statistical derivation of this formula. In conclusion, Balding and Nichols claim the "proposed method captures the primary

4

Chapter 1. Bayesian Networks and Population Substructure

effects [of population substructure] and other sources of uncertainty" [6].

The 1996 National Research Committee (NRC) report discussed the most appropriate way of accounting for population substructure when evaluating DNA evidence. They concluded in Recommendation 4.2 that "if the allele frequencies for the subgroup are not available, although data for the full population are, then the calculations should use the population-structure equations [derived by Balding and Nichols]" [14]. In light of this recommendation, and due to the simple nature of Balding and Nichols' method, it is used to calculate all match probabilities in this research.

In summary, the cited research demonstrates the impact of population substructure on the evaluation of DNA evidence. The chance of this background relatedness occurring in certain populations is large, and ignoring this potential could lead to errors in probability calculations. It seems reasonable that there is a higher amount of background relatedness among many populations, in addition to those discussed in Weir's 1994 article. Several cultures throughout the United States have a high occurrence of inbreeding, which speaks to the importance of ongoing research in this area. Today, DNA evidence is used routinely by courts to establish guilt or innocence. Population substructure must be considered or the credibility of this evidentiary tool could be called into question. Balding and Nichols have proposed a method of taking into account population substructure when evaluating DNA evidence. This methodology provides a simple, effective way to incorporate population substructure into our Bayesian Network.

Bayesian Networks in Forensics

Bayesian Networks are gaining popularity in the forensic sciences as a tool to graphically represent the complexities that arise in evaluating various types of evidence. These networks provide a means of performing calculations that are very involved, generally requiring extensive understanding of probability calculus. Bayesian Networks help scientists "follow a logical framework in complex situations" and "aid in

Chapter 1. Bayesian Networks and Population Substructure

constructing legal arguments" [15, 13]. Recently, Evett et al. claimed that BNs will play an increasingly important role in forensic science and that their power lies in "enabling the scientist to understand the fundamental issues in a case and to discuss them with colleagues and advocates [which] is something that has not been previously seen in forensic science" [16].

Researchers have examined a wide array of forensic cases over the past few years with the aid of BNs, ranging from simple car accident scenarios [17] to a highly complex murder case [15]. Other researchers have explored using BNs to model the most complex DNA evidence cases. The cases that have been examined to date are quite exhaustive and include: paternity determination [3, 8], taking into account mutation [3, 18], small quantities of DNA [16], cross-transfer evidence [19], and mixture cases with partial profiles involved [20, 21, 8].

Considering the importance of DNA evaluation to our legal system, further research into using Bayesian Networks seems prudent. Their graphical representations provide a vehicle for communication between practitioners when discussing very complex cases. They reduce the amount of confusion that can occur, by presenting important relationships between evidence in a logical way. No calculations are required to use these networks, which is a major benefit to the forensic scientist. In addition, once a network has been created, it can be used repeatedly in similar cases. For DNA evidence cases, the only modification needed is the specification of allele frequencies, inbreeding coefficient, and evidentiary profiles, as these values change from case to case. BNs are fulfilling a need in the forensic community, and this study intends to explore their usefulness in a wider array of cases. To date, BN studies have not taken into account the impact that population substructure may have on final DNA analysis. This study examines various DNA profile cases using BNs and explores potential improvements that can be made in DNA examination by considering population substructure.

Chapter 1. Bayesian Networks and Population Substructure

1.3   Research Methods

Each Bayesian Network we consider here is some variation of a paternity case. In these cases, the likelihood ratio given in Equation 1.1 is termed the *paternity index*, or PI. Let E denote the evidence, PF denote putative father, M denote mother, and C denote child. Here the prosecutor's and defendant's hypotheses are formed by considering whether or not the putative father is the true father:

H_p: PF is the father of C.

H_d: Some other man is the father of C.

Thus, the PI is

$$\text{PI} = \frac{\Pr(E|H_p)}{\Pr(E|H_d)}. \tag{1.2}$$

Denote the genotype of person X as G_X, and assume the only evidence is the gentoypes of the child, mother, and putative father. Then the PI from Equation 1.2 can be rewritten as

$$\text{PI} = \frac{\Pr(G_C, G_M, G_{PF}|H_p)}{\Pr(G_C, G_M, G_{PF}|H_d)}. \tag{1.3}$$

Using conditional probability properties (Box 1.2 of [2]), we have

$$\text{PI} = \frac{\Pr(G_C|G_M, G_{PF}, H_p)}{\Pr(G_C|G_M, G_{PF}, H_d)} \times \frac{\Pr(G_M, G_{PF}|H_p)}{\Pr(G_M, G_{PF}|H_d)}. \tag{1.4}$$

The mother's and putative father's observed genotypes do not depend on which hypothesis is true and thus the second term is one. Therefore, the PI for the simple paternity case is the ratio of two conditional probabilities:

$$\text{PI} = \frac{\Pr(G_C|G_M, G_{PF}, H_p)}{\Pr(G_C|G_M, G_{PF}, H_d)}. \tag{1.5}$$

The match probabilities needed to compute the denominator in Equation 1.5 can be calculated using the aforementioned methodology of Balding and Nichols [6]. Before we present this method, we introduce some notation (which differs from that presented in [6]). First, p_i is the frequency of the ith allele in the subpopulation being studied. The number of observed A_i alleles is denoted n_i, whereas n denotes the total number

Chapter 1.   Bayesian Networks and Population Substructure

of alleles observed. Finally, θ represents the inbreeding coefficient. With this notation in place, the probability of observing the ith allele, given n_i alleles have already been observed is denoted P_i, and its value can be calculated as shown in Equation 1.6:

$$P_i = \Pr(A_i|n_i) = \frac{n_i\theta + p_i(1 - \theta)}{1 + (n - 1)\theta}. \tag{1.6}$$

To illustrate the proper use of this formula, we give a short example. First, we refer to the kth founder allele observed as $Founder_k$. Suppose we have observed two alleles in our subpopulation and would like to obtain the appropriate allele frequencies for the third allele observed, $Founder_3$. Also, suppose that the locus under consideration has only two alleles, A_1 and A_2. The appropriate frequencies can be obtained from Equation 1.6 and are shown in Table 1.1.   For example, the formula given in the

Table 1.1: Algebraic P_i Values for $Founder_3$ using Equation 1.6.

$Founder_1$	A_1		A_2	
$Founder_2$	A_1	A_2	A_1	A_2
A_1	$\frac{2\theta+p_1(1-\theta)}{1+\theta}$	$\frac{\theta+p_1(1-\theta)}{1+\theta}$	$\frac{\theta+p_1(1-\theta)}{1+\theta}$	$\frac{p_1(1-\theta)}{1+\theta}$
A_2	$\frac{p_2(1-\theta)}{1+\theta}$	$\frac{\theta+p_2(1-\theta)}{1+\theta}$	$\frac{\theta+p_2(1-\theta)}{1+\theta}$	$\frac{2\theta+p_2(1-\theta)}{1+\theta}$

first cell of Table 1.1 corresponds with Equation 1.6 by letting $i = 1$ (the observed value of $Founder_3$ is A_1), $n_1 = 2$ (two A_1 alleles have already been seen), and $n = 2$, (we have observed a total of two alleles). As a numerical example, we could calculate these values in the hypothetical case where $\theta = 0.03$, $p_1 = 0.10$, and $p_2 = 0.90$. These values are presented in Table 1.2. As can be seen, the allele frequencies depend upon how many of that allele have already been observed. If two A_1 alleles have been seen already, then the probability of observing another from $Founder_3$ increases 50% from the original p_1 value of 0.10 to 0.1524. If no A_1 alleles have been observed, then the value decreases to 0.0942.

One of the major advantages of Balding and Nichols' method is its simplicity. This

Table 1.2: Numerical P_i Values for $Founder_3$ using Equation 1.6.

$Founder_1$	A_1		A_2	
$Founder_2$	A_1	A_2	A_1	A_2
A_1	0.1524	0.1233	0.1233	0.0942
A_2	0.8476	0.8767	0.8767	0.9058

allows us to enter formulas into HUGIN for most nodes, as opposed to having to enter each number by hand. The next section demonstrates how this method can be incorporated into a Bayesian Network.

1.4   Example One: A Simple Paternity Case with Two Alleles

Consider the simple paternity case, where the genotypes of the mother, child and putative father are known. For simplicity, we consider only one locus, with two alleles. In future networks created in this study, we incorporate evidence from multiple loci using the method endorsed by [14], which recommends that likelihood ratios be multiplied together. We also consider cases where we have several alleles at a particular locus. The BN for the simple paternity case with two alleles was first published by Dawid et al. in [3]. Here, we provide a brief description of their network, then extend it to account for population substructure.

In paternity cases, there is typically genotype data on three individuals; mother, child, and putative father. Three nodes are required in the BN to describe each individual. The first two nodes represent the maternal and paternal genes (or alleles) passed down to the individual. These nodes can take on values A_1 or A_2, where A_i represents the ith allele. To differentiate gene nodes, their names end in either "**pg**" for the paternal gene, or "**mg**" for the maternal gene. The third node needed for each

Chapter 1. Bayesian Networks and Population Substructure

individual represents their actual genotype. These node names will end in "**gt**," for genotype, and can take on values A_1A_1, A_1A_2, or A_2A_2. Arrows in the network show that the genotype node depends on the maternal and paternal gene nodes. Figure 1.1 shows the graphical representation for the putative father (**pf**).
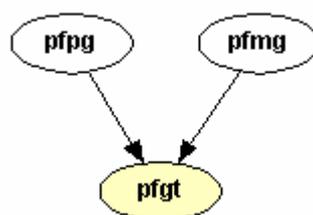
Figure 1.1: Putative Father's Node Trio.

Along with each node, there are associated probability tables. For example, the probability **pfpg** will take on the value A_1 is the population allele frequency of the first allele. Figure 1.2 illustrates how HUGIN represents the probability table, assuming the frequency for A_1 is 0.10. The probability table will look exactly the same for the

Figure 1.2: Probability Table for Putative Father's Paternal Gene Node.

node **pfmg**. For node **pfgt**, the probabilities are determined by the values of **pfpg** and **pfmg**. To demonstrate, Figure 1.3 shows probability table for **pfgt**, conditional on **pfpg** and **pfmg**. The first cell must be one, as it represents the probability **pfgt** takes on the value A_1A_1, given that both maternal and paternal alleles are A_1. Similar

10

Chapter 1. Bayesian Networks and Population Substructure

Figure 1.3: Conditional Probability Table for Putative Father's Genotype Node.

arguments are used to arrive at the other cell values.

As mentioned, each individual in the network will have node trios similar to that shown in Figure 1.1. The first letters of each node indicate which individual is being considered. The notation and descriptions for these nine nodes are given in Table 1.3.

Table 1.3: Notation for Putative Father, Mother and Child Nodes.

Node	Description
pfpg	Putative father's paternal gene
pfmg	Putative father's maternal gene
pfgt	Putative father's genotype
mpg	Mother's paternal gene
mmg	Mother's maternal gene
mgt	Mother's genotype
cpg	Child's paternal gene
cmg	Child's maternal gene
cgt	Child's genotype

Three final nodes are required to complete the Bayesian Network for this example. The first two are the true father's paternal and maternal genes, **tfpg** and **tfmg**. Their values will depend upon whether or not the putative father is the true father. This relationship is expressed by adding a boolean node, **tf=pf?**, that is either true or false.

Chapter 1.   Bayesian Networks and Population Substructure

This node is termed the *hypothesis* node, and it will eventually be used to compute the PI given by Equation 1.5. The relationships between these three nodes, along with the putative father nodes, are shown in Figure 1.4. For all of the networks presented
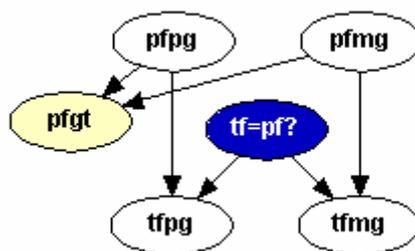
Figure 1.4: Network for Hypothesis, True Father and Putative Father Nodes.

here, we make the simplistic assumption that the prior odds of putative father being the true father is one. Thus, the two entries in the probability table for node **tf=pf?** are both 0.50. Conditional probabilities for nodes **tfpg** and **tfmg** are similar, thus only the table for **tfpg** is shown in Figure1.5. If the hypothesis node is true, then the values

Figure 1.5: Conditional Probability Table for True Father's Paternal Gene Node.

for **tfpg** and **tfmg** are directly determined by the values from **pfpg** and **pfmg**. If the hypothesis node is false, the probabilities are simply the respective allele frequencies.

Chapter 1. Bayesian Networks and Population Substructure

Again, the values in Figure 1.5 assume allele A_1 occurs with frequency 0.10. The entire network with all twelve nodes is shown in Figure 1.6.
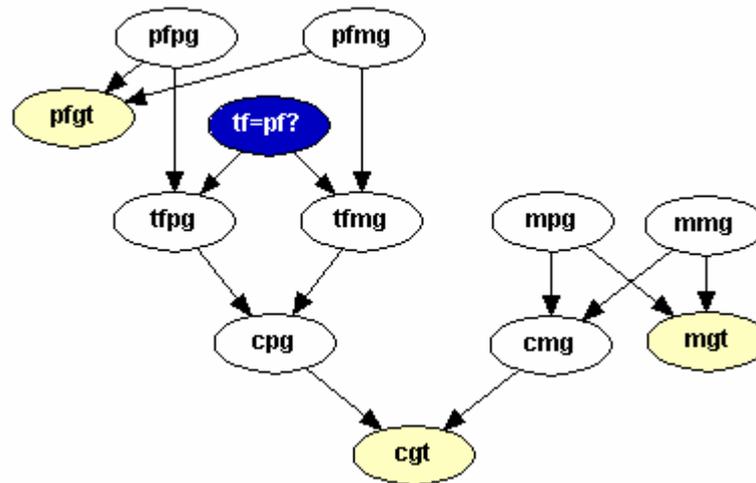
Figure 1.6: Simple Paternity Network from Dawid et al. [3].

To incorporate population substructure into this network we need to introduce several new nodes. First, we create a node for the value of θ and label it **theta**. This node takes on the value of θ we propose is associated with our population, and can take on any value the user chooses. Next, we add a node that contains the population's allele frequency for the A_1 allele. This is denoted **Specified p**, and the values can range from 0 - 1, as specified by the user. Now we need to keep track of how many A_i alleles have already been seen. This is easily done by introducing several counting nodes labeled **n2**, **n3**, **n4**, and **n5**. These replace the variable n_i that is present in Equation 1.6. In particular, **n2** is the value of n_1 after seeing two genes; **n3** is the value of n_1 after seeing three genes, etc. Note that no **n1** node is necessary, as we can simply place an arrow between the first gene node and the second gene node. We also keep track of the number of founder genes in the graph, by adding "_k" to the node name. For example, **pfmg** is labeled as the second founder gene and the node is named

Chapter 1. Bayesian Networks and Population Substructure

pfmg_2. The new network created appears in Figure 1.7.
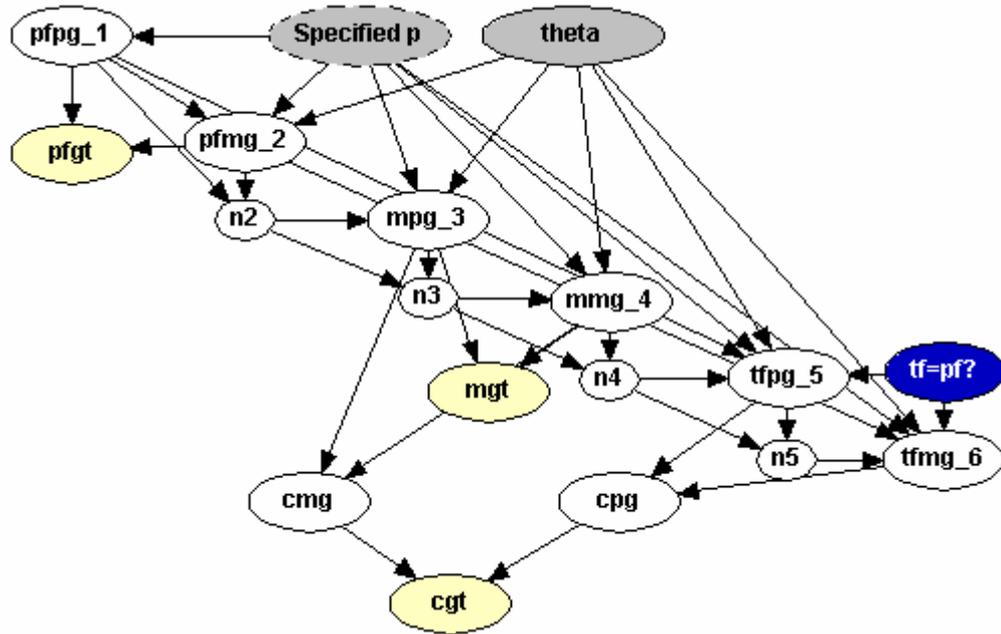
Figure 1.7: Population Substructure Simple Paternity Network.

We have rearranged the nodes in this network to ensure the reader can view all relationships present among our new nodes. The relationships, represented by arrows, are simply a result of what information is needed in our formulas to generate the allele frequencies, according to Equation 1.6. **Specified p** and **theta** are needed to calculate each founder's frequencies, therefore there are arrows from those nodes to every founder node in the graph. For the counting nodes, consider the node **n3**. It needs the information from **n2** to know how many A_i alleles have occurred up until that point, resulting in one arrow. The node **n3** also needs information from the current node to update the number of A_i occurrences, resulting in another arrow. This node is then used in the formulas to determine the allele frequencies for the fourth founder, resulting in an arrow from **n3** to **mmg_4**.

14

Chapter 1. Bayesian Networks and Population Substructure

Now we must discuss the numerical portion of our network. HUGIN allows the user to specify an *expression* to generate a conditional probability table. There are two ways to do this: enter a distribution or enter if-then-else statements. Here, we use the distribution method. To do this, the user types the following into the *Expression* line of the table: *Distribution(Formula for A_1, Formula for A_2)*. In our case, the formula for A_1 is taken directly from the formula given in Equation 1.6, with $n = 2$ as we have observed two founder alleles at this point, and $i = 1$. The formula for A_2 is simply one minus the value calculated for A_1. HUGIN then generates the conditional probability table, shown in Figure 1.8 for the node **mpg_3**, based on the distribution we entered.

mpg_3			
Edit Functions View			
Expression	Distribution ((n2 * theta + p * (1 - theta)) / (1 + theta), 1 - (n2 * theta + p * (1 - theta)) / (1 + theta))		
theta	0.03		
Specified p	0.1		
n2	0	1	2
A1	0.094175	0.123301	0.152427
A2	0.905825	0.876699	0.847573

Figure 1.8: Conditional Probability Table for Mother's Paternal Gene.

These values can then be verified against those calculated by hand in Table 1.2, as the same values for θ and p_1 were used. To do this, the numbers listed in Table 1.2 under $Founder_1 = A_1$ and $Founder_2 = A_1$ match with the numbers listed in Figure 1.8 under **theta** $= 0.03$, **Specified p** $= 0.1$, and **n2** $= 2$. The numbers listed in Table 1.2 under $Founder_1 = A_1$ and $Founder_2 = A_2$ as well as those listed under $Founder_1 = A_2$ and $Founder_2 = A_1$ match with those listed in Figure 1.8 under **theta** $= 0.03$, **Specified p** $= 0.1$, and **n2** $= 1$, and so on. The amount of time saved at this point may not seem overwhelming, however in more complex examples the formula entry option is an invaluable tool. We do not display all founder tables created, as they are very similar to this case. The counting node tables are given in Figure 1.9, and their derivation

15

Chapter 1. Bayesian Networks and Population Substructure

comes from simply counting how many times the A_1 allele is seen.

n2   Edit   Functions   View

pfpg_1	A1		A2	
pfmg_2	A1	A2	A1	A2
0	0	0	0	1
1	0	1	1	0
2	1	0	0	0

n3   Edit   Functions   View

n2	0		1		2	
mpg_3	A1	A2	A1	A2	A1	A2
0	0	1	0	0	0	0
1	1	0	0	1	0	0
2	0	0	1	0	0	1
3	0	0	0	0	1	0

n4   Edit   Functions   View

n3	0		1		2		3	
mmg_4	A1	A2	A1	A2	A1	A2	A1	A2
0	0	1	0	0	0	0	0	0
1	1	0	0	1	0	0	0	0
2	0	0	1	0	0	1	0	0
3	0	0	0	0	1	0	0	1
4	0	0	0	0	0	0	1	0

n5   Edit   Functions   View

n4	0		1		2		3		4	
tfpg_5	A1	A2	A1	A2	A1	A2	A1	A2	A1	A2
0	0	1	0	0	0	0	0	0	0	0
1	1	0	0	1	0	0	0	0	0	0
2	0	0	1	0	0	1	0	0	0	0
3	0	0	0	0	1	0	0	1	0	0
4	0	0	0	0	0	0	1	0	0	1
5	0	0	0	0	0	0	0	0	1	0

Figure 1.9: Probability Tables for Counting Nodes.

Once the network is created, HUGIN calculates the paternity index for various combinations of evidence. In [2] (Table 6.6), formulas for several cases are given using Balding and Nichols' methodology. An adapted version of this table is provided in

Chapter 1. Bayesian Networks and Population Substructure

Table 1.4, with actual PI values listed for the case when $\theta = 0.03$ and $p_1 = 0.1$. For

Table 1.4: Paternity Index Formulas Derived in [2].

mgt	cgt	pfgt	PI	$PI \quad (\theta = 0.03, p_1 = 0.1)$
A_1A_1	A_1A_1	A_1A_1	$\frac{1+3\theta}{4\theta+(1-\theta)p_1}$	5.02
A_1A_1	A_1A_1	A_1A_2	$\frac{1+3\theta}{2[3\theta+(1-\theta)p_1]}$	2.91
A_1A_1	A_1A_2	A_2A_2	$\frac{1+3\theta}{2\theta+(1-\theta)p_2}$	1.17
A_1A_1	A_1A_2	A_1A_2	$\frac{1+3\theta}{2[\theta+(1-\theta)p_2]}$	0.60
A_1A_2	A_1A_1	A_1A_1	$\frac{1+3\theta}{3\theta+(1-\theta)p_1}$	5.83
A_1A_2	A_1A_1	A_1A_2	$\frac{1+3\theta}{2[2\theta+(1-\theta)p_1]}$	3.47

example, consider the case when **mgt** $= A_1A_1$, **cgt** $= A_1A_1$, and **pfgt** $= A_1A_2$. We would like to verify that HUGIN matches the value of 2.91 seen in Table 1.4. After entering in the evidence provided by the mother, child, and putative father, HUGIN displays the tables shown in Figure 1.10. First, note that the evidence entered is
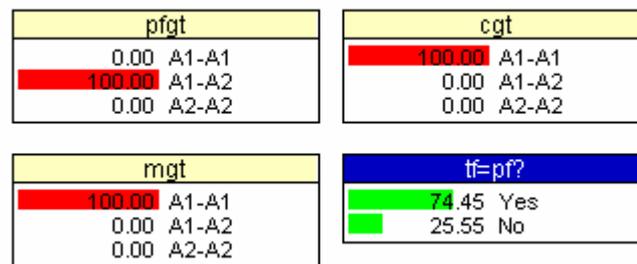
Figure 1.10: HUGIN's Output After Entering the Evidence, Simple Paternity Network.

represented by the 100% next to corresponding genotypes in the tables for **pfgt**, **cgt**, and **mgt**. The PI is obtained by taking the value shown in the **tf=pf?** table next to

17

Chapter 1. Bayesian Networks and Population Substructure

"Yes" and dividing it by the value displayed next to "No," and is given in Equation 1.7,

$$\text{PI} = \frac{74.45}{25.55} = 2.91. \tag{1.7}$$

We attempted all of the cases presented in Table 1.4 and obtained matching results using HUGIN.

Now we would like to compare our new network with the one presented in Figure 1.6. In total, we added only six new nodes. The nodes **Specified p** and **theta** require entering in only one number each, and do not increase the complexity of the conditional probability tables associated with the other nodes. The addition of the counting nodes do, however, increase the complexity of the probability tables of other nodes. For example, the node **mpg_3** previously required the entry of only two probabilities. Now there are two probability entries for each value of **n2**, leading to a total of six entries. This type of increase occurs with each founder node. However, with the use of the table generating feature and the use of the formulas given by Balding and Nichols, no data entry for any of these nodes is required. One must simply enter the correct formula in each table and let HUGIN calculate the actual values. As a result, the amount of time needed to create our new network, after the formulas have been established, turns out to be less than that of the previous network. In addition, the two networks take an equivalent amount of time to run using a reasonably equipped personal computer. It is important to note that our new network provides the exact same results as the previous network by simply entering in $\theta = 0$, making it flexible enough to handle both cases.

1.5 Example Two: A Simple Paternity Case with Multiple Alleles

Here we consider the case where there are more than two alleles at a particular locus. The mother and putative father could have at most four distinct alleles between them.

Chapter 1. Bayesian Networks and Population Substructure

We arbitrarily call them A_i, $i = 1, 2, 3, 4$. The allele frequencies in our population associated with these alleles are again denoted p_i. We then pool all other possible alleles into one group, denoted X where the probability of having one of these grouped alleles would be $1 - p_1 - p_2 - p_3 - p_4$. Our new network needs additional nodes to incorporate these new alleles. First, we create nodes **p_Ai**, for $i = 1, 2, 3, 4$. Each of these take on the values of the allele frequencies specified by the user. In this example, we assume that $p_i = 0.1$ for all i. The final nodes we need to modify in this network are the counting nodes. Previously, we recorded only how many A_1 alleles were seen. Now we must keep a count of how many A_1, A_2, A_3, and A_4 alleles are seen. We now have **n2_A1**, **n2_A2**, **n2_A3**, and **n2_A4** to replace **n2**, and **n3_A1**, **n3_A2**, **n3_A3**, and **n3_A4** to replace **n3**, and so on. The new network is displayed in Figure 1.11.
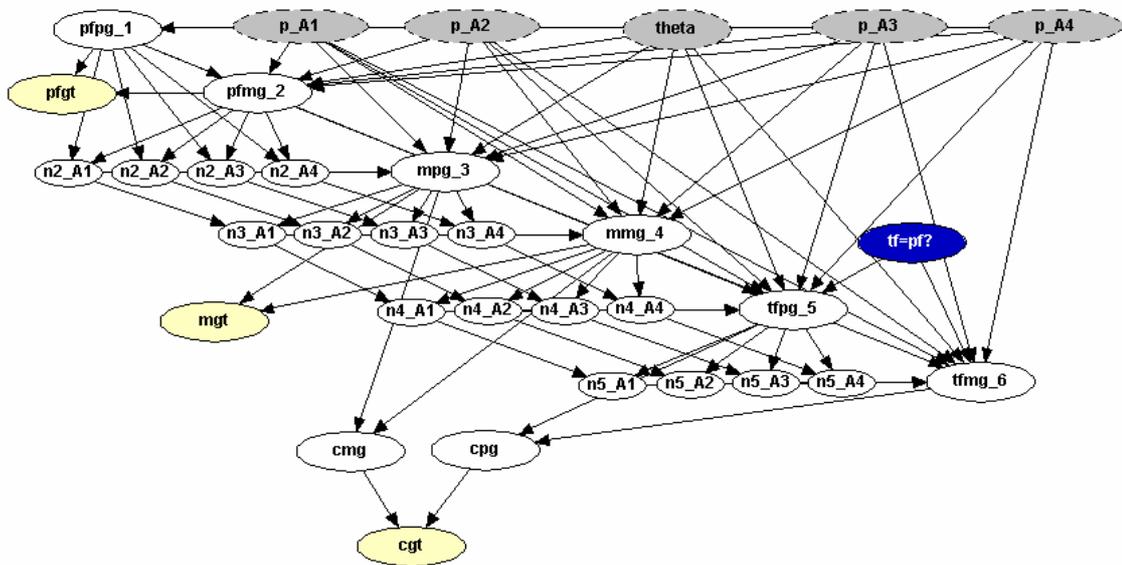
Figure 1.11: Population Substructure Paternity Network for Multiple Alleles.

The conditional probability tables for this network are generated in a similar fashion to those in our first example, with a few caveats. The most obvious difference is that there are now additional states that the nodes can take. For example, the node **mpg_3**

19

Chapter 1. Bayesian Networks and Population Substructure

previously only took on the values A_1 and A_2. Now, it can take on values A_1, A_2, A_3, A_4, and X. This means the entry in the *Expression* line has five items in the distribution statement, instead of only two.

A more subtle difference involves the counting nodes. In this network, there is a different counting node for each of the first four alleles. There is nothing inherent in our network that requires these nodes to add up to the number of alleles we have seen. For example, consider the counting nodes for the second allele observed, **n2_A1**, **n2_A2**, **n2_A3**, and **n2_A4**. Each of these nodes can take on values 0, 1, or 2. Thus, it is possible each node could each take on the value of two. If this situation were to occur, using Equation 1.6 with certain allele frequencies could produce negative values in some of the conditional probability table cells for the node **mpg_3**. To prevent this, we employ an *If* statement in the *Expression* line: *If X, Distribution(A), Distribution(B)*. This is interpreted as "If X is true, distribution A is used. Otherwise, distribution B is used." In this example, X represents the inequality **n2_A1 + n2_A2 + n2_A3 + n2_A4** $\leq$ 2. *Distribution(A)* is given by Equation 1.6 and *Distribution(B)* is given by the original allele frequencies. The complete statement for node **mpg_3** is as follows:

```
if (n2_A1+n2_A2+n2_A3+n2_A4 <= 2,
   Distribution ((n2_A1*theta+p_A1*(1-theta))/(1+theta),
   (n2_A2*theta+p_A2*(1-theta))/(1+theta),
   (n2_A3*theta+p_A3*(1-theta))/(1+theta),
   (n2_A4*theta+p_A4*(1-theta))/(1+theta),
   ((2-(n2_A1+n2_A2+n2_A3+n2_A4))*theta
     + (1-(p_A1+p_A2+p_A3+p_A4))*(1-theta))/(1+theta)),
    Distribution (p_A1, p_A2, p_A3, p_A4, 1-(p_A1+p_A2+p_A3+p_A4))).
```

For node **mmg_4**, the *If* statement will read `if (n3_A1+n3_A2+n3_A3+n3_A4 <= 3,` and so on. The counting node tables are created in the same manner as those in the previous example, and have not been included here due to space considerations.

The paternity index can now be obtained from HUGIN for various cases. Here we consider the case where the mother's genotype is A_1A_3, the putative father's genotype is A_2A_4, and the child's genotype is A_1A_2. Evett and Weir [2] provide a PI formula for

20

Chapter 1. Bayesian Networks and Population Substructure

this case and it is shown in Equation 1.8,

$$\text{PI} = \frac{1 + 3\theta}{2\{\theta + (1 - \theta)p_2\}}. \tag{1.8}$$

When $\theta = 0.03$ and $p_2 = 0.1$, this formula gives PI $= 4.29$. Using HUGIN, we obtain the same result. Figure 1.12 gives HUGIN's output after entering in the evidence. The corresponding PI is given in Equation 1.9,

$$\text{PI} = \frac{81.10}{18.90} = 4.29. \tag{1.9}$$

Figure 1.12: HUGIN's Output After Entering the Evidence, Multiple Allele Network.

In contrast to this network, one not taking population substructure into account would appear exactly as the network proposed for the two allele case (Figure 1.6). The changes needed to go to a multiple allele case would occur when specifying the

21

Chapter 1. Bayesian Networks and Population Substructure

conditional probability tables. Each founder node would have five states instead of just two, as there are five possible alleles (A_1, A_2, A_3, A_4, or X). Each genotype node would have a total of ten states, as there are 10 ways to select two alleles from a total of five possible alleles. Previously, each genotype had only three states (A_1A_1, A_1A_2, and A_2A_2).

Our network shown in Figure 1.11 adds a total of 21 nodes to the network which does not consider population substructure. The first five (**theta** and **p_Ai**, $i = 1, 2, 3, 4$) only require one number entered for each node. However, the various counting nodes do add quite a bit of complexity. Typing in each of the tables associated with the counting nodes is quite time consuming, although not very complex to derive. Again, the use of the table generating feature simply nullifies any added complexity that may occur in the founder nodes due to the addition of the counting nodes. The only data entry required is the formulas for each node, which is essentially the same amount of work required in the two allele case. In terms of running time, this network takes approximately one minute to run, whereas the non-population substructure network takes approximately three seconds (again, on a reasonably equipped personal computer). This time difference is substantial, however computing time is not as much of a concern in recent times, due to increasing technology. Overall, our new network is substantially more complex than its counterpart. However, this complexity is by no means prohibitive, as it needs to be created only once. From then on, the network is flexible enough to handle any type of paternity case that could arise when all three genotypes are given (including the scenario in Example One).

1.6 Example Three: A Complex Paternity Case with Two Alleles

Our final example considers the more complex situation that can occur when forensic scientists do not have access to the putative father's DNA. Instead, suppose they have

22

Chapter 1. Bayesian Networks and Population Substructure

a sample from a relative of the putative father. In particular, consider the case when DNA is available from a brother of the putative father. A simple network depicting this situation is provided in Figure 1.13. A table listing the new notation used in this
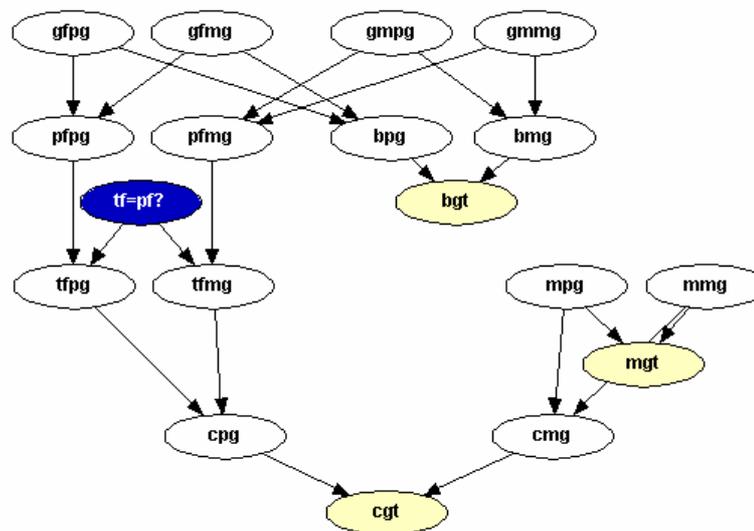
Figure 1.13: Complex Paternity Network.

network is shown in Table 1.5.

Table 1.5: Notation for Network in Figure 1.13.

Node	Description
gmpg	Mother of Putative father's paternal gene
gmmg	Mother of Putative father's maternal gene
gfpg	Father of Putative father's paternal gene
gfmg	Father of Putative father's maternal gene
bpg	Brother of Putative father's paternal gene
bmg	Brother of Putative father's maternal gene
bgt	Brother of Putative father's genotype

Incorporating population substructure requires nodes to be added to the current

23

Chapter 1. Bayesian Networks and Population Substructure

network, similar to those added in the previous two examples. We add one node
containing our theta value (**theta**), one containing our allele frequencies (**Specified
p**), and several counting nodes (**n2 - n7**). For simplicity this network only considers
the two allele case, however it can be extended to incorporate multiple alleles in a
manor similar to Example Two. The final network, with the new nodes included, is
displayed in Figure 1.14.
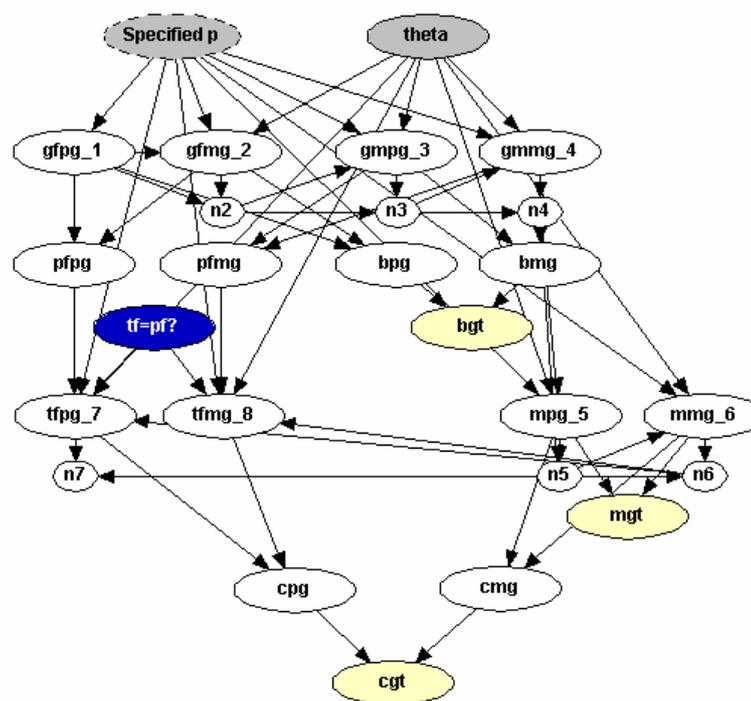
Figure 1.14: Population Substructure Complex Paternity Network.

This scenario was examined very early on in [22] and later appeared in [2]. The
likelihood ratio in this case is sometimes referred to as the *Avuncular Index* (AI), as
opposed to the paternity index. The plaintiff's new hypothesis is that tested man is
a paternal uncle of the child. The defense hypothesis contends that the tested man
is unrelated to the child. A simple mathematical relationship between the paternity

24

Chapter 1. Bayesian Networks and Population Substructure

index and the avuncular index was discovered in [22], and it is given by Equation 1.10.

$$\text{AI} = (1/2)\text{PI} + 1/2 \tag{1.10}$$

Recall the PI given in Example One (Equation 1.5) where we observed genotypes from the putative father, mother and child. If instead of observing $pfgt = A_1 A_2$, we observe $bpg = A_1 A_2$, according to Equation 1.10, we should obtain the AI shown in Equation 1.11,

$$\text{AI} = (1/2)(2.91) + 1/2 = 1.96. \tag{1.11}$$

Now, we attempt to arrive at this same result using our new BN given in Figure 1.14. To arrive at the AI above, we assumed $\theta = 0.03$ and $p_1 = 0.1$. If we make those same assumptions now, and we enter in our observed genotypes, HUGIN displays the results shown in Figure 1.15. We do in fact arrive at the same result given in Equation 1.11 by

Figure 1.15: HUGIN's Output After Entering the Evidence, Complex Paternity Network.

dividing the percentages displayed in the table for **tf=pf?**, as is shown in Equation 1.12,

$$\text{AI} = \frac{66.18}{33.82} = 1.96. \tag{1.12}$$

Here, we added a total of eight nodes (**theta**, **Specified p**, and the six counting nodes). The resultant network has similar advantages and disadvantages to the network created in Example One. It is a much more flexible network, and is actually simpler to create than its non-population substructure counterpart (again, as a result of the table generating feature).

25

Chapter 1.   Bayesian Networks and Population Substructure

1.7   Discussion

Bayesian Networks are clearly a useful tool for DNA evidence evaluation. They allow scientists to point and click their way to solutions for very difficult probability calculations. They also provide a graphical representation of, at times, highly complex forensic scenarios. One way to fully make use of this valuable tool is to provide several "shell" networks that can be used over and over again by anyone. This work contributes a few "shells" that allow scientists to make inferences based on DNA evidence while taking into account population substructure. With the advent of HUGIN, along with the table generating feature, these networks are not only possible, but relatively simple to create. Graphical methods, such as BNs, are bringing the power of complex statistical methodology into the forensic laboratory. Here, we have presented an extension of an already established graphical tool to further empower the forensic scientist.

CHAPTER 2

Pairwise Relatedness and Population Substructure

2.1 Introduction

Pairwise relatedness describes the amount of relatedness between two individuals or organisms. In our context, the amount of genetic similarity observed can be used as a measure or indicator of relatedness. To illustrate, suppose two individuals are full siblings. Their DNA will be made up of DNA passed down through their respective ancestors. Since they are siblings, they have the exact same ancestors. As a result, they will have a higher level of genetic similarity than an unrelated pair of individuals. That is, the greater the number of ancestors in common (increasing relatedness) leads to greater amounts of genetic similarity.

An important concept that helps describe genetic similarity is commonly referred to as *identity by descent* or IBD. Two alleles are IBD if they are direct copies of a single ancestral allele. For example, suppose X and Y are full siblings. Let X have alleles labeled a and b, and let Y have alleles labeled c and d. This particular situation is diagrammed in Figure 2.1. Here, there is a chance that a and c are IBD as they could both be a copy of the same maternal allele.

An inbred individual is one that carries IBD alleles. Most populations will always have a low level of inbreeding, due to population substructure. Inbreeding, of any amount, will necessarily have an effect on pairwise relatedness estimates. If two individuals share some background relatedness due to inbreeding we would arrive at inflated estimates of relatedness. It would be useful to quantify the effects of background relat-

Chapter 2.   Pairwise Relatedness and Population Substructure

Mother   Father

a $\quad c$ $\quad b$ $\quad d$

X Y
ab cd
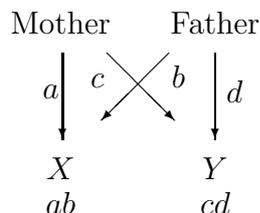
Figure 2.1: Diagram of IBD Relationship Between Two Siblings X and Y.

edness and incorporate them into our estimation technique. However, most pairwise relatedness estimators developed thus far have ignored population substructure.

Accurately estimating pairwise relatedness is important in many diverse fields, including forensic genetics, quantitative genetics, conservation genetics, and evolutionary biology [23]. Perhaps the most common forensic application of pairwise relatedness is in remains identification. Traditionally, dental records or fingerprints are used to identify remains. However, in many cases these methods are impractical (high temperature fires, explosive impact, etc.). Pairwise relatedness estimation can facilitate the identification process in these cases. Indeed, within the last decade, several remains identification projects have made extensive use of pairwise relatedness (kinship) estimation [24, 25, 26, 27, 28]. In addition, there are scenarios where pairwise relatedness estimates may be helpful in the courtroom. For example, the defense may suggest that a relative of the suspect is the true culprit. An estimate of the amount of relatedness between the suspect and the donor of the crime stain may be useful in this case. When authorities are unable to apprehend a suspect and a crime stain is available, relatedness estimation could be invaluable. If a known relative's DNA is available, pairwise relatedness estimation may give the authorities evidence to infer innocence or guilt.

Chapter 2. Pairwise Relatedness and Population Substructure

Measuring Pairwise Relatedness

One common measure of pairwise relatedness is referred to as the coancestry coefficient, denoted θ_{XY}. It is defined as the probability a random allele from individual X is IBD to a random allele from individual Y. To illustrate, consider the case where X and Y are parent and child, respectively. Also assume there is no underlying population substructure (non-inbred). Suppose X has alleles a and b. Due to Mendelian inheritance laws, with equal probability X will pass Y either allele a or allele b. Without loss of generality, we assume that a is passed from X to Y. In this case, the probability of randomly selecting allele a from X is $1/2$. In addition, the probability of randomly selecting allele a from Y is also $1/2$. This leads to an overall probability of $(1/2)(1/2) = 1/4$, which is θ_{XY} in the parent-child case. Similar arguments can be used to arrive at the other θ_{XY} values listed in Table 2.1. The relatedness coefficient is another common measure, and is simply $2\theta_{XY}$ (in the non-inbred case).

Table 2.1: Common θ_{XY} Values.

Relationship	θ_{XY}
Unrelated	0
Cousins	1/16
Full Siblings, Parent/Child	1/4
Identical Twins	1/2

The final and most descriptive method of measuring non-inbred pairwise relatedness was first introduced by Cotterman [29]. It involves the use of three parameters, whose definition here follows the notation of Evett and Weir [2]. Define P_0, P_1, and P_2 as the probability, at a particular locus, that two individuals share 0, 1, or 2 alleles IBD, respectively. Figure 2.2 is a diagram of the possible IBD relationships (or patterns) that could occur between four alleles taken from two individuals, X and Y. Later we see when population substructure exists, there are nine possible IBD patterns. For now we assume two alleles within the same individual cannot be IBD, thus only three

29

Chapter 2. Pairwise Relatedness and Population Substructure
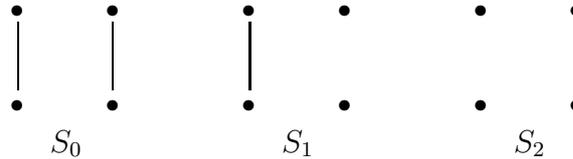
Figure 2.2: IBD Patterns Between Two Individuals, for the Non-Inbred Case. In each group, the two upper dots represent the alleles in individual X. The two lower dots represent the alleles in Y. A line between two dots indicates those alleles are IBD.

patterns are required. Consider the first diagram in Figure 2.2. There are two alleles shared between X and Y that are IBD. Thus, the probability of this pattern occurring is P_2. The probability of the second pattern is then P_1, and P_0 is the probability of the final pattern.

The coancestry coefficient can be written as a function of these "P-coefficients". Recall θ_{XY} is the probability a random allele from individual X is IBD to a random allele from individual Y. In the first pattern, with probability $1/2$ any random allele from X will be IBD to a random allele from Y (half the time the IBD allele from Y will be selected and half the time the non-IBD allele from Y will be selected). In the second pattern, only half of the time will you select the IBD allele from X. When this is coupled with the chance of selecting the IBD allele from Y ($1/2$), you arrive at an overall probability of $1/4$. The remaining pattern has no lines connecting X's alleles to Y's alleles and therefore does not contribute to the value of θ_{XY}. Thus the following holds:

$$\theta_{XY} = \frac{1}{4}P_1 + \frac{1}{2}P_2. \tag{2.1}$$

The coancestry coefficient, relatedness coefficient and P-coefficients are just a few of the existing parameters which can be used to measure pairwise relatedness. The purpose of this research is to adapt an existing estimator of pairwise relatedness. A reliable and simple estimator of pairwise relatedness is sought that can account for the

30

Chapter 2. Pairwise Relatedness and Population Substructure

potential effects of population substructure.

2.2   Review of Relevant Literature

Pairwise relatedness estimation is important in several diverse fields of study. As a result, several estimators of pairwise relatedness have been proposed using a variety of methodologies. The most commonly used technique (Queller and Goodnight [30]) was derived from a quantitative genetics point of view. The second group of estimators we consider makes use of the method of moments. Finally, maximum likelihood estimators will be reviewed. Note that the maximum likelihood approach will receive the most attention, as it is the foundation for the new estimator proposed. A comprehensive review of all techniques listed above is found in [23] and a biologist's perspective is given in [31]. A statistical comparison of several estimators (oddly excluding maximum likelihood) is found in [32].

In 2003, Milligan performed a simulation study designed to compare various pairwise relatedness estimators [33]. Several currently used estimators, including those we consider here, were examined. The results obtained are in agreement with most other studies. As a general rule, the amount of available genetic information impacts the quality of any pairwise relatedness estimator(i.e. number of loci, number of alleles, allele frequency distributions). Thus, Milligan used several simulated data sets. The number of loci ranged from five to thirty, and the number of alleles ranged from two to twenty. Allele frequencies were taken from three types of distributions: equal frequencies, one highly frequent allele (0.8), Dirichlet distribution with all parameters one. The findings of this study will be referred to often when comparing the various methods we consider in this section.

Chapter 2. Pairwise Relatedness and Population Substructure

Queller and Goodnight's Estimator

A commonly used technique for estimating pairwise relatedness was studied by Queller and Goodnight [30], though it was first derived by Grafen [34]. The estimate is of the relatedness coefficient (r_{XY}) as opposed to the coancestry coefficient (θ_{XY}). They derive an estimator for the average relatedness between groups of individuals, as opposed to pairs. However, they provide a modification of this method for pairwise estimation. The derivation provided in both [30, 34] is based on quantitative genetic theory. The reader is referred to [30] for details, as they are outside the scope of this review. Here, we will simply describe the estimator and discuss the advantages and disadvantages of using this technique.

First, define alleles to be identical in state (IBS) if they are of the same allelic type. It is important to note the difference between IBS and IBD. Alleles which are IBD are required to be IBS as well, because they are copies of the exact same ancestral allele. However, the reverse is not true. If two alleles are IBS, they could have descended from two different individuals (therefore not IBD). Next, label individual X's alleles as a and b, and individual Y's alleles as c and d (these are just labels and do not necessarily imply different allelic types). Now we define indicator variables,

$$S_{ij} = \begin{cases} 1 & \text{if allele } i \text{ is IBS to allele } j, \\ 0 & \text{otherwise.} \end{cases} \tag{2.2}$$

Finally, let p_i represent the population frequency of the ith allele. Queller and Goodnight's estimate of r_{XY} is then

$$\hat{r}_{xy} = \frac{0.5(S_{ac} + S_{ad} + S_{bc} + S_{bd}) - p_a - p_b}{1 + S_{ab} - p_a - p_b}. \tag{2.3}$$

The value of $\hat{r}_{xy}$ will depend on which individual is assigned the label X and which is Y. To arrive at an overall estimate, they propose using the average:

$$\frac{\hat{r}_{XY} + \hat{r}_{YX}}{2}. \tag{2.4}$$

Chapter 2. Pairwise Relatedness and Population Substructure

Queller and Goodnight's estimator is undefined when individual X is a heterozygote and there are only two alleles. In addition, it is possible to arrive at estimates that are outside the meaningful parameter space $(0, \frac{1}{2})$. According to Milligan's [33] simulations, this estimator is unbiased, although it tends to have a left skewed distribution. Thus, the most probable estimate will often be an incorrect one. The standard error for this estimate, as with all others considered, decreases with increasing numbers of loci and alleles. A major advantage of this method is that the creators have posted a program online that is free to download and simple to use [1].

Moment Estimators

Several moment estimators have been developed to estimate pairwise relatedness [35, 36, 37, 23, 1, 38]. Two techniques are reviewed here: Li et al.'s [36] modification of Lynch's [35] estimator; Lynch and Ritland's [23] estimator. Of the other moment estimators, some are algebraically complex and others are very similar to those described below and are thus not considered in this review. Appendix B contains comments and corrections to the paper by Jinliang Wang [1].

Lynch and Li Estimator

First we consider Lynch's [35] moment estimator, incorporating a slight modification by Li et al. [36]. They are also estimating the relatedness coefficient. To begin, define the similarity index (S_{XY}) as the average fraction of alleles at a locus in either X or Y for which there is another allele in the other individual which is IBS. For example, suppose X has genotype $A_i A_i$ and Y has genotype $A_i A_j$. Both of X's alleles are IBD to an allele from Y. Additionally, one of Y's two alleles are IBD to an allele from X. Thus S_{XY} equals the average of $\frac{2}{2}$ and $\frac{1}{2}$ which is $\frac{3}{4}$. Table 2.2 lists the S_{XY} values for all nine possible IBS patterns, denoted $\lambda_1, \ldots, \lambda_9$. The concept behind Lynch's estimator is if two individuals are related to a degree r_{XY}, the expected value of S_{XY} is

---

[1]http://www.gsoftnet.us/GSoft.html

Chapter 2. Pairwise Relatedness and Population Substructure

Table 2.2: Similarity Index (S_{XY}) Values for All IBS Patterns.

	IBS Patterns	S_{XY}
λ_1	$A_iA_i, A_iA_i \;\; \forall i$	1
λ_2	$A_iA_i, A_jA_j \;\; \forall i, \forall j \neq i$	0
λ_3	$A_iA_i, A_iA_j \;\; \forall i, \forall j \neq i$	3/4
λ_4	$A_iA_i, A_jA_k \;\; \forall i, \forall j \neq i, \forall k > j, k \neq i$	0
λ_5	$A_iA_j, A_iA_i \;\; \forall i, \forall j \neq i$	3/4
λ_6	$A_jA_k, A_iA_i \;\; \forall i, \forall j \neq i, \forall k > j, k \neq i$	0
λ_7	$A_iA_j, A_iA_j \;\; \forall i, \forall j > i$	1
λ_8	$A_iA_j, A_iA_k \;\; \forall i, \forall j \neq i, \forall k \neq i, j$	1/2
λ_9	$A_iA_j, A_kA_l \;\; \forall i, \forall j > i, \forall k \neq i, j, \forall l > k, l \neq i, j$	0

simply the sum of two terms. The first quantity is the fraction of alleles shared because they are identical by descent and the second is the fraction shared because they are identical in state. This leads to the following equation:

$$E(S_{XY}) = r_{XY} + (1 - r_{XY})S_0, \tag{2.5}$$

where S_0 is the expected value of S_{XY} at a locus for two unrelated individuals in a randomly mating population. The value of S_0 is rarely known, and Li et al. [36] propose $\hat{S}_0 = \sum_{i=1}^{n} p_i^2(2 - p_i)$, where n is the number of alleles at the locus and p_i is the population frequency of the ith allele. Setting S_{XY} equal to its expectation and substituting in estimates for the unknown values, we have

$$S_{XY} = \hat{r}_{XY} + (1 - \hat{r}_{XY})\hat{S}_0. \tag{2.6}$$

The moment estimator is then found by solving Equation 2.6 for $\hat{r}_{XY}$,

$$\hat{r}_{XY} = \frac{S_{XY} - \hat{S}_0}{1 - \hat{S}_0}. \tag{2.7}$$

To obtain a multi-locus estimate, the $\hat{r}_{XY}$ values are simply averaged over loci. Wang criticizes this approach, stating "although relatedness estimates from unlinked

Chapter 2. Pairwise Relatedness and Population Substructure

loci ... are independent, they could be dramatically different in sampling variance and ideally should not be simply averaged to give the overall estimate" [1]. Meaningful values for r_{XY} range from 0 to 1. It is important to note that Equation 2.7 does require the estimates to be less than one, as S_{XY} must be less than or equal to one. It is possible to obtain a negative estimate, which would fall outside of the parameter space. This happens whenever $S_{XY} < S_0$, which occurs at times due to sampling error [23]. Also note this estimator is always defined, as long as at least one allele frequency is greater than zero.

Lynch and Ritland's Estimator

The next moment estimator was proposed by Lynch and Ritland [23]. To begin, define two new parameters: ϕ_{XY} is the probability of X and Y having one pair of IBD alleles; Δ_{XY} is the probability of X and Y having two pairs of IBD alleles. In our notation, these two parameters are equivalent to P_1 and P_2. Lynch and Ritland use these parameters because in quantitative genetics, they are both involved in measuring the genetic covariance between individuals. In particular, the additive genetic covariance between individuals is a function of r_{XY}, whereas the dominance genetic covariance is a function of Δ_{XY}. The relatedness coefficient can then be written in terms of these parameters:

$$r_{XY} = \frac{\phi_{XY}}{2} + \Delta_{XY}. \tag{2.8}$$

Lynch and Ritland focus on the conditional probabilities of individual Y's genotype given individual X's genotype. Here we will consider when Y is homozygous and refer the reader to [23] for the other possible cases. Let $\Pr(ii|ii)$ denote the probability of X and Y having two pairs of alleles in common and let $\Pr(i\bar{i}|ii)$ denote the probability of them having only one pair in common. Lynch and Ritland give these probabilities as

$$\Pr(ii|ii) = p_i^2 + p_i(1 - p_i)\phi_{XY} + (1 - p_i^2)\Delta_{XY}, \tag{2.9}$$

$$\Pr(i\bar{i}|ii) = 2p_i(1 - p_i) + (1 - p_i)(1 - 2p_i)\phi_{XY} - 2p_i(1 - p_i)\Delta_{XY}. \tag{2.10}$$

35

Chapter 2. Pairwise Relatedness and Population Substructure

It is assumed that the population allele frequencies are known. To use the method of moments, two functions are required whose expected values are $\Pr(ii|ii)$ and $\Pr(i\bar{i}|ii)$. Lynch and Ritland propose two indicator variables, that are assigned 1 if the corresponding genotype pattern is observed and 0 is assigned for all other patterns. These equations, with the indicator functions substituted in, can then be solved to obtain estimates for ϕ_{XY} and Δ_{XY}. Using Equation 2.8, and substituting in $\hat{\phi}_{XY}$ and $\hat{\Delta}_{XY}$ will give the estimator:

$$\hat{r}_{XY} = \frac{\hat{\Pr}(i\bar{i}|ii) + 2\hat{\Pr}(ii|ii) - 2p_i}{2(1 - p_i)}. \tag{2.11}$$

As mentioned, the equation above holds only when Y is a homozygote. Lynch and Ritland additionally provide a general form of their estimator that holds for all cases (Equation 5 in [23]). Since their estimates will differ depending on which person is labeled Y, they suggest averaging the two cases, as done by Queller and Goodnight in Equation 2.4. Finally, to obtain multi-locus estimates they propose using a weighting system. The actual weights that will minimize the variance of their estimator are functions of parameters and thus cannot be obtained. Lynch and Ritland use approximations which make the inconsistant assumption that X and Y are unrelated.

A major limitation of this estimation technique is this necessity to assume X and Y are unrelated. It requires assuming a particular value for relatedness (namely 0), when it is relatedness itself that we are trying to estimate. As with Queller and Goodnight's estimator above, this estimate can also be undefined. This occurs when X is a heterozygote for a locus with two equally frequent alleles.

Another potential disadvantage is that negative estimates of r_{XY} can occur. Obtaining estimates outside of the meaningful parameter space is an issue that deserves some attention. Mainly due to the competing perspectives that exist about its meaning. Lynch and Ritland state that these estimates are in fact meaningless, and it is a drawback to using their estimators. Milligan and Wang agree [33, 1]. However, Hardy states

It is important to keep in mind that relatedness coefficients depend on a

Chapter 2. Pairwise Relatedness and Population Substructure

> 'reference population' (or 'reference sample'), and express a degree of genetic similarity between individuals relative to the average genetic similarity between the individuals found in the reference population. Consequently, negative values of the relatedness coefficient may be obtained, meaning X and Y are less related on average than random individuals from the 'reference' population.

He also states "a relatedness coefficient must always be defined relative to some reference level of relatedness" [38].

Milligan [33] evaluated both moment estimators described here. Both were unbiased; however for both first cousins and unrelated individuals, almost half of the estimates fell outside the meaningful parameter space. Thus, if we were to truncate the values to lie in the meaningful space, there would be some amount of bias observed. The standard error for Lynch and Ritland's estimator was lower than Lynch and Li's estimator, especially in cases of low relatedness. For both estimators, standard errors are extremely dependent on the sampling conditions and on the actual degree of relatedness. A free software program, IDENTEX, has been created by Belkhir et al. that calculates pairwise relatedness estimates using either Lynch and Ritland's methodology or Queller and Goodnight's technique [39].

Perhaps the most detrimental attribute of moment estimators overall, is the challenges that arise when attempting to extend them to other data types. New derivations are required to handle any deviations from the typical sampling scheme. For example, there are large differences in the derivations for dominant versus codominant allele structures. Also, no easy way exists to incorporate the effects of population substructure into their estimators. These moment estimators, which estimate a continuous parameter of relatedness, cannot be easily converted to a discrete relationship estimator. All of these difficulties have been handled quite easily using maximum likelihood techniques; a major reason why this methodology was implemented here. The next section fully examines these techniques.

Chapter 2. Pairwise Relatedness and Population Substructure

Maximum Likelihood Estimators

As mentioned above, maximum likelihood techniques have been derived and adapted to handle a wide variety of cases. They have been used to arrive at both a discrete estimate (as done by Thompson [40]) and a continuous estimate of relatedness (as in [33]). The likelihood technique has also been extended to incorporate the effects of linkage between loci [41]. Hypothesis testing using the likelihood function has also been explored [42]. A comprehensive review of earlier work in maximum likelihood estimation and the handling of various extensions is provided in [43]. First we describe the original maximum likelihood estimator (MLE) proposed in 1975 by Thompson [40]. Then we discuss how Milligan proposed expanding Thomson's model from three to nine parameters in order to allow for population substructure.

Three Parameter MLE

Likelihood techniques estimate the coancestry coefficient (θ_{XY}) defined in Section 2.1. The invariance property states if $\hat{\theta}$ is the maximum likelihood estimator of θ, then for any function $\tau(\theta)$, the MLE of $\tau(\theta)$ is $\tau(\hat{\theta})$. This property implies that once we obtain the MLEs for the three P-coefficients (defined in Section 2.1), we can use Equation 2.1 to find the MLE for θ_{XY}.

Assume we observe data on the genotypes of two individuals at several unlinked loci. Nine distinct IBS patterns, λ_i, $i = 1, \ldots 9$, were discussed in the previous section (Table 2.2). The likelihood of $\mathbf{P}$ given an observed IBS pattern λ_i is

$$L_i(\mathbf{P}|\lambda_{\mathbf{i}}) = \Pr(\lambda_{\mathbf{i}}|\mathbf{P}). \tag{2.12}$$

The subscript i on the likelihood makes it explicit that the likelihood function varies based on which IBD pattern is observed. Let the three IBD patterns in Figure 2.2 be S_7, S_8, and S_9 (the purpose for this notation will become clear when we discuss the nine parameter MLE). Then, making use of law of total probability (see Appendix A),

Chapter 2. Pairwise Relatedness and Population Substructure

we have

$$L_i(\mathbf{P}|\lambda_\mathbf{i}) = \Pr(\lambda_i|S_7)\Pr(S_7) + \Pr(\lambda_i|S_8)\Pr(S_8) + \Pr(\lambda_i|S_9)\Pr(S_9)$$
$$= \Pr(\lambda_i|S_7)P_2 + \Pr(\lambda_i|S_8)P_1 + \Pr(\lambda_i|S_9)P_0. \tag{2.13}$$

If we denote the frequency of the ith allele as p_i, the values for $\Pr(\lambda_i|S_j)$ are given in Table 2.3. To illustrate, consider the first cell of Table 2.3. In this case, all alleles

Table 2.3: Conditional Probabilities $\Pr(\lambda_i|S_j)$, with No Population Substructure.

IBS Pattern		S_7	S_8	S_9
			IBD Pattern	
λ_1	A_iA_i, A_iA_i	p_i^2	p_i^3	p_i^4
λ_2	A_iA_i, A_jA_j	0	0	$p_i^2p_j^2$
λ_3	A_iA_i, A_iA_j	0	$p_i^2p_j$	$2p_i^3p_j$
λ_4	A_iA_i, A_jA_k	0	0	$2p_i^2p_jp_k$
λ_5	A_iA_j, A_iA_i	0	$p_i^2p_j$	$2p_i^3p_j$
λ_6	A_jA_k, A_iA_i	0	0	$2p_i^2p_jp_k$
λ_7	A_iA_j, A_iA_j	$2p_ip_j$	$p_ip_j(p_i+p_j)$	$4p_i^2p_j^2$
λ_8	A_iA_j, A_iA_k	0	$p_ip_jp_k$	$4p_i^2p_jp_k$
λ_9	A_iA_j, A_kA_l	0	0	$4p_ip_jp_kp_l$

are of type i and we are given that two pairs of alleles are IBD. Thus, the probability of this event is the chance that X randomly gets two i alleles. When there is no population substructure, X receives the i alleles independently. Therefore it is simply the frequency of the ith allele squared. The other cells can be determined using similar arguments. This likelihood equation will be further examined and an example of its use is provided in Section 2.3.

To obtain the MLEs for the P-coefficients we need to maximize the likelihood with respect to the parameters of interest. In some cases, this can be performed analytically (see Appendix A of [33]). However, in the majority of cases the maximum must be found using some numerical maximizing technique. Here we use the downhill simplex method which will be discussed at length in Section 2.3. To obtain multi-locus

Chapter 2. Pairwise Relatedness and Population Substructure

estimates, the likelihoods for each loci are simply multiplied together to arrive at one overall likelihood function, as loci are assumed independent. This overall likelihood is then maximized to obtain the MLE. Recalling the weighting method of Lynch and Ritland that required the (perhaps incorrect) assumption that X and Y were unrelated, this multiplicative property of likelihoods is quite an advantage.

A disadvantage of the three dimensional maximum likelihood estimator is the large biases that occur for some relationships. This problem can be severe if the relationship is close to the endpoints of the parameter space. This bias occurs because the maximum likelihood technique requires its estimates to fall within the valid space. For example, if the true relationship is unrelated ($\theta_{XY} = 0$), we will never get an unbiased result as we are unable to obtain values less than zero. Milligan found that genetic sampling has a large effect on the amount of bias, stating that it can be reduced by sampling loci with more alleles (>20), with non-skewed frequency distributions [33]. Another disadvantage is that software is not freely available to implement this method.

An advantage of the three parameter likelihood technique is the small standard errors observed. Milligan showed, depending on sampling conditions, that the standard errors for the non-likelihood based estimators were between 2% and 250% larger. In addition he found that the errors for the MLE were less influenced by degree of actual relatedness. This was not the case for the other estimators considered. When the root mean-squared error was studied, the likelihood maintains very low values. To conclude, Milligan writes "although some non-likelihood estimators exhibit better performance with respect to specific metrics under some conditions, none approach the high level of performance exhibited by the likelihood estimator across all conditions and all metrics of performance."

Overall, it seems clear that a maximum likelihood approach has many advantages over the other estimators reviewed here. According to current studies, the bias that is observed can be overcome by sampling a large number of loci, as well as increasing the number of alleles. In previous decades, this has meant that the likelihood method has fallen by the wayside. However, as technology is improving, vast amounts of

Chapter 2. Pairwise Relatedness and Population Substructure

genetic data are becoming available on a much larger number of species. Thus, the likelihood method is gradually becoming a more popular method of pairwise relatedness estimation.

Nine Parameter MLE

In 2003, Milligan extended the work of Thompson by defining the maximum likelihood estimator in a way that can account for population substructure [33]. This natural extension increases the number of parameters needed from three to nine. The previous approach allowed for only three IBD patterns, as presented in Figure 2.2. When population substructure exists, there are more possibilities. There is now a chance that X's (or Y's) parents have ancestors in common. This implies that the two alleles received by an individual from their parent could be IBD. In particular, six additional IBD patterns must be considered. The full set of nine IBD states S_j are shown in Figure 2.3. This expanded set of patterns requires that nine parameters be estimated:

$$\Delta_j = \Pr(S_j) \text{ for } j = 1, \ldots, 9. \tag{2.14}$$

They are referred to as Jacquard's coefficients, as they were first developed by Jacquard in [44]. The data we observe are the possible IBS patterns, λ_i, given in Table 2.3. Thus, the nine parameter likelihood function is

$$L_i(\boldsymbol{\Delta}|\lambda_i) = \sum_{j=1}^{9} \Pr(\lambda_i|S_j)\Delta_j, \tag{2.15}$$

as $\Delta_j = \Pr(S_j)$, and where $\Pr(\lambda_i|S_j)$ values are given in Table 2.4, adapted from [33]. We derive two cells here and refer the reader to [33] for further details.

Consider the cell in Table 2.4 corresponding to IBD pattern S_4 (see Figure 2.3) and IBS pattern λ_3 $(A_i A_i, A_i A_j)$. In this case, the two alleles from X are IBD to each other, but no other alleles are IBD. Thus, we only need to include the probability of obtaining allele A_i once (p_i). The probability of Y having alleles $A_i A_j$, given there are no IBD relationships involving these alleles is $2p_i p_j$. The factor of 2 is because order is

41

Chapter 2. Pairwise Relatedness and Population Substructure
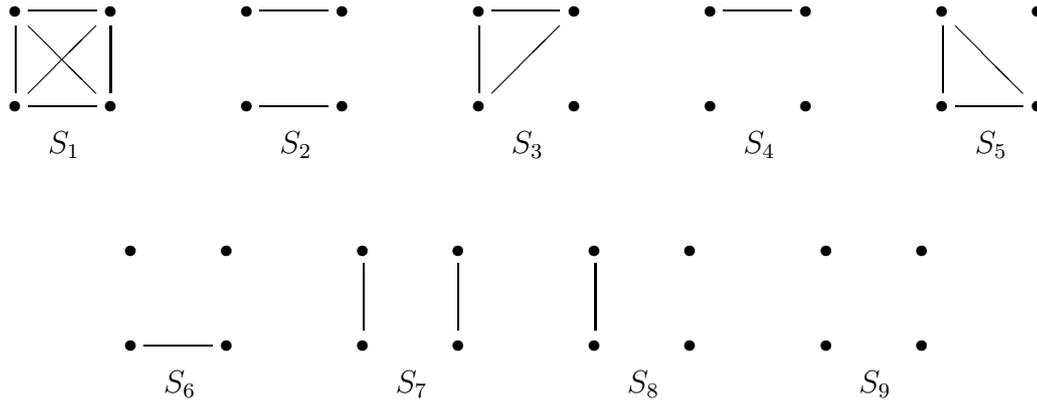
Figure 2.3: IBD Patterns Between Two Individuals, for the Inbred Case.
In each group, the two upper dots represent the alleles from individual X. The two lower dots represent the alleles from Y. A line between two dots indicates those alleles are IBD.

Table 2.4: Conditional Probabilities $\Pr(\lambda_i | S_j)$, with Population Substructure.

	S_1	S_2	S_3	S_4	S_5	S_6	S_7	S_8	S_9
λ_1	p_i	p_i^2	p_i^2	p_i^3	p_i^2	p_i^3	p_i^2	p_i^3	p_i^4
λ_2	0	p_ip_j	0	$p_ip_j^2$	0	$p_i^2p_j$	0	0	$p_i^2p_j^2$
λ_3	0	0	p_ip_j	$2p_i^2p_j$	0	0	0	$p_i^2p_j$	$2p_i^3p_j$
λ_4	0	0	0	$2p_ip_jp_k$	0	0	0	0	$2p_i^2p_jp_k$
λ_5	0	0	0	0	p_ip_j	$2p_i^2p_j$	0	$p_i^2p_j$	$2p_i^3p_j$
λ_6	0	0	0	0	0	$2p_ip_jp_k$	0	0	$2p_i^2p_jp_k$
λ_7	0	0	0	0	0	0	$2p_ip_j$	$p_ip_j(p_i+p_j)$	$4p_i^2p_j^2$
λ_8	0	0	0	0	0	0	0	$p_ip_jp_k$	$4p_i^2p_jp_k$
λ_9	0	0	0	0	0	0	0	0	$4p_ip_jp_kp_l$

Chapter 2. Pairwise Relatedness and Population Substructure

not considered within an individual; Y's alleles could be $A_i A_j$ or $A_j A_i$. Therefore, the probability of observing IBS pattern λ_3 given IBD pattern S_4 is $2p_i^2 p_j$. Now consider $\Pr(\lambda_7 | S_8)$. Here we observe IBS pattern $A_i A_j, A_i A_j$ and one allele from X is IBD to one allele from Y. One possibility is that the A_i alleles are IBD. In this case, the probability of observing the pattern is $p_i p_j^2$. If, instead, the A_j alleles are IBD the probability of observing λ_7 is $p_i^2 p_j$. When these two probabilities are summed, we arrive at $p_i p_j (p_i + p_j)$.

Thus, Milligan has defined a likelihood that can be maximized to find the MLEs of Jacquard's coefficients. Making use of the MLE's invariance property, an MLE for θ_{XY} can be obtained. Recall θ_{XY} is the probability a random allele from individual X is IBD to a random allele from individual Y. Using this definition, we can relate Jacquard's parameters to θ_{XY}:

$$\theta_{XY} = \Delta_1 + \frac{1}{2}(\Delta_3 + \Delta_5 + \Delta_7) + \frac{1}{4}\Delta_8. \tag{2.16}$$

To arrive at this equation, consider the state S_1 in Figure 2.3. In this case, with probability one, any random allele from X will be IBD to a random allele from Y. In state S_3, with probability $1/2$ any random allele from X will be IBD to a random allele from Y (half the time the IBD allele from Y will be selected and half the time the non-IBD allele from Y will be selected). The same is true for patterns S_5 and S_7. In S_8 only half of the time will you select the IBD allele from X. When this is coupled with the chance of selecting the IBD allele from Y $(1/2)$, you arrive at an overall probability of $1/4$. The remaining states $(S_2, S_4, S_6,$ and $S_9)$ have no lines connecting X's alleles to Y's alleles and therefore do not contribute to the value of θ_{XY}.

After providing this derivation, Milligan finishes his study performing simulations comparing the various aforementioned estimators. He simply ignores the effects of population substructure, and performs his studies using the simplified three parameter model presented above. No detailed study of the properties of the nine parameter estimator has been done. For this reason, the nine parameter estimator is further examined in the next section.

Chapter 2. Pairwise Relatedness and Population Substructure

2.3 Research Methods

This section extends the body of work on the estimation of relatedness using maximum likelihood techniques. First, an example of the use of the nine parameter MLE is provided. Similar to the three parameter MLE, analytical expressions for the MLE do not exist and numerical methods must be employed. The downhill simplex method is reviewed an examples of its use are provided. A new seven parameter estimator is also derived that still accounts for population substructure while reducing the number of parameters to estimate. Finally, a new methodology is developed that can infer relationships from any of the three types of MLE estimates. We conclude by describing the design of the simulation study used to compare the three, seven and nine paramter MLEs.

Nine Parameter MLE, Continued

To facilitate the understanding of the nine parameter likelihood function given by Equation 2.15, consider the following scenario. Suppose we observe genotype data for two individuals at two loci. Let individual X have alleles $A_1 A_2$ at locus one and $B_1 B_2$ at locus two. Let individual Y have alleles $A_1 A_1$ at locus one and $B_1 B_2$ at locus two. Label the allele frequencies p_1, p_2 and q_1, q_2 at the two loci, respectively. Consider the first locus, with IBS pattern λ_5 $(A_i A_j, A_i A_i)$. Using Equation 2.15, coupled with the appropriate line from Table 2.4 we find the likelihood for locus one is

$$L_5(\boldsymbol{\Delta}|\lambda_5) = \sum_{j=1}^{9} \Pr(\lambda_5|S_j)\Delta_j = p_1 p_2 \Delta_5 + 2p_1^2 p_2 \Delta_6 + p_1^2 p_2 \Delta_8 + 2p_1^3 p_2 \Delta_9. \qquad (2.17)$$

Now consider the second locus, and assume it is independent (unlinked) from the first locus. Here, the IBS pattern is λ_7 $(B_i B_j, B_i B_j)$. The corresponding line from Table 2.4 leads to the likelihood

$$L_7(\boldsymbol{\Delta}|\lambda_7) = \sum_{j=1}^{9} \Pr(\lambda_7|S_j)\Delta_j = 2q_1^2 q_2 \Delta_7 + q_1 q_2 (q_1 + q_2)\Delta_8 + 4q_1^2 q_2^2 \Delta_9. \qquad (2.18)$$

Chapter 2.   Pairwise Relatedness and Population Substructure

Since the loci are independent, we simply multiply the two likelihoods together to obtain an overall likelihood,

$$L(\mathbf{\Delta}) = \left(p_1 p_2 \Delta_5 + 2p_1^2 p_2 \Delta_6 + p_1^2 p_2 \Delta_8 + 2p_1^3 p_2 \Delta_9\right) \\ \times \left(2q_1^2 q_2 \Delta_7 + q_1 q_2 (q_1 + q_2) \Delta_8 + 4q_1^2 q_2^2 \Delta_9\right).$$

(2.19)

Now we need to maximize the likelihood, using some numerical method. Additional complexity is introduced as we have the following constraints on our parameters:

- $\sum_{i=1}^{9} \Delta_i = 1$,
- $0 \leq \Delta_i \leq 1$, $\forall i$.

The first constraint is due to the fact that the nine IBD states are exhaustive, thus their total probability must equal one. The second constraint is simply a result of each parameter representing a probability, thus must lie between zero and one. One numerical technique that caters to functions with constraints is the downhill simplex method. For a complete description of the method, see [45]. The next section briefly describes the method and continues this example.

Downhill Simplex Method

The downhill simplex method was first described by Nelder and Mead [46]. This method was chosen because it is fast and accurate. Additional random walk methods were attempted, however the estimates obtained were exactly those of the simplex method. Additionally, the random walk programs took several hours to run, whereas the simplex method only needed seconds. The simplex method was also employed in Milligan's study [33], allowing for verification of results.

The downhill simplex method is a numerical minimizing technique that facilitates functions with constraints. An N-dimensional simplex is a geometrical figure of $N+1$ points and all connecting line segments and faces. (In 2-dimensions it is a triangle.) To begin, an initial simplex must be given. The method will then take a series of steps changing the dimensions of the simplex. Each step either reflects, expands, or contracts the simplex allowing the simplex to "blob" around the surface of the function, always

Chapter 2. Pairwise Relatedness and Population Substructure

searching for lower values. Eventually the simplex will pull itself in around the lowest point, which will be the minimum value. Throughout the process, there are constant checks to ensure the constraints are met. A C++ program was created implementing this method (see Appendix C), adapting code provided in [45]. As mentioned, this is a minimizing routine. Here we obtain the maximum value by minimizing the negative likelihood.

Recall the likelihood equation for the example provided in the previous section:

$$L(\boldsymbol{\Delta}) = \left(p_1 p_2 \Delta_5 + 2p_1^2 p_2 \Delta_6 + p_1^2 p_2 \Delta_8 + 2p_1^3 p_2 \Delta_9\right)$$
$$\times \left(2q_1^2 q_2 \Delta_7 + q_1 q_2(q_1 + q_2)\Delta_8 + 4q_1^2 q_2^2 \Delta_9\right). \tag{2.20}$$

We would like to maximize the likelihood with respect to $\boldsymbol{\Delta}$. For demonstration purposes, we consider the special case where no population substructure exists. This assumption requires $\Delta_1 = \ldots = \Delta_6 = 0$. If we additionally assume (arbitrarily) that $p_1 = p_2 = q_1 = q_2 = 0.30$, and note that $\Delta_9 = 1 - \Delta_7 - \Delta_8$, the likelihood is reduced to

$$L(\boldsymbol{\Delta}) = -0.0215\Delta_7^2 - 0.0037\Delta_8^2 + 0.0168\Delta_7 + 0.0063\Delta_8 + 0.0047. \tag{2.21}$$

Figure 2.4 provides a graph of this function.

To get a better idea of where the maximum occurs, Figure 2.5 shows the likelihood with an intercepting plane, showing the maximum occurs when $\Delta_7 \approx 0.40$ and $\Delta_8 \approx 0$. We can use the simplex method to obtain exact results. The following is output from our program:

```
Delta 7 = 0.390
Delta 8 = 0.0
Delta 9 = 0.610
Maximum = 0.008
Theta_XY  = 0.195
This method required 254 function evaluations
```

As predicted above, the MLEs for Δ_7 and Δ_8 are 0.390 and 0, respectively. The MLE for Δ_9 is simply one minus the MLE values for Δ_7 and Δ_8. The output gives us the actual value of the likelihood at the maximum, 0.008, which also agrees with our plots

Chapter 2. Pairwise Relatedness and Population Substructure
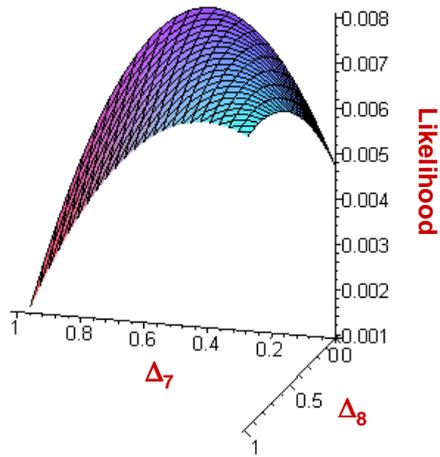
Figure 2.4: Graph of Likelihood Function.
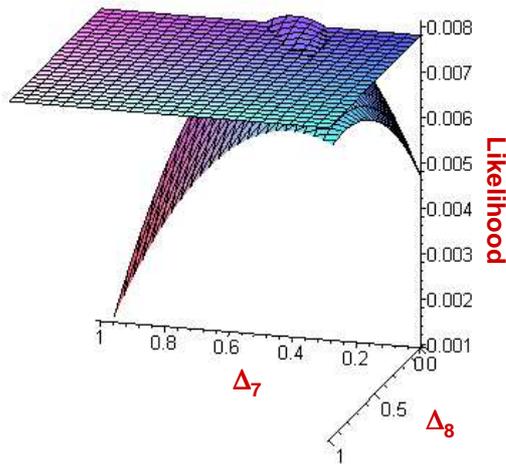
Figure 2.5: Graph of Likelihood Function with Intercepting Plane.

47

Chapter 2. Pairwise Relatedness and Population Substructure

in Figures 2.4 and 2.5. The MLE for θ_{XY} is given, which we can verify using using Equation 2.16:

$$(\theta_{XY})_{MLE} = \frac{1}{2}(0.390) + \frac{1}{4}(0) = 0.195. \tag{2.22}$$

Finally, the number of function evaluations required is also listed in the output. This refers to how many times the likelihood function was computed for a particular set of parameter values before the "best" value was obtained. The computationally demanding portion of this program is the function evaluations. Thus, the number of evaluations is reported to give an idea of how long the program took to run. In this case, it only took a fraction of a second. While this simplified example was in two dimensions, the simplex method works exactly the same in N-dimensions ($N = 8$ in the population substructure case).

The nine dimensional method requires a distinction between X and Y. In some cases, this distinction is not necessary. For example, if X and Y are drawn from the same subpopulation, the probability that X has two IBD alleles is equal to the probability that Y has two IBD alleles. The nine parameter model assumes these two probabilities are distinct. If the distinction between X and Y is unnecessary the nine parameter model is at a disadvantage, as extraneous parameters are being estimated. This is the motivation for the seven parameter model proposed in the next section.

Seven Parameter MLE

As mentioned, in the nine parameter case different estimates can occur depending on which individual is labeled X and which is labeled Y. This phenomenon occurs because the patterns shown in Figure 2.3 are ordered with respect to X and Y. For example, if we were to ignore the ordering of X and Y, S_3 and S_5 would be the same pattern. In addition, S_4 and S_6 would also be the same pattern. If we assume X and Y come from the same subpopulations, one new parameter could replace Δ_3 and Δ_5. If another parameter replaced Δ_4 and Δ_6, the total number of parameters is reduced to seven.

A new set of notation is needed to define the seven parameter estimate. To begin,

Chapter 2. Pairwise Relatedness and Population Substructure

there are now only seven distinct IBD patterns possible between the four alleles from X and Y. These patterns are denoted $S'_1, \ldots S'_7$ and are shown in Figure 2.6. Pattern
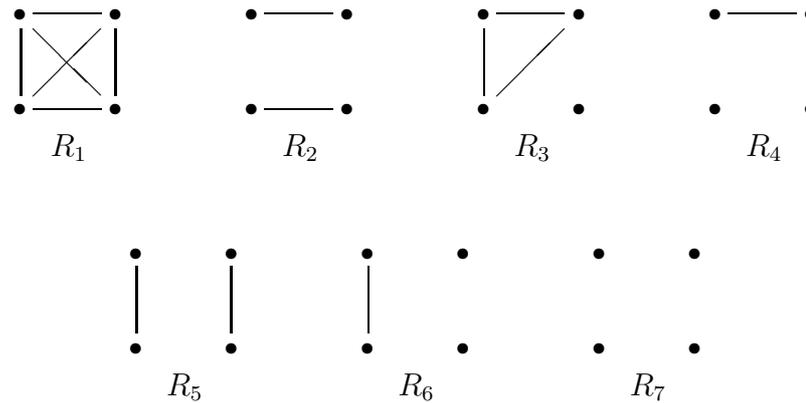
Figure 2.6: IBD Patterns Between Two Individuals, for the Seven Parameter Inbred Case.

S'_3 replaces both S_3 and S_5 from Figure 2.3, as the ordering between X and Y does not matter. Similarly, S'_4 replaces both S_4 and S_6. Thus, the new parameters of interest are

$$\phi_j = \Pr(S'_j) \text{ for } j = 1, \ldots, 7. \tag{2.23}$$

A description of the relationships among the new ϕ's, Jacquard's coefficients, and Evett and Weir's commonly used δ coefficients [2] is given in Table 2.5.

In addition to reducing the number of IBD states, we also reduce the number of IBS states. Now that ordering between X and Y no longer matters, pattern λ_3 (A_iA_i, A_iA_j) is the same as pattern λ_5 (A_iA_j, A_iA_i). Similarly, λ_4 (A_iA_i, A_jA_k) is the same as λ_6 (A_jA_k, A_iA_i). Thus, we define a new set of IBS patterns, $\lambda'_1, \ldots, \lambda'_7$ and they are listed in Table 2.6. The likelihood is similar to that in Equation 2.15,

$$L_i(\mathbf{\Delta}|\lambda'_i) = \sum_{j=1}^{7} \Pr(\lambda'_i|S'_j)\phi_j, \tag{2.24}$$

where $\Pr(\lambda'_i|S'_j)$ is given by Table 2.6.

49

Chapter 2.   Pairwise Relatedness and Population Substructure

Table 2.5: Relationships Among Various Relateness Coefficients.

New	Jacquard [44]	Evett & Weir [2]
ϕ_1	Δ_1	δ_{abcd}
ϕ_2	Δ_2	$\delta_{ab.cd}$
ϕ_3	$\Delta_3 + \Delta_5$	$\delta_{abc} + \delta_{abd} + \delta_{acd} + \delta_{bcd}$
ϕ_4	$\Delta_4 + \Delta_6$	$\delta_{ab} + \delta_{cd}$
ϕ_5	Δ_7	$\delta_{ac.bd} + \delta_{ad.bc}$
ϕ_6	Δ_8	$\delta_{ac} + \delta_{bd} + \delta_{ad} + \delta_{bc}$
ϕ_7	Δ_9	δ_0

Table 2.6: Conditional Probabilities based on Seven Parameters.

$IBS Patterns$	S'_1	S'_2	S'_3	S'_4	S'_5	S'_6	S'_7
$\lambda'_1 = A_iA_i, A_iA_i$	p_i	p_i^2	p_i^2	p_i^3	p_i^2	p_i^3	p_i^4
$\lambda'_2 = A_iA_i, A_jA_j$	0	p_ip_j	0	$p_ip_j^2$	0	0	$p_i^2p_j^2$
$\lambda'_3 = A_iA_i, A_iA_j$	0	0	$\frac{p_ip_j}{2}$	$p_i^2p_j$	0	$p_i^2p_j$	$2p_i^3p_j$
$\lambda'_4 = A_iA_i, A_jA_k$	0	0	0	$p_ip_jp_k$	0	0	$2p_i^2p_jp_k$
$\lambda'_5 = A_iA_j, A_iA_j$	0	0	0	0	$2p_ip_j$	$p_ip_j(p_i + p_j)$	$4p_i^2p_j^2$
$\lambda'_6 = A_iA_j, A_iA_k$	0	0	0	0	0	$p_ip_jp_k$	$4p_i^2p_jp_k$
$\lambda'_7 = A_iA_j, A_kA_l$	0	0	0	0	0	0	$4p_ip_jp_kp_l$

To demonstrate the conversion from the nine by nine Table 2.4 to the seven by seven table here, consider the first row. The value for $\Pr(S'_3|\lambda'_1)$ is simply the average of the appropriate probabilities from Table 2.4:

$$\Pr(S'_3|\lambda'_1) = \frac{\Pr(S_3|\lambda_1) + \Pr(S_5|\lambda_1)}{2} = \frac{p_i^2 + p_i^2}{2} = p_i^2. \qquad (2.25)$$

Similarly,

$$\Pr(S'_4|\lambda'_1) = \frac{\Pr(S_4|\lambda_1) + \Pr(S_6|\lambda_1)}{2} = \frac{p_i^3 + p_i^3}{2} = p_i^3. \qquad (2.26)$$

The other entries in the first row are the exact same as those in Table 2.4, noting $S_7 = S'_5, S_8 = S'_6, S_9 = S'_7$. The same process is used to arrive at the values for rows

Chapter 2. Pairwise Relatedness and Population Substructure

2, 5, 6, and 7. Now consider the third row of Table 2.6. The first two and last three cells are obtained by averaging the corresponding values from Table 2.4 in the third and fifth rows. For example, $\Pr(\lambda_3'|S_6'$ is the average of $p_i^2 p_j$ and $p_i^2 p_j$. $\Pr(S_3'|\lambda_3')$ is obtained by averaging four cells from Table 2.4,

$$\Pr(S_3'|\lambda_3') = \frac{\Pr(S_3|\lambda_3) + \Pr(S_5|\lambda_3) + \Pr(S_3|\lambda_5) + \Pr(S_5|\lambda_5)}{4}. \tag{2.27}$$

A similar average is used for the next cell,

$$\Pr(S_4'|\lambda_3') = \frac{\Pr(S_4|\lambda_3) + \Pr(S_6|\lambda_3) + \Pr(S_4|\lambda_5) + \Pr(S_6|\lambda_5)}{4}. \tag{2.28}$$

The fourth row is derived in a similar manner to row three.

Therefore, we have defined a likelihood that can be maximized to find the MLEs for $\phi_1, \ldots \phi_7$. The relationship between these parameters and the coancestry coeficient,

$$\theta_{XY} = \phi_1 + \frac{1}{2}(\phi_3 + \phi_5) + \frac{1}{4}\phi_6, \tag{2.29}$$

allows us to obtain the MLE for θ_{XY}, similar to the nine parameter case.

Both the seven and nine parameter models give one summary value (MLE of θ_{XY}) which can then be used to infer a relationship. For example, if we get an estimate of 0.24 and if there is no inbreeding, and the ages of X and Y are fairly close (to rule out the parent-child possibility), we could predict that it is a full sibling pair. Unfortunately, this is not the most satisfying result. We would like to say they are full siblings with absolute certainty, or with at least some idea of the error rates associated with our estimate. In addition, we may not have information about the individuals' ages. Thus, it would be impossible to differentiate between full sibling and parent-child pairs. Ideally, we would like to have some sort of classification mechanism that could place paired observations into one of several groups. Then an estimated relationship could be given, as well as some accuracy rates based on simulation study results. To this end, a distance metric method of classifying pairwise relationships was developed.

Chapter 2. Pairwise Relatedness and Population Substructure

Distance Metric Method of Relationship Classification

Through maximizing the likelihood, we have obtained estimates for either Jacquard's nine coefficients or the seven ϕ's. When estimating the continuous parameter θ_{XY}, we use only a function of these parameters. Additionally, that function only contains five of the nine (or four of the seven) parameters estimated. In our classification method we make use of all available MLE values; hypothesizing that the more information used, the better the estimates.

To begin, we can quantify the amount of population substructure that exists using what is commonly referred to as the inbreeding coefficient, denoted ψ. (Note that this is the same parameter as θ defined in Chapter 1, it is relabeled here to avoid confusion with θ_{XY}.) If we assume the value of ψ is known, it is possible to determine the true values for either Jacquard's coefficients or the seven ϕ's for any imaginable relationship. The true values of Jacquard's coefficients, in terms of ψ, for some common relationships are given in Table 2.7. Numerical values for the full sibling case, at several different values of ψ, are given in Table 2.8.

Next, define $\boldsymbol{\Delta}_U$, $\boldsymbol{\Delta}_F$, ... to be the known relationship vectors for unrelated pairs, full sib pairs, etc. We can then compute the Euclidean distance (D_U, D_F, ...) between the estimated vector ($\hat{\boldsymbol{\Delta}}$) and several of the true vectors. For example, the distance formula for unrelated individuals in the nine parameter case is

$$D_U = \|\hat{\boldsymbol{\Delta}} - \boldsymbol{\Delta}_U\| = \sqrt{\sum_{i=1}^{9}(\hat{\Delta}_i - \Delta_{U,i})^2}, \tag{2.30}$$

These distances can be computed for any number of competing relationships. The relationship that obtains the minimum distance will then become our discrete estimate. To illustrate the classification method, suppose we obtain the following nine parameter MLE:

$$\hat{\boldsymbol{\Delta}} = (0.0524, 0.0000, 0.0336, 0.0358, 0.0517, 0.0631, 0.0527, 0.4605, 0.2502). \tag{2.31}$$

Assume we have prior knowledge that unrelated, cousin, half sib, and full sib pairs are

Chapter 2. Pairwise Relatedness and Population Substructure

Table 2.7: Jacquard's Coefficients in Terms of the Inbreeding Coefficient (ψ) for Some Common Relationships.

	Relationship			
Coefficient	Unrelated	Cousins	Half Siblings	Full Siblings
Δ_1	$\frac{6\psi^3}{(1+\psi)(1+2\psi)}$	$\frac{\psi^2(1+11\psi)}{2(1+\psi)(1+2\psi)}$	$\frac{\psi^2(1+5\psi)}{(1+\psi)(1+2\psi)}$	$\frac{\psi(1+7\psi+16\psi^2)}{4(1+\psi)(1+2\psi)}$
Δ_2	$\frac{\psi^2-\psi^3}{(1+\psi)(1+2\psi)}$	$\frac{3(\psi^2-\psi^3)}{4(1+\psi)(1+2\psi)}$	$\frac{\psi^2(1-\psi)}{2(1+\psi)(1+2\psi)}$	$\frac{\psi^2(1-\psi)}{4(1+\psi)(1+2\psi)}$
Δ_3	$\frac{4(\psi^2-\psi^3)}{(1+\psi)(1+2\psi)}$	$\frac{\psi(1+13\psi-14\psi^2)}{4(1+\psi)(1+2\psi)}$	$\frac{\psi(1+5\psi-6\psi^2)}{2(1+\psi)(1+2\psi)}$	$\frac{\psi(1+3\psi-4\psi^2)}{2(1+\psi)(1+2\psi)}$
Δ_4	$\frac{\psi(1-2\psi+\psi^2)}{(1+\psi)(1+2\psi)}$	$\frac{3\psi(1-2\psi+\psi^2)}{4(1+\psi)(1+2\psi)}$	$\frac{\psi(1-2\psi+\psi^2)}{2(1+\psi)(1+2\psi)}$	$\frac{\psi(1-2\psi+\psi^2)}{4(1+\psi)(1+2\psi)}$
Δ_5	$\frac{4(\psi^2-\psi^3)}{(1+\psi)(1+2*\psi)}$	$\frac{\psi(1+13\psi-14\psi^2)}{4(1+\psi)(1+2\psi)}$	$\frac{\psi(1+5\psi-6\psi^2)}{2(1+\psi)(1+2\psi)}$	$\frac{\psi(1+3\psi-4\psi^2)}{2(1+\psi)(1+2\psi)}$
Δ_6	$\frac{\psi(1-2\psi+\psi^2)}{(1+\psi)(1+2\psi)}$	$\frac{3\psi(1-2\psi+\psi^2)}{4(1+\psi)(1+2\psi)}$	$\frac{\psi(1-2\psi+\psi^2)}{2(1+\psi)(1+2\psi)}$	$\frac{\psi(1-2\psi+\psi^2)}{4(1+\psi)(1+2\psi)}$
Δ_7	$\frac{2(\psi^2-\psi^3)}{(1+\psi)(1+2\psi)}$	$\frac{\psi(7\psi-8\psi^2-1)}{4(1+\psi)(1+2\psi)}$	$\frac{\psi(1+3\psi-4\psi^2)}{2(1+\psi)(1+2\psi)}$	$\frac{1+4\psi+3\psi^2-8\psi^3}{4(1+\psi)(1+2\psi)}$
Δ_8	$\frac{4\psi(1-2\psi+\psi^2)}{(1+\psi)(1+2\psi)}$	$\frac{14\psi^3-27\psi^2+12\psi+1}{4(1+\psi)(1+2\psi)}$	$\frac{2+7\psi-20\psi^2+11\psi^3}{4(1+\psi)(1+2\psi)}$	$\frac{1+2\psi-7\psi^2+4\psi^3}{2(1+\psi)(1+2\psi)}$
Δ_9	$\frac{1-3\psi+3\psi^2-\psi^3}{(1+\psi)(1+2\psi)}$	$\frac{3(1-3\psi+3\psi^2-\psi^3)}{4(1+\psi)(1+2\psi)}$	$\frac{1-3\psi+3\psi^2-\psi^3}{2(1+\psi)(1+2\psi}$	$\frac{1-3\psi+3\psi^2-\psi^3}{4(1+\psi)(1+2\psi}$

Table 2.8: Jacquard's True Parameter Values for Full Siblings.

	ψ			
Parameter	0	0.05	0.10	0.20
Δ_1	0	0.0150	0.0352	0.0905
Δ_2	0	0.0005	0.0017	0.0048
Δ_3	0	0.0247	0.0477	0.0857
Δ_4	0	0.0098	0.0153	0.0190
Δ_5	0	0.0247	0.0477	0.0857
Δ_6	0	0.0098	0.0153	0.0190
Δ_7	0.25	0.2411	0.2693	0.2762
Δ_8	0.50	0.4688	0.4295	0.3429
Δ_9	0.25	0.1856	0.1381	0.0762
θ_{XY}	0.25	0.2875	0.3250	0.40

the only possible relationships. Also suppose the population we are considering has a (rather large) inbreeding coefficient of 0.10. Then for each possible relationship, we can list the true vectors and compute D_U, D_C, D_H, and D_F which appear in Table 2.9. From these results, we estimate the true relationship to be half siblings, as 0.0048 is

Table 2.9: MLE, True $\boldsymbol{\Delta}$ Vectors, and Euclidean Distances for Example in Section 2.3.

$\hat{\boldsymbol{\Delta}}$	$\hat{\boldsymbol{\Delta}}_U$	$\hat{\boldsymbol{\Delta}}_C$	$\hat{\boldsymbol{\Delta}}_H$	$\hat{\boldsymbol{\Delta}}_F$
0.0524	0.0045	0.0080	0.0114	0.0352
0.0000	0.0068	0.0051	0.0034	0.0017
0.0336	0.0273	0.0409	0.0545	0.0477
0.0358	0.0614	0.0460	0.0307	0.0153
0.0517	0.0273	0.0409	0.0545	0.0477
0.0631	0.0614	0.0460	0.0307	0.0153
0.0527	0.0136	0.0307	0.0477	0.2693
0.4605	0.2455	0.3682	0.4909	0.4295
0.2502	0.5523	0.4142	0.2761	0.1381
Distances	0.1427	0.0385	0.0048	0.0637

the minimum distance observed. In fact, these data were simulated assuming half sib relationship. The same methodology applies to the two or seven parameter model, and comparisons among the these classification methods are included in the simulation study described in the next section.

Experimental Design

A simulation study was designed to evaluate the performance of the seven and nine parameter MLE, as well as the various distance metric methods of classification. We wanted to determine the advantage (or disadvantage) of accounting for population substructure in various population types. Thus, we simulated data assuming inbreeding coefficients of 0, 0.05, 0.10. As Milligan notes, the quality of our estimates will depend highly on the number of loci and the number of alleles per locus [33]. We considered

Chapter 2. Pairwise Relatedness and Population Substructure

2, 5, and 10 alleles for 20, 40, 60, 80 and 100 loci to evaluate these effects. When $\psi > 0$, allele frequencies were assumed to come from a Dirichlet distribution, with parameter $(1 - \psi)p_i/\psi$. This particular Dirichlet distribution is appropriate in the population substructure case [2]. Equal allele frequencies were assumed when $\psi = 0$. Finally, we varied the true relationship to include unrelated, cousin, half sibling, and full sibling pairs. For each combination of estimation method, allele number, loci number, inbreeding coefficient and true relationship we simulated 500 observations. In this study, the other pairwise relatedness estimators discussed in Section 2.2 were not included, as previous comparison studies have been done [33, 23, 32].

2.4   Results

Continuous Estimation of θ_{XY}

We refer to the three parameter estimator as the 2D MLE as the maximization takes place in two dimensional space. 6D MLE and 8D MLE refer to the seven and nine parameter estimates, respectively. Several plots representing the mean values 2D MLE are shown in Figure 2.7. Increasing the number of both loci and alleles increases the accuracy of the estimator in the non-inbred case ($\psi = 0.0$). However, this trend does not continue as ψ increases. In fact, in most cases the average estimated values are moving further away from the true value as loci and alleles increase. These results are expected, as this estimator assumes $\psi = 0$. In the non-inbred case the bias increases as the true relationship decreases. This is also expected, as we are approaching the edge of the parameter space. To demonstrate the potential effects of population substructure, consider the plot for cousins when $\psi = 0.05$. In this case, the 95% confidence interval is (0.0963, 0.1043). If we assume no population substructure, the true θ_{XY} value for cousins is 0.0625. It is quite tempting to incorrectly conclude a higher degree of relatedness than truly exits.

Similar plots for the 8D MLE are displayed in Figure 2.8. In every case, increasing

Chapter 2.   Pairwise Relatedness and Population Substructure
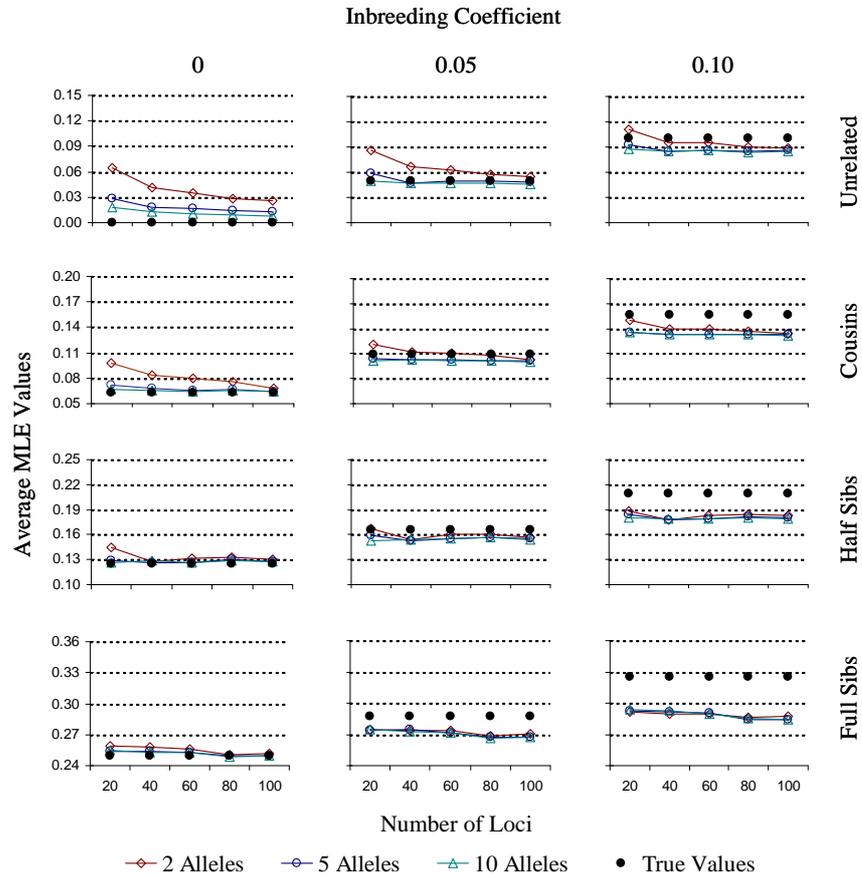
Figure 2.7: Means Plots for 2D MLE, Based on 500 Simulated Data Points per Plot.

the number of loci and the number of alleles improves the accuracy of the MLE. In addition, it appears that the bias is decreasing as ψ is increasing. Except for the unrelated case, the bias of this estimator does not seem influenced by the true relationship. This is quite an advantage over other estimators [33]. Again, consider cousins when $\psi = 0.05$. If we allow for population substructure, the true θ_{XY} value is 0.1094, which falls within the 95% confidence interval, (0.1089, 0.1177).

To examine the differences between all three estimators, Figure 2.9 plots the means for the 2D, 6D, and 8D MLEs for unrelated and full sibling pairs, with ten alleles per

Chapter 2.   Pairwise Relatedness and Population Substructure
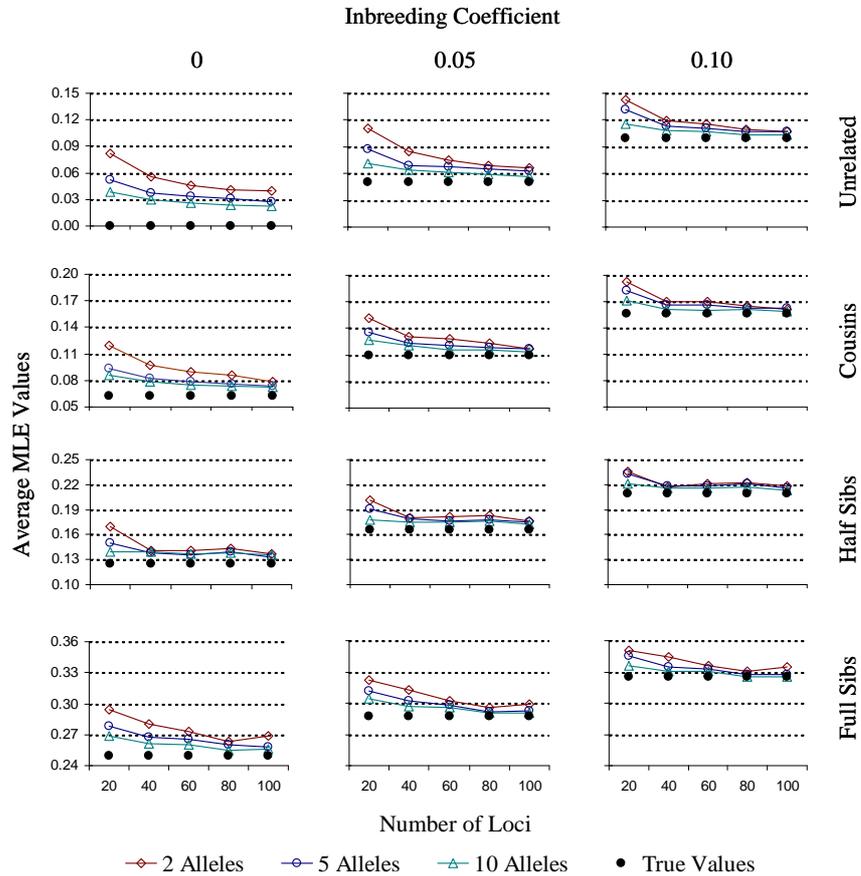
Figure 2.8: Means Plots for 8D MLE, Based on 500 Simulated Data Points per Plot.

locus. There is an increase in accuracy when reducing the number of parameters from nine to seven, markedly so in the non-inbred, unrelated case. Based on the assumptions made during the simulation, the nine parameter model is estimating extra parameters, that are in fact not necessary. We assumed individuals X and Y are simulated from the same subpopulation, and thus their ordering is not significant. Therefore, the increase in accuracy for the seven parameter model is expected. These graphs also show the underestimation that occurs when using the 2D MLE for inbred individuals ($\psi > 0$). Similar results were found for cousin and half sibling pairs, and for loci with two and

57

Chapter 2. Pairwise Relatedness and Population Substructure
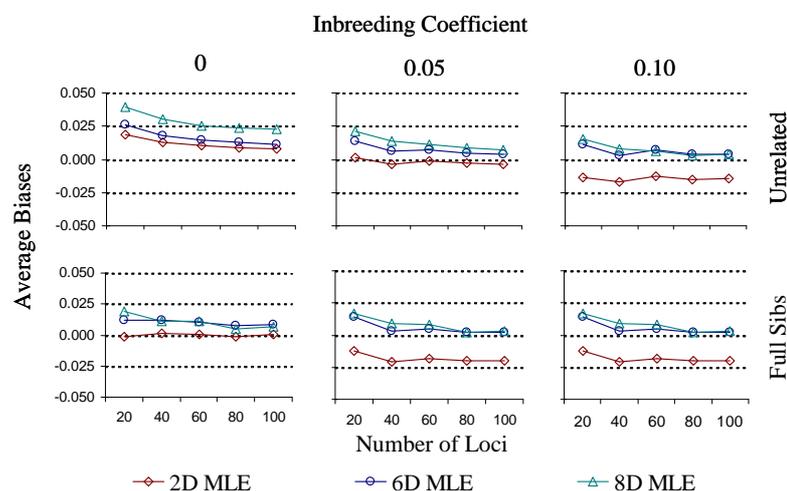
Figure 2.9: Plots of the Bias for 2D, 6D, and 8D MLEs, Based on 500 Simulated Data Points per Plot, Ten Alleles per Locus.

five alleles (results not shown).

The standard deviations for the 2D and 8D MLEs are shown in Figures 2.10 and 2.11. In most cases, the standard deviations for the 8D MLE are a small amount larger than those observed with with the 2D MLE. This is to be expected, as the new MLE requires the estimation of all 8 independent Jacquard's coefficients whereas the 2D MLE only estimates two. In all cases the standard deviations are reduced by increasing the number of both loci and alleles. In particular, there is a larger advantage when moving from two to five alleles, as compared to the effect of moving from five to ten alleles. Varying the true relationship does not appear to have a large effect on the standard deviations of either estimator. In addition, the true value of ψ also has little to no effect on the standard deviations.

When reducing the number of parameters from nine to seven, we hypothesized the amount of variation of the MLE would be reduced. Figure 2.12 plots the standard deviations of the 2D, 6D, and 8D MLE for unrelated and full sibling pairs, with ten alleles per locus. Surprisingly, no significant reduction in variation is observed when

Chapter 2. Pairwise Relatedness and Population Substructure
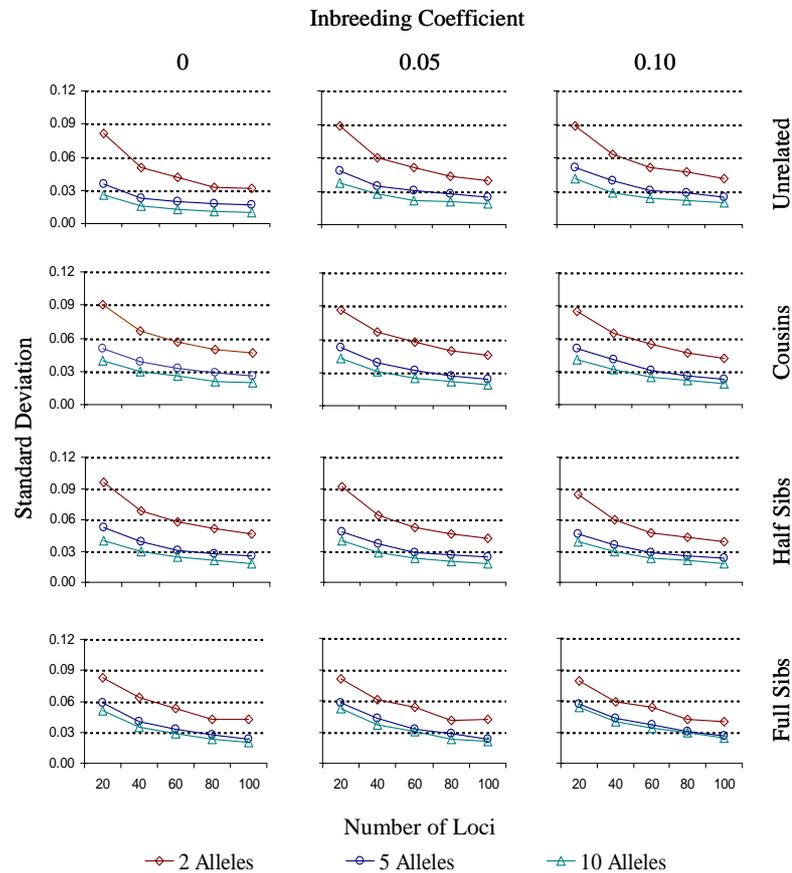
Figure 2.10: Standard Deviations for 2D MLE, Based on 500 Simulated Data Points per Plot.

moving from nine to seven parameters. In each case, the standard errors are smaller for the 2D MLE than the other two estimators. Similar results were again found for cousin and half sibling pairs, and for loci with two and five alleles (results not shown).

Chapter 2. Pairwise Relatedness and Population Substructure
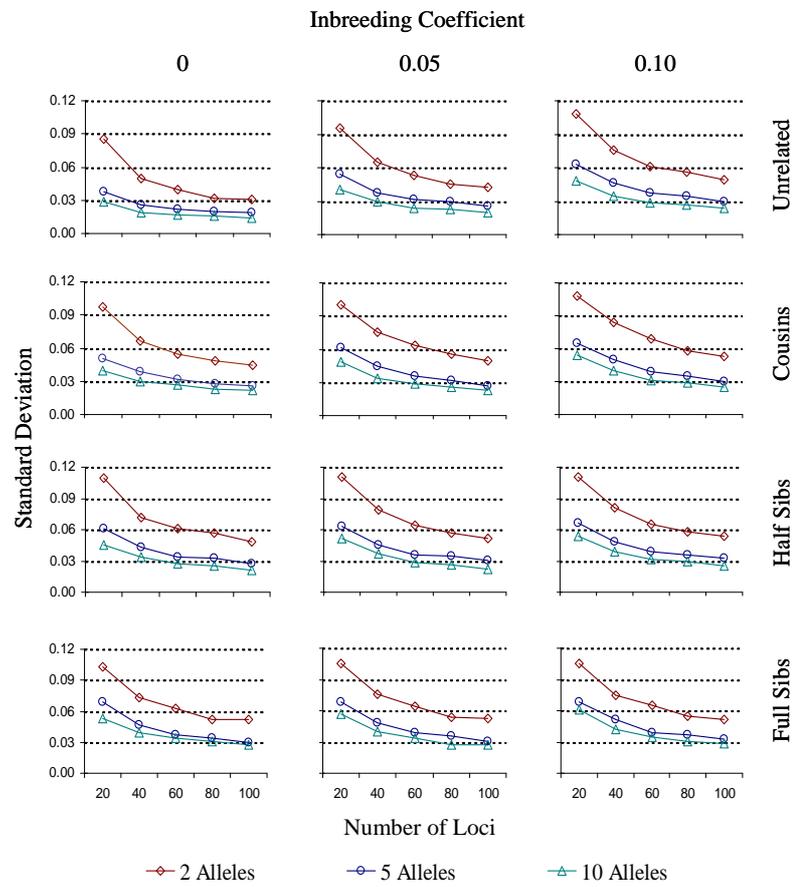
Figure 2.11: Standard Deviations for 8D MLE, Based on 500 Simulated Data Points per Plot.

Chapter 2. Pairwise Relatedness and Population Substructure
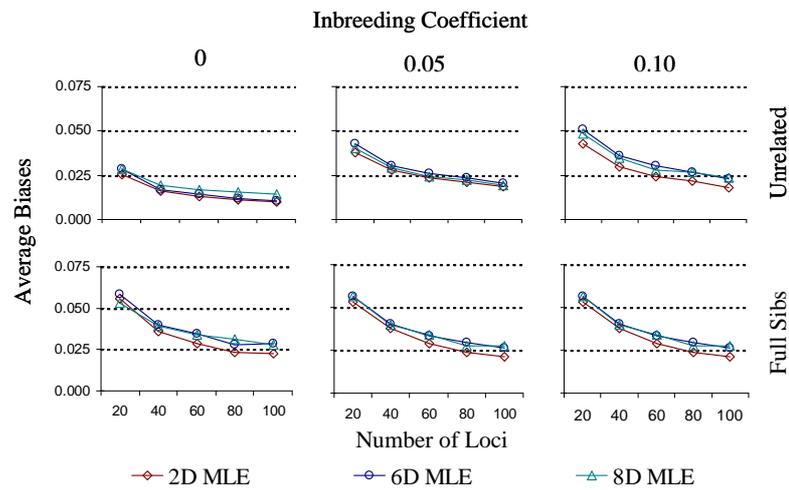
Figure 2.12: Plots of the Standard Deviations for 2D, 6D, and 8D MLEs, Based on 500 Simulated Data Points per Plot, Ten Alleles per Locus.

Chapter 2. Pairwise Relatedness and Population Substructure

Discrete Estimation of Relationships

Both the 2D estimates and the 8D estimates were used to evaluate the performance of the distance metric method of classification. Preliminary studies showed that the results for the 6D estimator were approximately the same as those of the 8D estimator, and is thus was not considered separately in this study. It is important to note that the true values for each case were used assuming the appropriate ψ values. To demonstrate, suppose we generate a pair of individuals taken from a population with $\psi = 0.05$. Also suppose the 8D estimates are (0.018, 0.000, 0.026, 0.000, 0.058, 0.000, 0.144, 0.510, 0.244), and the 2D estimates are (0.175, 0.596, 0.229). To arrive at the full sibling distance, we calculate the Euclidian distance between the 8D estimate and the values given in Table 2.8: (0.015, 0.001, 0.025, 0.010, 0.025, 0.010, 0.241, 0.469, 0.186). In the 2D case, we calculate the Euclidian distance between the estimate the last three of the true values, (0.241, 0.469, 0.186). Another option for the 2D case would be to calculate the distances using the true values when $\psi = 0$ for all cases, regardless of the ψ value used to simulate the data. In this sense we are not comparing estimators that do and do not account for population substructure. We are simply investigating if there is any advantage to using all nine estimates, as opposed to just three.

Table 2.10 gives the accuracy rates for the two methods, under the best possible conditions: 100 loci each having 10 alleles. For both estimators, the accuracy rates were

Table 2.10: Simulated Accuracy Rates for the Distance Metric Classification Methods. For each cell, the rates are based on 500 simulated pairs with 100 loci, ten alleles per loci.

	$\psi = 0.0$		$\psi = 0.05$		$\psi = 0.10$	
	2D	8D	2D	8D	2D	8D
Unrelated	0.976	0.828	0.966	0.876	0.936	0.844
Cousins	0.900	0.850	0.770	0.748	0.644	0.622
Half Sibs	0.958	0.896	0.910	0.850	0.906	0.856
Full Sibs	0.998	0.984	0.994	0.980	0.986	0.984

the highest for unrelated, and full sib pairs. In the majority of cases, the 2D estimate

62

Chapter 2. Pairwise Relatedness and Population Substructure

tends to be more accurate. The performance of both estimators was poorest when the true relationship was cousins. These trends were found in all cases, regardless of the number of loci or the number of alleles (results not shown). The accuracy rates for the 2D estimate, under all of the various sampling scenarios, appear in Figure 2.13. The
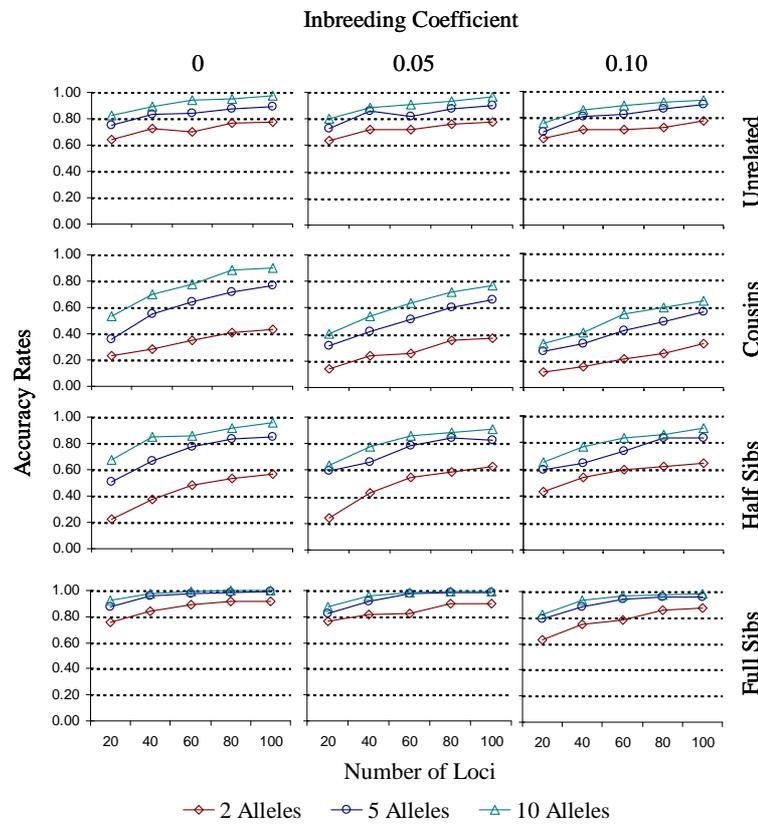
Figure 2.13: Accuracy Rates for 2D Method, Based on 500 Simulated Data Points per Plot.

accuracy rates for unrelated, half sib and full sib pairs are all above 90% when there are high numbers of alleles (≥ 10) and loci (≥ 100). Performance of both estimators using biallelic data from large quantities of loci is studied further in Chapter 3.

In light of the results shown here, we recommend using the 2D version as a cursory estimate of relationships that are distant from each other, such as unrelated and full

63

Chapter 2. Pairwise Relatedness and Population Substructure

sib pairs. This method is quick, easy, and not nearly as computationally demanding as other methods [42, 47]. It also accounts for population substructure, so it is highly recommended for populations with large estimated inbreeding. However, for the purposes of forensic identification, existing techniques are superior. For example, likelihood ratio methodology has already been used and established in US courts. Thus, the methods used in the Kinship software program [48] would provide a better alternative when no population substructure is suspected. However, further research in this area is needed to incorporate population substructure into existing estimates.

2.5   Discussion

In summary, when estimating the continuous parameter θ_{XY}, the nine parameter method described here displays both smaller bias and smaller standard errors than the three parameter maximum likelihood estimate whenever population substructure exists. With the exception of unrelated pairs and when $\psi = 0$, the 95% confidence intervals for the 8D MLE always include the true value. The same cannot be said for the 2D MLE. When no population substructure is suspected, two dimensional methods provide accurate estimates with somewhat smaller standard errors. If one is comfortable making the additional assumption that the pair of individuals under consideration are from the same subpopulation, the 6D MLE provides a more accurate alternative to the 8D MLE. When attempting to describe relatedness with a discrete estimate, the two dimensional version provided here is a simple and accurate method that appropriately accounts for population structure.

Accurately estimating relatedness is an important topic across scientific disciplines. In many circumstances, population substructure exists and can thus have a large impact on the estimates. Most estimators in current use simply ignore this potential, and are therefore not always appropriate. Here we have provided much needed alternative estimates that should prove useful for researchers with genetic data from structured populations.

CHAPTER 3

Applications to Real Data

3.1 Introduction

Various genetic data sets for individuals from various populations are available online. We use three such data sets to explore applications of both Bayesian Networks and pairwise relatedness estimation. Pairwise relatedness is estimated using two, six, and eight dimensional maximum likelihood estimates. We also evaluate a new classification technique, based on the maximum likelihood estimates. This method is designed to predict, or classify, the actual relationship between two individuals. Three data sets are used to estimate relatedness, as they each have different numbers of loci, ranging from 20 to over 500. To demonstrate the multiple allele Bayesian Network from Chapter 1, a fictitious inbred paternity case is considered. Genotypes are available for the mother, putative father, and child at twenty loci with varying numbers of alleles. All of the results presented in this chapter support the notion of accounting for population substructure when analyzing genetic data. The following examples show that underestimation of pairwise relatedness occurs when population substructure is ignored. The final example considered shows that vastly different paternity index values can be obtained when accounting for structured populations.

Chapter 3. Applications to Real Data

3.2   Pairwise Relatedness Estimation

CEPH Family Data

The first data set is maintained by the Fondation Jean Dausset (CEPH) laboratory and is available online[1]. The version of the database used here (V10.0 - November 2004) contains genotypes for 65 families at 32,356 genetic markers or loci. Up to fifty loci from ten chromosomes were selected for the various analyses, with up to seventeen alleles per locus. Appendix D lists the name, location and allele frequency values for each locus.

Ten families were selected (CEPH Family Numbers: 102, 884, 1331, 1332, 1333, 1346, 1347, 1362, 1413, 1424) and a representative pedigree is shown in Figure 3.1. Eight families are residents of Utah with ancestry from northern and western Europe.
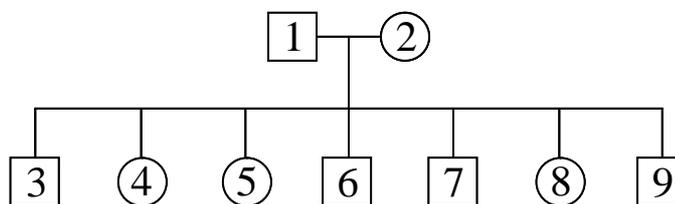
Figure 3.1: Representative CEPH Family Pedigree.
A square indicates the individual is male, circle indicates female. Individuals 1 and 2 are the parents of individuals 3 - 9.

Family 102 is from Venezuela and 884 is an Amish family. These particular families were chosen because they had the most data available for the selected loci. Relatedness was estimated for pairs of individuals with varying true relationships. One unrelated pair (individuals 1 and 2 in Figure 3.1), one random full sibling pair and one random parent child pair were selected from each family.

---

[1]http://www.cephb.fr/cephdb/php/

Chapter 3. Applications to Real Data

Results

Continuous Estimation of Relatedness. The maximum likelihood techniques described in Section 2.3 were used to obtain maximum likelihood estimators (MLEs) of the coancestry coefficient (θ_{XY}). The two, six, and eight dimensional MLE values for the unrelated pairs of individuals are plotted in Figure 3.2. Based on twenty loci, two
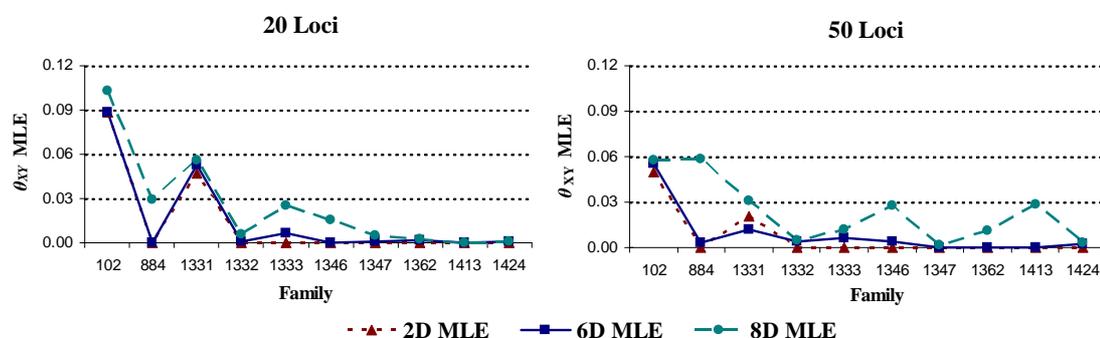
Figure 3.2: 2D, 6D and 8D MLEs for Unrelated CEPH Individuals, based on 20 or 50 loci.

families (102 and 1331) appear to have higher estimated relatedness than would be expected for unrelated individuals. As we increase loci, the estimates decrease, but family 102 still has particularly large estimates. Another anomaly occurs in the 8D MLE when increasing the number of loci. Several families estimates actually increase; 884, 1346, 1362, 1413. Assuming no inbreeding, the biases should be getting smaller (estimates getting closer to zero) as the number of loci increase. More investigation is needed to determine the cause of these inflated estimates.

The variability of the MLEs can be estimated using a bootstrap technique. For each pair of individuals, 1000 bootstrap samples were generated by randomly selecting the corresponding number of loci, without replacement. For each bootstrap sample, the MLE was obtained using the three different methods. The variance of these MLEs approximates the true variance of the estimate. Table 3.1 shows the MLE, estimated variances, and bootstrap confidence intervals for the unrelated pairs from families 102

67

Chapter 3. Applications to Real Data

and 1331. The bootstrap confidence interval endpoints are the fifth and ninety-fifth

Table 3.1: 2D, 6D and 8D MLEs, Bootstrap (BS) Standard Errors and 90% BS CIs.
Husband wife pairs from CEPH families 102 and 1331. 1000 BS replicates were generated in
each case.

Method	Loci	Family 102		Family 1331	
		MLE (BS SE)	BS CI	MLE (BS SE)	BS CI
2P	20	0.0887 (0.0584)	(0.0021, 0.2038)	0.0467 (0.0418)	(0.0000, 0.1359)
	50	0.0494 (0.0418)	(0.0000, 0.1276)	0.0209 (0.0246)	(0.0000, 0.0693)
6P	20	0.0881 (0.0600)	(0.0109, 0.2164)	0.0531 (0.0454)	(0.0007, 0.1426)
	50	0.0550 (0.0380)	(0.0031, 0.1297)	0.0121 (0.0252)	(0.0003, 0.0802)
8P	20	0.1028 (0.0589)	(0.0319, 0.2339)	0.0562 (0.0447)	(0.0113, 0.1549)
	50	0.0573 (0.0352)	(0.0131, 0.1266)	0.0305 (0.0260)	(0.0047, 0.0860)

percentile values of the 1000 bootstrap MLEs obtained in each case. Each estimation
method provides similar results. In all cases, increasing the number of loci tends to
decrease the MLE value by about half. It also reduces the width of the confidence
interval by about half. The standard errors for all three estimators are similar, and
are reduced by increasing the number of loci. It is important to note that the results
for these families are extreme. The average 20 loci CI lengths for the other eight
families were 0.0450, 0.0626, and 0.0894, for the 2D, 6D, and 8D estimation methods,
respectively. In the 50 loci case, these average lengths reduced to 0.0128, 0.0297, and
0.0591.

Plotting the estimated values of P_0 versus P_1 is a more informative way to visualize
the results. Recall, from Section 2.1, the measures P_0, P_1, and P_2. They represent
the probability that two individuals share 0, 1, or 2 alleles identical by descent (IBD),
respectively. These values can be expressed as functions of Jacquard's coefficients,

$$P_0 = \Delta_2 + \Delta_4 + \Delta_6 + \Delta_9,$$
$$P_1 = \Delta_3 + \Delta_5 + \Delta_8,$$
$$P_2 = \Delta_1 + \Delta_7,$$

Chapter 3. Applications to Real Data

and as functions of the seven parameter model ϕ-coefficients,

$$P_0 = \phi_2 + \phi_4 + \phi_7,$$

$$P_1 = \phi_3 + \phi_8,$$

$$P_2 = \phi_1 + \phi_7.$$

The plots for unrelated estimates based on 20 and 50 loci are shown in Figure 3.3. The true, non-inbred values for any particular relationship are also plotted along with the estimates. The plot based on 20 loci clearly indicates the husband-wife pair for family
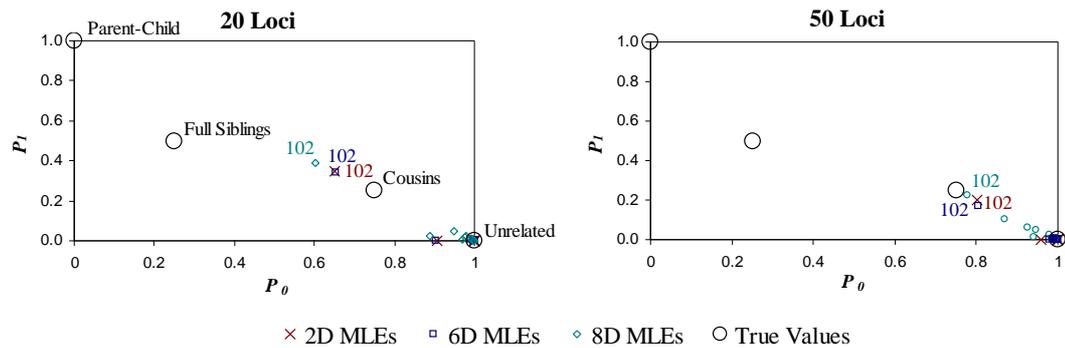
Figure 3.3: P_0 versus P_1 Plots for Unrelated CEPH Individuals.

102 are highly related. In fact, all MLEs fall in between the true values for cousins and full siblings. The plot based on 50 loci indicates a lesser relationship, as the plotted values now fall between unrelated and cousins. Thus, increasing the number of loci has reduced the estimated relatedness for families 102 and 1331. More investigation is needed (increasing the numbers of loci) to determine if the husband and wife pairs for these two families are in fact related.

Plots of full sibling and parent child pair MLE estimates and their associated bootstrap confidence intervals appear in Figure 3.4. In each family, one sibling pair and one parent child pair were randomly selected, and the estimates are based on fifty loci. In most of the full sibling cases, the true value for θ_{XY} falls within the bounds of the

Chapter 3. Applications to Real Data
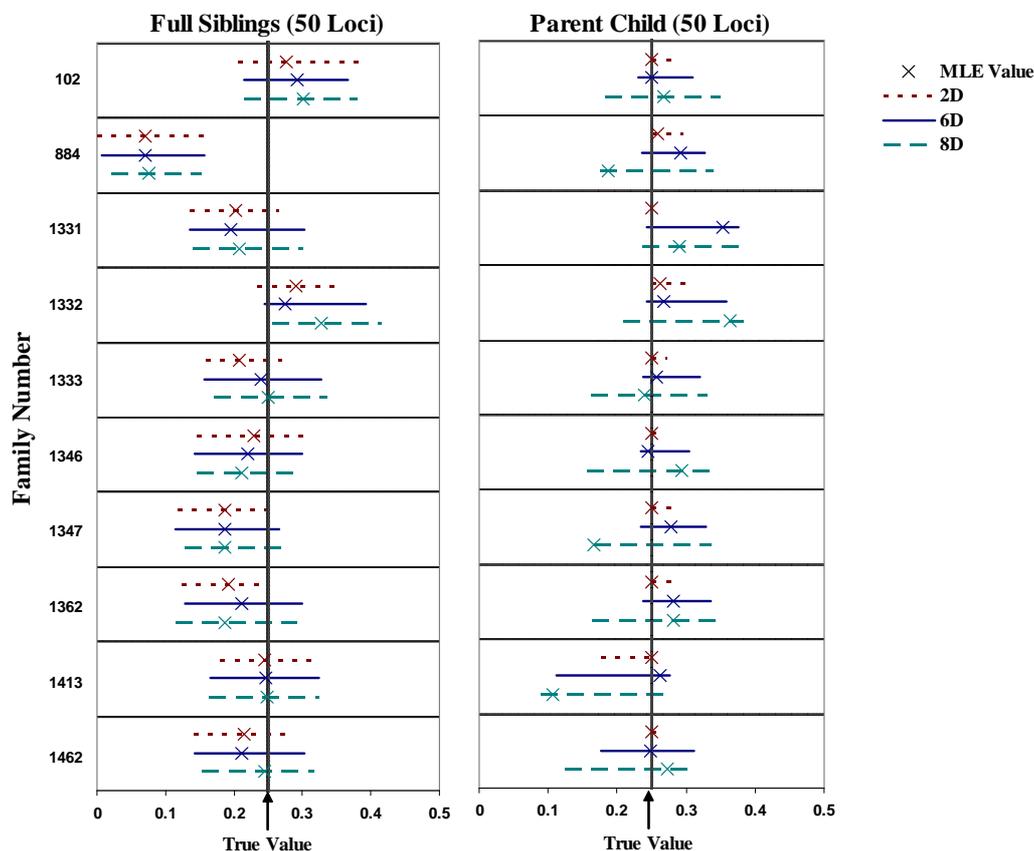
Figure 3.4: 2D, 6D and 8D MLEs for Full Sibling and Parent Child CEPH Pairs Based 50 loci, interval around MLE values based on 1000 bootstrap samples. True value based on the assumption of no inbreeding.

bootstrap CIs. The major exception occurs with the pair from family 884. The 2D, 6D, and 8D estimates in this case were 0.0705, 0.0706, and 0.0749. More investigation is needed here to determine if these individuals are actually siblings. It worth entertaining the idea that perhaps they are half siblings, and the CEPH database entries were incorrect. For most of the full sibling pairs the three estimates were very similar, and tend to underestimate the true relationship. The average biases over families (excluding family 884), were -0.0164, -0.0189, and -0.0095 for the 2D, 6D, and 8D MLEs

Chapter 3. Applications to Real Data

respectively. The average CI lengths were also very similar: 2D = 0.1402, 6D=0.1583, 8D=0.1582.

The plot in Figure 3.4 based on parent child pairs clearly show the advantages of reducing the number of parameters in the model. Both the 2D and 6D methods are performing quite well, whereas the 8D method is showing less reliable results. The 8D estimator is showing large biases, and the MLE values tend to lie closer to the endpoints of the CIs. This effect does is not evident in the 2D and 6D cases These plots also help show the performance of all three estimators is highly dependent on the true relationship. The CIs for the 2D and 6D estimates were much smaller than those observed for full sibs (averages were 0.0331 and 0.1060 respectively). This reduction in CI length was not observed for the 8D estimate, as the average length increased to 0.1747. The true value of θ_{XY} is contained in the CIs for every family.

Based on these results, we conclude the 8D estimator is more biased and exhibits higher standard errors than the 2D counterpart. The increase in variance can be attributed to the large number of estimates required for the 8D estimator. This could also affect the bias, as in the non-inbred case the true values for $\Delta_1, \ldots, \Delta_6$ are zero, regardless of the true relationship. Thus, we have increased the dimensionality when in fact it was unnecessary. When the number of parameters is reduced to six, some improvement was seen when the true relationships were unrelated and parent child. Based on the estimates obtained here, the parents of family 102 are more related than we would expect. In this case, the 8D and 6D methods for full sibs and parent-child will be more accurate. For example, one full sib pair from this family had a 2D MLE of 0.2234, a 6D MLE of 0.2424, and an 8D MLE of 0.2754. If we set the inbreeding coefficient equal to 0.09 (the smaller estimated relatedness between individuals 1 and 2) the true value of θ_{XY} is 0.3175. Thus, the 8D MLE is much closer to the true value than the 2D MLE.

Discrete Estimation of Relatedness. The classification techniques described in Section 2.3 were used to obtain discrete estimates of relatedness. The two, six, and

Chapter 3. Applications to Real Data

eight dimensional accuracy rates for unrelated, full sib, and parent-child pairs are shown in Figure 3.5. The 10 unrelated pairs are simply the husband-wife pairs from
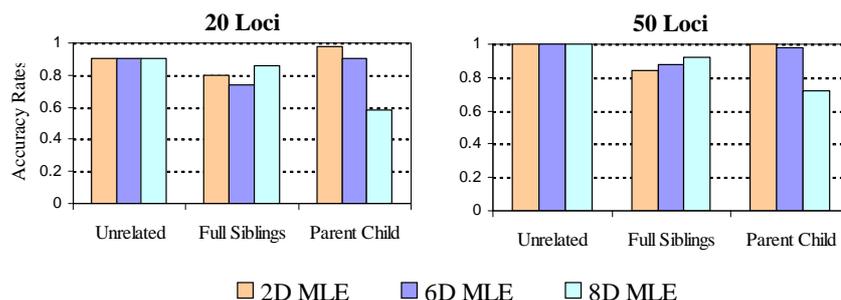
Figure 3.5: CEPH Data Accuracy Rates for 2D, 6D and 8D Discrete Relatedness Estimates. The rates are based on 10 unrelated pairs, 50 full sibling pairs, and 50 parent-child pairs.

each family. The five full sibling and five parent child pairs were randomly chosen from each family, giving rise to 50 observations in those cases. The accuracy rates based on twenty loci are relatively high with the exception of the 8D rate for parent-child pairs. In this case, 29 out of the 50 pairs were misclassified as full sibling pairs, and one pair was misclassified as unrelated. These, for the most part, were evenly spread among the 10 families. The exception was family 102, where 4 of the 5 parent-child pairs were misclassified. Again, this is most likely due to the high relatedness observed between the parents. Overall, it is difficult to conclude from these results which method proved more accurate. A similar statement can be made concerning the results from 50 loci. Accuracy rates do improve in every category, but which one is "best" is still not clear. The 6D and 8D methods work well for full siblings, but the 2D method is superior for parent-child pairs. Overall, the 6D method provides adequate results, even in the non-inbred case.

As a final note, recall that all estimates reported here are based on only 20 or 50 loci. According to the simulation results provided in Chapter 2, these numbers are not sufficient to expect accurate estimators. As such, the results stated here are tentative

Chapter 3. Applications to Real Data

and need further verification using more loci.

FBI Data

Another data set available online is provided by the FBI[2]. Genotypes at several loci are provided for samples obtained from six different human populations; 210 US African Americans (AA), 162 Bahamians (BA), 244 Jamaicans (JA), 209 US Hispanics (HI), 85 Trinadadians (TR) and 203 US Caucasians (CA). All samples were genotyped at the thirteen CODIS[3] loci. In addition, the African American, Caucasian, and Hispanic samples were also typed for the loci HLA-DQA1, LDLR, GYPA, HBGG, D7S8, Gc, and D1S80. The number of alleles per locus vary from 2 to 28. Allele frequencies were estimated from each population separately, using all observations from each sample. Within each sample, 500 randomly selected pairs comprised the unrelated data set. Additionally, 500 random pairs were selected and "mated" to obtain parent-child pairs and full sibling pairs.

Results

Continuous Estimation of Relatedness. If we assume no population substructure exists in these six populations, all three estimators are biased high (Figure 3.6). In most cases, the biases observed for the 8D and 6D MLEs were much larger than those observed for the 2D MLE. The most extreme difference occurred when the true relationship was parent child. Reducing the dimensionality from eight to six did not have an effect on the biases, as few differences exist between the 6D and 8D MLE. Since pairs are "mated" to arrive at full sibling and parent child pairs, the variability can be estimated by computing the standard deviation of the 500 estimates in each case. This is in contrast to the bootstrap technique used for the CEPH data, where we were relying on the data to determine true relationships. The standard deviations

---

[2]http://www.fbi.gov/hq/lab/fsc/backissu/july1999/budowle.htm

[3]See http://www.fbi.gov/hq/lab/codis/ for more information about the FBI's CODIS program.

Chapter 3. Applications to Real Data
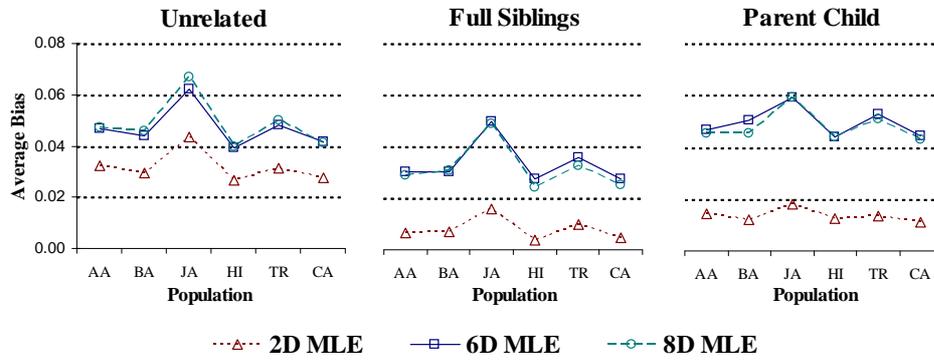
Figure 3.6: Plotted Biases of the 2D, 6D and 8D MLEs, FBI Data.
Each plot based on 500 observations, biases were calculated assuming no population substructure

for each case are shown in Figure 3.7. The standard deviations are very similar across
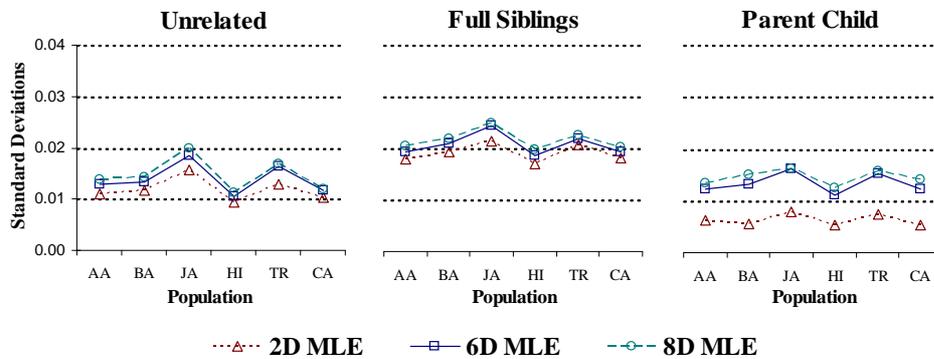
Figure 3.7: Plotted Standard Deviations of the 2D, 6D and 8D MLEs, FBI Data.
Each plot based on 500 observations.

estimators in the unrelated and full sibling cases. The 2D MLE shows much smaller values in the parent child case. The variation between populations appears to be a direct function of the bias. For example, the Jamaican sample showed the highest MLE values and they also display the highest standard deviations.

Chapter 3. Applications to Real Data

If the no population structure assumption is incorrect, then the bias for the 8D and 6D MLEs would be reduced. In [49], Weir and Hill calculated single-population estimates of the inbreeding coefficient for three of the six populations, based on the 13 CODIS loci: African American, $\hat{\psi} = 0.010$; Caucasian, $\hat{\psi} = 0.017$; Hispanic, $\hat{\psi} = 0.032$. The biases were recalculated for the 2D and 8D estimates, using these estimated inbreeding coefficients, and are presented in Table 3.2. The 6D MLE is not included

Table 3.2: Biases and Standard Errors for the 2D and 8D MLEs, FBI Data. Each estimate is based on 500 observations. Biases were calculated assuming inbreeding coefficients of 0.010, 0.017, 0.032 for the AA, CA, and HI samples, respectively. Standard deviations are given in parentheses.

	Unrelated		Full Siblings		Parent-Child	
	2D	8D	2D	8D	2D	8D
AA	0.022(0.040)	0.037(0.050)	-0.001(0.065)	0.021(0.074)	0.007(0.023)	0.038(0.049)
CA	0.010(0.034)	0.022(0.041)	-0.020(0.061)	0.000(0.072)	-0.011(0.019)	0.020(0.045)
HI	-0.004(0.037)	0.010(0.043)	-0.008(0.065)	0.013(0.073)	-0.002(0.019)	0.030(0.051)

in this table, as the estimates are very similar to the 8D case. The biases for both estimators have been reduced by accounting for population substructure. When using the 2D MLE, the biases are mostly negative confirming the simulation results provided in Chapter 2. The standard deviations are highest for full siblings, though not by a significant amount. The 2D standard deviations are approximately 0.01 less than the 8D standard deviations in all cases except for parent-child. Here, the standard deviations for the 8D MLE are at least twice the size of the 2D MLE standard deviations.

To examine the variability and bias of the estimates further, consider the P_0 versus P_1 plots shown in Figure 3.8 for the African American sample. These plots show clearly the additional variation in both the six and eight dimensional MLEs, when compared to the 2D MLE. In the non-inbred case, parent-child pairs must share one allele IBD. Thus, the probability of sharing zero alleles is alway zero in the 2D case. With the 6D and 8D MLE, this is not the case. For example, the probability of zero alleles IBD in

Chapter 3. Applications to Real Data

the 8D case consists of several IBD patterns (S_2, S_4, S_6, S_9 from Chapter 2, Table 2.3), all of which could have probability greater than zero, if population substructure exists. This causes the extra variation seen in the higher dimension P_0 versus P_1 plots, and their MLEs. For this reason, if no inbreeding is suspected we recommend using the 2D MLE.

Figure 3.8 also demonstrates the advantages of techniques estimating more than one parameter. Recall from Figure 3.7 that the 6D and 8D θ_{XY} estimates displayed very similar standard deviations. Thus, if the estimates were only one dimensional (like the moment estimators of Chapter 2) we would conclude both estimates are equally biased and have similar variability. However, different conclusions would be drawn based on the two dimensional P_0-P_1 plots. They show many 8D estimates falling in the full sibling range, whereas the 6D estimates are more confined to the parent child range. Thus we would conclude that the 6D method is in fact superior to the 8D method,
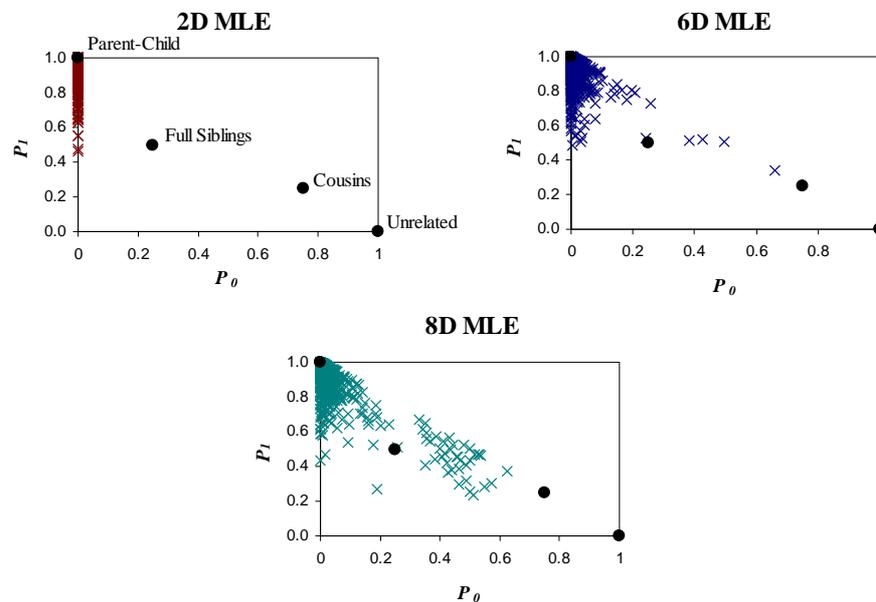
Figure 3.8: P_0 versus P_1 Plots for Simulated Parent-Child Pairs from AA Sample.

76

Chapter 3. Applications to Real Data

with respect to both bias and variability.

Discrete Estimation of Relatedness. Figure 3.9 presents the accuracy rates, averaged over the 6 populations. The results here are very similar to those obtained
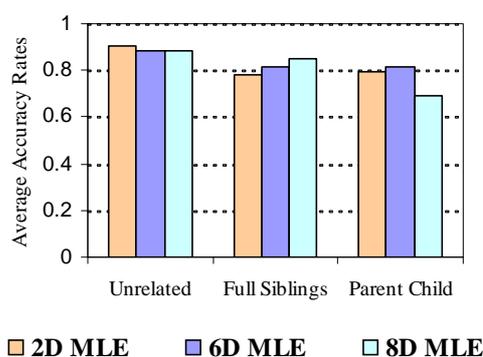
Figure 3.9: Mean Accuracy Rates for FBI Data.
Means were obtained by averaging all accuracy rates obtained for the six samples.

for the CEPH data set, except the 8D accuracy rates are higher. Table 3.3 provides individual accuracy rates for each of the six samples. As in the CEPH example, the

Table 3.3: Individual Accuracy Rates for FBI Data.

Sample	Unrelated			Full Siblings			Parent-Child		
	2D	6D	8D	2D	6D	8D	2D	6D	8D
AA	0.890	0.900	0.896	0.816	0.842	0.878	0.914	0.834	0.704
BA	0.902	0.888	0.886	0.782	0.814	0.864	0.782	0.820	0.668
JA	0.840	0.808	0.806	0.704	0.758	0.788	0.704	0.738	0.626
HI	0.932	0.926	0.922	0.786	0.810	0.846	0.786	0.842	0.712
TR	0.906	0.860	0.864	0.792	0.818	0.848	0.792	0.798	0.708
CA	0.940	0.924	0.940	0.806	0.840	0.882	0.806	0.848	0.720

accuracy rates are relatively high for most cases, considering only twenty loci were

Chapter 3.   Applications to Real Data

used. The estimator with the highest accuracy varies between populations and true relationships. The accuracy rates for all methods are affected by the increased variability evident in the MLEs for the Jamaican sample. The lower rates for the 8D estimate in the parent-child case are most likely due to the additional variation observed in the 8D MLE (see Figure 3.8). Again, it is difficult to conclude from these results which method is more accurate. The next data set provides genetic data on a large number of loci, and should thus provide less ambiguous results.

HapMap Data

The International HapMap Project is a multi-country effort to genotype humans from several populations [50]. The samples are from a total of 209 individuals, including 60 Yoruba people in Ibadan, Nigeria, 44 Japanese in Tokyo, 45 Han Chinese in Beijing, and 60 Americans from the CEPH families previously mentioned. The amount of data the HapMap Consortium has made available is massive. We consider here only observations from loci on chromosome 2. There are a total of 54,649 equally spaced loci typed, each with two alleles. In this study, we use every $100th$ locus, for a total of 547 loci. Allele frequencies were again estimated from each individual sample. Unrelated, parent-child, and full sib pairs were generated using the same methods as for the FBI data set, taking care that repeat pairs did not occur.

Results

Continuous Estimation of Relatedness.   Plots of the biases, assuming no population structure are shown in Figure 3.10. First note the drastic reduction in bias for this data set, as compared to the biases for the FBI data set given in Figure 3.6. For example, for unrelated pairs, the 2D MLE biases ranged between 0.02 and 0.05. With the increase in loci, the range is now reduced to (0.006, 0.008). Similar results are seen with the 6D and 8D MLEs. It is encouraging to see these results, considering there are only 2 alleles per locus. In most cases the 6D and 8D MLEs are still displaying higher

Chapter 3.   Applications to Real Data
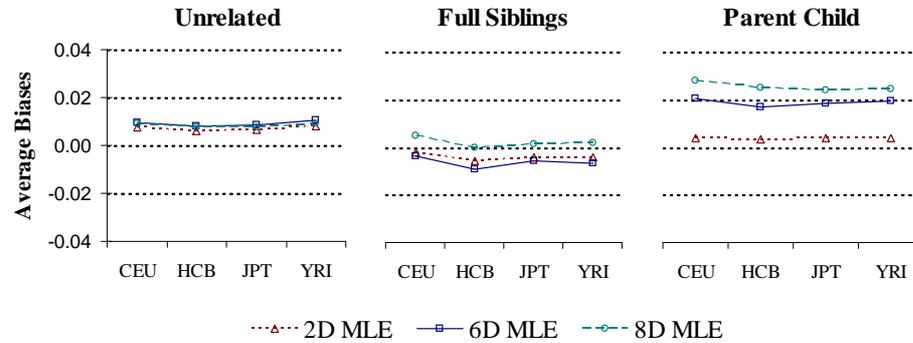
Figure 3.10: Plotted Biases of the 2D and 8D MLEs, HapMap Data. Each plot based on 500 observations, biases were calculated assuming no population substructure.

biases than the 2D estimate, as population substructure is not suspected in these populations. In the full sibling case however, the 6D MLE is actually underestimating θ_{XY}. These biases are small, and range from -0.009 to -0.003.

Increasing the number of loci also had an impact on the amount of variation seen in the estimates. Table 3.4 gives the standard deviation values for two samples, the FBI African American sample and the HapMap CEU sample. These results confirm

Table 3.4: Standard Errors of the 2D, 6D and 8D MLE for Selected Samples.

	Unrelated			Full Siblings			Parent-Child		
Sample	2D	6D	8D	2D	6D	8D	2D	6D	8D
FBI(AA)	0.040	0.046	0.294	0.065	0.069	0.074	0.023	0.044	0.049
HAP (CEU)	0.012	0.011	0.011	0.020	0.030	0.023	0.006	0.019	0.023

that increasing the number of loci, even if they are biallelic, increases all estimators' accuracy and precision. Next, we consider the impact of increasing loci on the discrete estimation of relationships.

Chapter 3. Applications to Real Data

Discrete Estimation of Relatedness.   When estimating discrete relatedness every relationship was estimated with at least 90% accuracy using all three methods. The accuracy rates averaged over populations appear in Figure 3.11. The lowest values
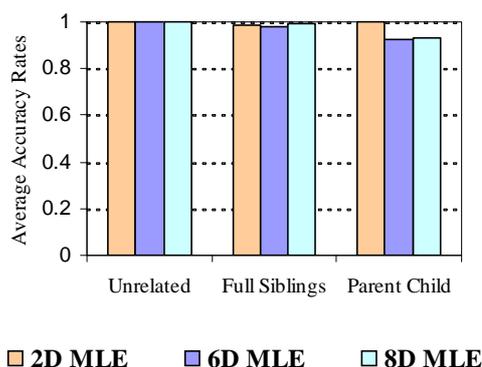
Figure 3.11: Mean Accuracy Rates for Hapmap Data.
Means were obtained by averaging all accuracy rates obtained for the four samples.

obtained were 0.908 (8D, Parent Child, HI data) and 0.92 (6D, Parent Child, AA and BA data). All cases showed drastic improvement from the accuracy using the FBI data set. Consider the two P_0 versus P_1 plots for the CEU sample shown in Figure 3.12. In the first plot, there are distinct clusters for each of the groups. In addition, within each cluster, the observations are all closest to the appropriate true relationship value. This is not the case in the second two plots. Similar to the results shown in Figure 3.8, we see quite a bit of scatter when the true relationship is parent child. Several 8D observations are still closer to the true value for full siblings than parent-child.

The results we have shown here have assumed that there were only three possible relationship categories: unrelated, full sibling, and parent-child. However, there are realistic circumstances where the number of categories will be more than three. As such, we obtained accuracy rates for the case when there are five possible relationship types: unrelated, cousins, half siblings, full siblings, and parent-child. These results are summarized in Table 3.5. Increasing the number of alternatives did not impact

Chapter 3. Applications to Real Data
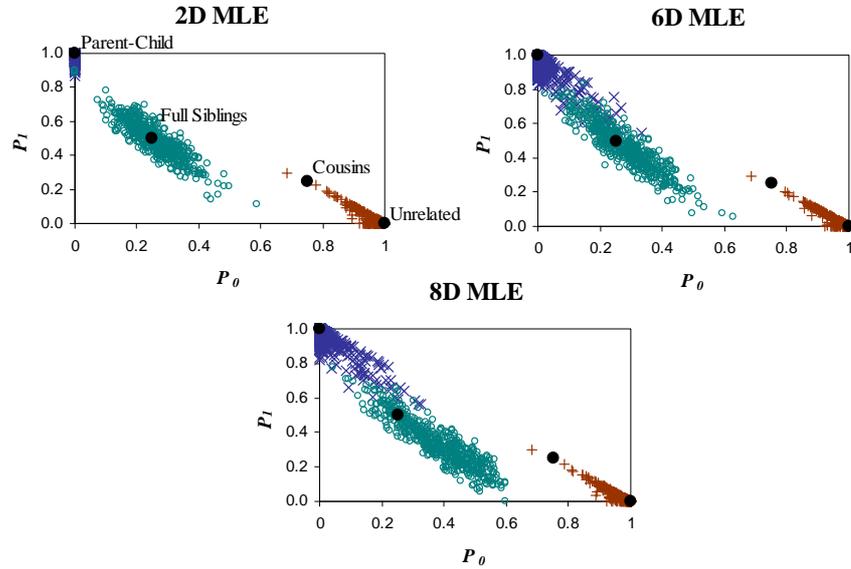
Figure 3.12: P_0 versus P_1 Plots for Simulated Pairs from CEU Sample.

Table 3.5: Individual Accuracy Rates for HapMap Data.
These results were obtained by considering five different relationship types, instead of three.

	Unrelated			Full Siblings			Parent-Child		
Sample	2D	6D	8D	2D	6D	8D	2D	6D	8D
CEU	0.976	0.968	0.966	0.972	0.958	0.752	1.000	0.920	0.930
HCB	0.974	0.972	0.970	0.982	0.954	0.728	1.000	0.920	0.944
JPT	0.982	0.970	0.972	0.964	0.972	0.802	1.000	0.938	0.946
YRI	0.966	0.954	0.948	0.980	0.956	0.760	1.000	0.930	0.908

the accuracy of the 2D estimator significantly. The 2D classification method is now at least 96% accurate, whereas in the three alternative case it was at least 98% accurate. However, there was a large impact on the 8D estimator for full sibling case. This is due to the additional scatter that is seen in the 8D P_0 versus P_1 plots in Figure 3.12.

Chapter 3. Applications to Real Data

Reductions in accuracy also occurred with the 6D method for full siblings, although not as extreme. Both full sibs and unrelated pairs were most commonly misclassified as cousins (detailed results for the 8D full sibling case are given in Figure 3.13). A reduction in the accuracy in the parent-child case was not seen, as no other competing relationship was added that is closer than full siblings to the parent child space.
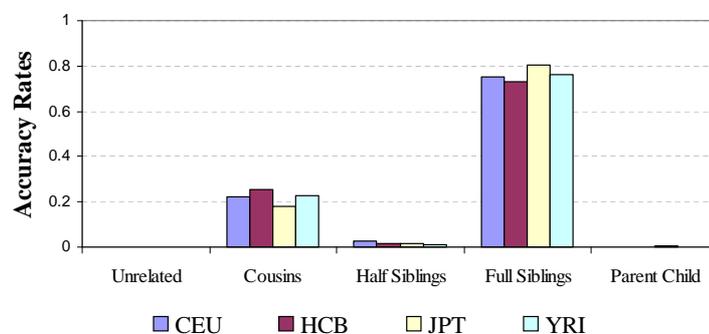
Figure 3.13: Classification Rates for the 8D Method when True Relationship is Full Sibling.

To conclude, the 2D method of classification is very accurate when large numbers of loci are given. They provides results that are over 97% accurate in every case considered here. Future studies are needed before the 6D and 8D estimators can be recommended for forensic uses. First, one should investigate whether or not the accuracy for parent-child improves with larger number of alleles per locus. In addition, studies such as those performed here should be conducted with real data that is known to have a large inbreeding coefficient. Studies such as these would help determine if the best discrete estimator to use depends upon population substructure, which it most likely will. Finally, simulation studies should be done comparing the discrete estimators discussed here with other existing methods of relationship classification.

Chapter 3. Applications to Real Data

3.3   Multiple Allele Paternity Network Example

The Bayesian Network (BN) examples considered in Chapter 1 used data from only
one locus. We present here a more realistic example. Consider family 102 from the
CEPH data set. From the analyses performed in the previous section, we have reason
to believe this family has an inbreeding coefficient (ψ) greater than zero. Thus, this
family would be an interesting case to consider for the BN described in Example Two
from Chapter 1 (Figure 1.11). The genotypes for the mother and child (individual 3)
are available at 19 loci (the mother's genotype is missing for locus GATA41A01). We
can then suppose the "putative" father is individual 1 (the actual father) and use the
BN to calculate paternity indices (PIs) for each locus.

For this example, we set the inbreeding coefficient to be 0.0917, the 2D MLE for the
coancestry coefficient between the mother and putative father. The PI for each locus
was also calculated using a non-population substructure network, which assumes $\psi = 0$.
The genotypes and PIs for each locus are provided in Table 3.6. Assuming these loci are
independent, the overall paternity index is obtained by multiplying all of the individual
PI values. When $\psi = 0.0917$, the overall PI is 22405 and when $\psi = 0$ the PI is 551,758.
Both PIs are large and either case would lead us to conclude that the putative father
is the father of the child in question. However, when population structure is ignored
the overall PI is about 25 times larger. In certain circumstances, this overestimation
could lead to an incorrect statement about paternity. This example helps demonstrate
the high dependence of the PI upon the population substructure assumptions. Thus,
if there is evidence to conclude that there is a moderate amount of substructure, the
BN of Figure 1.11 should be employed.

Approximately one hour was needed to enter in the allele frequencies, genotypes,
and to obtain the output from HUGIN using the population substructure network.
This is in contrast to the twenty minutes needed for the non-population substructure
network. In practice, both of these times are inadequate. These calculations can be
done using existing software in a matter of seconds. Before Bayesian Networks can be

Chapter 3. Applications to Real Data

Table 3.6: CEPH Family 102 Genotypes and PI Values.

The genotypes are given by pairs of allele numbers, where the numbers correspond with Appendix D. Paternity index (PI) values were obtained using the Bayesian Nework in Figure 1.11.

Locus	Chr.	Genotypes			PI	
		P. Father	Mother	Child	$\psi = 0$	$\psi = 0.0917$
ATA1G10	8	32	32	32	1.13	1.09
CEB42	8	12	34	23	2.00	2.00
FB12B7	8	56	22	25	1.91	1.93
GATA23C09	8	31	22	32	1.57	1.68
MFD159A	8	17	37	13	6.16	3.85
GATA27G11	12	31	11	31	1.40	1.53
LMS43	12	12	13	13	1.33	1.03
MFD84	12	13	15	15	1.55	1.12
PTHIZ53	12	22	22	22	1.21	1.14
ACT1A01	18	42	55	52	3.26	2.76
AFM123YA1	18	12	23	23	1.02	0.88
ATA1H06	18	52	56	62	17.66	5.43
GATA28D12	18	32	32	32	2.21	1.64
GATA30C02	18	43	44	43	0.95	1.12
MFD302	18	13	13	33	3.44	2.02
CYP2DP8	22	12	13	12	1.70	1.78
GCT10C10	22	11	14	14	1.49	1.31
IL2RB	22	12	11	12	1.30	1.45
PH41A	22	24	22	24	2.69	2.45

widely accepted and used by forensic scientists, this time constraint must be addressed. One simple solution would be to automate the data entry. If HUGIN could read in genotypes and allele frequencies from a data file and then perform the appropriate calculations, the time needed would be greatly reduced. Additional time would be saved if HUGIN could output the results into another data file. This is one area that needs more research, in collaboration with BN software providers.

Chapter 3. Applications to Real Data

3.4   Discussion

When estimating pairwise relatedness, we have shown that accounting for substructure is possible. In fact, the methodology does not differ substantially from methods already in use. We provided a very simple extension from a two dimensional maximization problem to a six or eight dimensional problem. The first two data sets considered here have helped to demonstrate the need for a large number of loci for both methods. The HapMap Consortium projects 6.8 million single nucleotide polymorphisms or SNPs, each with a unique genomic position, will be genotyped for a total of 270 individuals included in their study [50]. The vast majority of these SNPs are biallelic. Recent technology advances allow genotyping of large samples of individuals at thousands of SNP loci [51]. The results presented here using a subset of the HapMap data showed that SNP data is sufficient to accurately estimate pairwise relatedness, especially when we can assume no population substructure exists (2D MLE).

Bayesian Networks are commonly used to calculate various probabilities from forensic genetic data. We have shown that accounting for substructure is possible. In addition, the resultant networks are not significantly more complex than those that already exist. The real data example provided in this chapter demonstrates the vastly different results that can be obtained. This example also shows that more research on Bayesian Networks is needed, primarily to explore reducing data entry time.

Literature Cited

[1] J. Wang. An estimator for pairwise relatedness using molecular markers. *Genetics*, 160:1203–1215, 2002.

[2] I.W. Evett and B.S. Weir. *Interpreting DNA Evidence*. Sinauer, Sunderland, MA., 1998.

[3] A.P. Dawid, J. Mortera, V.L. Pascali, and D. Van Boxel. Probabilistic expert systems for forensic inference from genetic markers. *Scandinavian Journal of Statistics*, 29:577–595, 2002.

[4] J.M. Curran, C.M. Triggs, J. Buckleton, and B.S. Weir. Interpreting DNA mixtures in structured populations. *Journal of Forensic Sciences*, 44(5):987–995, 1999.

[5] D.J. Balding and R.A. Nichols. A method for quantifying differentiation between populations at multi-allelic loci and its implications for investigating identity and paternity. *Genetica*, 96:3–12, 1995.

[6] D.J. Balding and R.A. Nichols. DNA profile match probability calculation - How to allow for population stratification, relatedness, database selection and single bands. *Forensic Science International*, 64(2–3):125–140, 1994.

[7] N. Fenton and M. Neil. The jury observation fallacy and the use of Bayesian Networks to present probabilistic legal arguments. *Mathematics Today*, 36(6):180–187, 2000.

[8] R.G. Cowell. FINEX: A probabilistic expert system for forensic identification. *Forensic Science International*, 134:196–206, 2003.

[9] R.G. Cowell, A.P. Dawid, S.L. Lauritzen, and D.J. Speidelhalter. *Probabilistic Networks and Expert Systems*. Springer-Verlag, Berlin-Heidelberg-New York, 1999.

[10] B.S. Weir. Quantifying the genetic structure of populations with application to paternity calculations. In M.E. Halloran and S. Geisser, editors, *Statistics in Genetics Volume 112 of IMA Volumes in Mathematics and its Applications*, pages 31–44. Springer-Verlag, New York, 1998.

Literature Cited

[11] B.S. Weir. Effects of inbreeding on forensic calculations. *Annual Review of Genetics*, 28:597–621, 1994.

[12] J.M. Curran, J.S. Buckleton, and C.M. Triggs. What is the magnitude of the subpopulation effect? *Forensic Science International*, 135(1):1–8, 2003.

[13] P. Garbolino and F. Taroni. Evaluation of scientific evidence using Bayesian Networks. *Forensic Science International*, 125(2–3):149–155, 2002.

[14] National Research Council. *The Evaluation of Forensic DNA Evidence*. National Academy Press, Washington, DC, 1996.

[15] T.S. Levitt and K.B. Laskey. Computational inference for evidential reasoning in support of judicial proof. *Cardozo Law Review*, 22:1691–1731, 2001.

[16] I.W. Evett, P.D. Gill, G. Jackson, J. Whitaker, and C. Champod. Interpreting small quantities of DNA: the hierarchy of propositions and the use of Bayesian Networks. *Journal of Forensic Sciences*, 47(3):520–530, 2002.

[17] P.E.M. Huygen. Use of Bayesian Belief Networks in legal reasoning. In *17th BILETA Annual Conference*, 2002.

[18] A.P. Dawid. An object-oriented Bayesian Network for estimating mutation rates. In *Ninth International Workshop on Artificial Intelligence and Statistics*, 2003.

[19] C. Aitken, F. Taroni, and P. Garbolino. A graphical model for the evaluation of cross-transfer evidence in DNA profiles. *Theoretical Population Biology*, 63:179–190, 2003.

[20] J. Mortera, A.P. Dawid, and S.L. Lauritzen. Probabilistic expert systems for DNA mixture profiling. *Theoretical Population Biology*, 63:191–205, 2003.

[21] J. Mortera. Analysis of DNA mixtures using Bayesian Networks. In P.J. Green, N.L. Hjort, and S. Richardson, editors, *Highly Structured Stochastic System*, pages 39–44. Oxford University Press, 2003.

[22] J.W. Morris, R.A. Garber, J. d'Autremont, and C.H. Brenner. The avuncular index and the incest index. *Advances in Forensic Haemogenetics 1*, pages 607–611, 1988.

[23] M. Lynch and K. Ritland. Estimation of pairwise relatedness with molecular markers. *Genetics*, 152:1753–1766, 1999.

Literature Cited

[24] B. Olaisen, M. Stenersen, and B. Mevag. Identification by DNA analysis of the victims of the August 1996 Spitsbergen civil aircraft disaster. *Nature Genetics*, 15(4):402–405, 1997.

[25] B. Leclair, C.J. Fregeau, K.L. Bowen, and R.M. Fourney. Enhanced kinship analysis and STR-based DNA typing for human identification in mass fatality incidents: The Swissair Flight 111 disaster. *Journal of Forensic Sciences*, 49(5):939–953, 2004.

[26] C.H. Brenner and B.S. Weir. Issues and strategies in the DNA identification of World Trade Center victims. *Theoretical Population Biology*, 63(3):176–178, 2003.

[27] C.H. Brenner. Some mathematical problems in the DNA identification of Tsunami victims. Unpubished, June 2005.

[28] C.M. Hsu, N.E. Huang, L.C. Tsai, L.G. Kao, C.H. Chao, A. Linacre, and J.C.-I. Lee. Identification of victims of the 1998 Taoyuan Airbus crash accident using DNA analysis. *International Journal of Legal Medicine*, 113(1):43–46, 1999.

[29] C.W. Cotterman. *A Calculus for Statistico-Genetics*. PhD thesis, Ohio State University, 1940.

[30] D.C. Queller and K.F. Goodnight. Estimating relatedness using molecular markers. *Evolution*, 43:258–275, 1989.

[31] M.S. Blouin. DNA-based methods for pedigree reconstruction and kinship analysis in natural populations. *Trends in Ecology and Evolution*, 18(10):503–511, 2003.

[32] T. Van De Casteele, P. Galbusera, and E. Matthysen. A comparison of microsatellite-based pairwise relatedness estimators. *Molecular Ecology*, 10(6):1539–1549, 2001.

[33] B.G. Milligan. Maximum likelihood estimation of relatedness. *Genetics*, 163:1153–1167, 2003.

[34] A. Grafen. A geometric view of relatedness. *Oxford Surveys in Evolutionary Biology*, 2:39–89, 1985.

[35] M. Lynch. Estimation of relatedness by DNA fingerprinting. *Molecular and Biological Evolution*, 5:584–599, 1988.

[36] C.C. Li, D.E. Weeks, and A. Chakravarti. Similarity of DNA fingerprints due to chance and relatedness. *Human Heredity*, 43:45–52, 1993.

Literature Cited

[37] K. Ritland. Estimators for pairwise relatedness and individual inbreeding coefficients. *Genetical Research*, 67:175–185, 1996.

[38] O.J. Hardy. Estimation of pairwise relatedness between individuals and characterization of isolation-by-distance processes using dominant genetic markers. *Molecular Ecology*, 12:1577–1588, 2003.

[39] K. Belkhir, V. Castric, and F. Bonhomme. IDENTIX, a software to test for relatedness in a population using permutation methods. *Molecular Ecology*, 2:611–614, 2002.

[40] E.A. Thompson. The estimation of pairwise relationships. *Annals of Human Genetics*, 39:173–188, 1975.

[41] E.A. Thompson and T.R. Meagher. Genetic linkage in the estimation of pairwise relationship. *Theoretical and Applied Genetics*, 97:857–864, 1998.

[42] M. McPeek and L. Sun. Statistical tests for detection of misspecified relationships by use of genome-screen data. *American Journal of Human Genetics*, 66:1076–1094, 2000.

[43] E.A. Thompson. Estimation of relationships from genetic data. In C.R. Rao and R. Chakraborty, editors, *Handbook of Statistics, Vol. 8*, pages 225–269. Elsevier Science Publishers, 1991.

[44] A. Jacquard. Genetic information given by a relative. *Biometrics*, 28:1101–1114, 1972.

[45] W.H. Press, S.A. Teukolsky, W.T. Vetterling, and B.P. Flannery. *Numerical Recipes in C: The Art of Scientific Computing*. Cambridge University Press, Cambridge, UK., 1992.

[46] J.A. Nelder and R. Mead. A simplex method for function minimization. *Computer Journal*, 7(4):308–313, 1965.

[47] C.H. Brenner. Kinship analysis by DNA when there are many possibilities. In *Progress in Forensic Genetics 8*, 1999.

[48] C.H. Brenner. Symbolic kinship program. *Genetics*, 145:535–542, 1997.

[49] B.S. Weir and W.G. Hill. Estimating F-statistics. *Annual Review of Genetics*, 36:721–750, 2002.

Literature Cited

[50] The International HapMap Consortium. The International HapMap Project. *Nature*, 426:789–796, 2003.

[51] J.C. Glaubitz, E. Rhodes Jr., and J.A. DeWoody. Prospects for inferring pairwise relationships with SNPs. *Molecular Ecology*, 12:1039–1047, 2003.

APPENDIX A

A Simple Bayesian Network

This example will provide a basic introduction to Bayesian Networks. It is not intended to provide a realistic example in which a Bayesian Network can be used, but simply intended to give an illustrative example. Several unrealistic assumptions are made purely for the sake of simplicity.

To begin, every BN will have a graphical portion which contains nodes and directed lines. Each node in the graph represents a variable (or an event), and each directed line describes the associations that may exist between the variables in the graph. To demonstrate, a very simple example will be presented that has been adapted from Aitken et al. [19]. Suppose a crime was committed. The police have a suspect, and have recovered a blood stain from the crime scene. The proposition that the suspect is the source of the stain (for simplicity we will say this represents guilt), versus the proposition that the suspect is not the source of the stain (is not guilty) will be examined, using the evidence provided by the crime stain. To this end, we will calculate the following likelihood ratio:

$$LR = \frac{\Pr(\text{Evidence}|\text{Guilty})}{\Pr(\text{Evidence}|\text{NotGuilty})}. \tag{A.1}$$

Three nodes (or variables) will be needed in the BN:

Guilty (G) = Proposition that the suspect is guilty

True Match (M) = Evidence of a true match

91

Appendix A. A Simple Bayesian Network

Reported Match (RM) = Evidence of a reported match

It is important to mention if we have a "true match" this means that the evidentiary DNA matches exactly to the suspect's DNA. We are assuming this implies the culprit and the suspect are one and the same. In practice, this is not a valid assumption. The culprit and the suspect could match on a particular set of loci, and it still may not be reasonable to conclude that they are one in the same.

Each of the variables listed above has two different possible states, either yes or no. This is an over simplified case, and it is important to note that the variables within a BN can take on binary (as in this example), categorical, or continuous values. This allows the flexibility to consider various types of evidence within the same BN. Figure A.1 is the graphical representation of this hypothetical case.
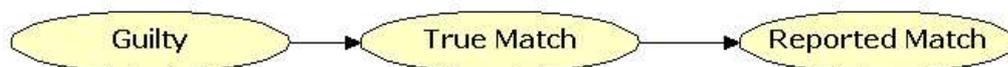
Figure A.1: A Simple Bayesian Network.

The directed lines in this network indicate the relationships between the three variables. The arrow from **Guilty** to **True Match** indicates that the variable **True Match** is dependent upon the variable **Guilty**. In other words, if **Guilty** takes on the value of false, the **True Match** variable must also take on the value false. The arrow from **True Match** to **Reported Match** indicates the same type of relationship. When there is a true match, the probability of a **Reported Match** will necessarily increase, as long as the match reporting mechanism is working correctly. It is important to note the absence of a relationship between **Guilty** and **Reported Match**. The

Appendix A. A Simple Bayesian Network

probability of a reported match should not depend upon the state of **Guilty** directly, only indirectly through the variable **True Match**.

Along with this graphical representation, the BN will also have a numerical representation through various conditional and unconditional probability tables. A probability table will be associated with every node in a graph. If a node is a *parent node*, meaning it does not have any arrows pointing to it, then the probabilities will be unconditional. This means that the probability of each state of this variable does not depend on the states of any other variables. There is one such node in this example; **Guilty**. For this network, the assumption is that the suspect has a 50% chance of being guilty, and a 50% chance of being innocent. This implies that the prior odds (Probability Guilty / Probability Not Guilty) of being guilty are 1; a frequentist assumption. If one were to appeal to Bayesian reasoning, the prior odds could be specified otherwise, based upon prior information about the suspect. See [2] for a detailed discussion of the specification of prior odds for likelihood ratio calculations. The assumption we have made will lead to the unconditional probability table shown in Table A.1.

Table A.1: Unconditional Probability Table for **Guilty** Node.

	$\Pr(G)$
Yes	0.50
No	0.50

The other two nodes are considered *child nodes*, as they have arrows pointing to them. Each will have a conditional probability table associated with it, as they are both dependent on other nodes in the graph. The **True Match** node probabilities will depend on the current state of **Guilty**. For example, if **Guilty** takes on the value

93

Appendix A. A Simple Bayesian Network

false, then the probability of having a true match must be 0. Table A.2 presents the entire probability table. Note that $\overline{G}$ indicates Not **Guilty**.

Table A.2: Conditional Probability Table for **True Match** Node.

	$\Pr(M|G)$	$\Pr(M|\overline{G})$
Yes	1	0
No	0	1

The final node to be considered is **Reported Match**. The probabilities of this node will depend on the value of **True Match**. For example, if **True Match** takes on the value No, then the probability of **Reported Match** is determined by the chance that the reporting tool will present a false positive. In this example, arbitrary assumptions are made that the chance of reporting a false positive is 2% and the chance of reporting a false negative is 1%. This is required to differentiate between **True Match** and **Reported Match**. In practice, these numbers are significantly lower if not zero. The need to incorporate them into this network is a result of the previous assumption that a true match implies the culprit and the suspect are one in the same. Note that we are not implying that these are reasonable values, they are simply chosen for illustrative purposes. These assumptions concerning the match reporting mechanism lead to the conditional probabilities presented in Table A.3. One can enter the probabilities into

Table A.3: Conditional Probability Table for **Reported Match** Node.

	$\Pr(RM|M)$	$\Pr(RM|\overline{M})$
Yes	0.99	0.02
No	0.01	0.98

Appendix A. A Simple Bayesian Network

HUGIN, and the resultant tables are shown in Figure A.2.

Figure A.2: Probability Tables from HUGIN.

The current example requires a calculation of the likelihood ratio shown in Equation A.1. The evidence mentioned in this equation is replaced with the variable Reported Match. When coupled with the notation $\overline{G} = $ Not Guilty, the following equation represents the likelihood ratio:

$$LR = \frac{\Pr(RM|G)}{\Pr(RM|\overline{G})} \tag{A.2}$$

To calculate this value, we will make use of the law of total probability, adapted from [2]:

Law of Total Probability

If A_1 and A_2 are mutually exclusive and exhaustive events, then for any other event

H,
$$\Pr(H|E) = \Pr(H|A_1, E)\Pr(A_1|E) + \Pr(H|A_2, E)\Pr(A_2|E).$$

Now $\Pr(RM|G)$ can be calculated:

$$\Pr(RM|G) = \Pr(RM|M, G)\Pr(M|G) + \Pr(RM|\overline{M}, G)\Pr(\overline{M}|G)$$

Appendix A. A Simple Bayesian Network

by the law of total probability, as M and $\overline{M}$ are mutually exclusive and exhaustive events. Keeping in mind that the variable Reported Match is independent of the variable Guilty, and that $\Pr(\overline{M}|G) = 1 - \Pr(M|G)$, we have

$$\Pr(RM|G) = \Pr(RM|M)\Pr(M|G) + \Pr(RM|\overline{M})(1 - \Pr(M|G)).$$

Finally, taking similar steps we find $\Pr(RM|\overline{G})$:

$$\begin{aligned}
\Pr(RM|\overline{G}) &= \Pr(RM|M,\overline{G})\Pr(M|\overline{G}) + \Pr(RM|\overline{M},\overline{G})\Pr(\overline{M}|\overline{G}) \\
&= \Pr(RM|M)\Pr(M|\overline{G}) + \Pr(RM|\overline{M})(1 - \Pr(M|\overline{G}).
\end{aligned} \tag{A.3}$$

The resultant likelihood ratio is

$$LR = \frac{\Pr(RM|M)\Pr(M|G) + \Pr(RM|\overline{M})(1 - \Pr(M|G))}{\Pr(RM|M)\Pr(M|\overline{G}) + \Pr(RM|\overline{M})(1 - \Pr(M|\overline{G})}. \tag{A.4}$$

Given the formula in Equation A.4, and entering the values from the probability tables above, Equation A.5 results.

$$LR = \frac{0.99 * 1 + 0.02 * 0}{0.99 * 0 + 0.02 * 1} = \frac{0.99}{0.02} = 49.5. \tag{A.5}$$

HUGIN can be used to perform the same calculations in this BN. Figure A.3 is HUGIN's display before any evidence is entered. After entering the evidence of obtaining a

Figure A.3: Before Entering the Evidence.

reported match, HUGIN will display the tables shown in Figure A.4. First, note that

Appendix A. A Simple Bayesian Network

Figure A.4: After Entering the Evidence that we have a **Reported Match**.

the evidence entered is represented by the 100% next to "Yes" in the **Reported Match** table. The likelihood ratio is obtained by taking the value shown in the **Guilty** table next to "Yes" and dividing it by the value displayed next to "No."

$$LR = \frac{98.02}{1.98} = 49.5. \tag{A.6}$$

This value is the result shown in Equation A.5.

APPENDIX B

Corrections and Comments on Wang's Paper [1]

In a paper published in 2002 by Jinliang Wang [1], there appear to be several mistakes. To begin, in the third paragraph of page 1204, Wang states "For a marker locus with n co-dominant alleles indexed by i, j, k, $l = 1, 2, \ldots, n$ there would be $G = n(n+1)/2$ possible genotypes and $C = n(n+1)[n(n+1)+2]/8$ possible combinations of genotypes for a pair of individuals." This statement is false. Consider the counter example of $n = 3$. Then $G = 6$, therefore $C = \binom{6}{2} = 15$. However $C = 3(3+1)[3(3+1)+2]/8 = 21 \neq 15$.

Another discrepancy occurs on page 1205, Table 1. There are several probabilities that are incorrect, namely $\Pr(ij, ij), \Pr(ii, ij), \Pr(ij, kl)$. These same probabilities are derived by Evett and Weir in [2], pages 112-115[1]. Noting the definitions for P_0, P_1, and P_2 given by Equation 4.12 in [2], Table B.1 summarizes the errors found in [1].

As a final note, Wang states

> The ML method can be used to distinguish among different relationships. Though it can also be used to estimate relatedness, it results in much larger biases and sampling variances that the moment estimators unless the number of marker loci is unrealistically large...This is perhaps because the

---

[1]There is a typographical error in the first equation on page 113 of [2]. It should read $P(A_i A_i, A_j A_k) = 2(\delta_0 p_i^2 p_j p_k + \delta_{ab} p_i p_j p_k)$

Appendix B. Corrections and Comments on Wang's Paper [1]

ideal properties of the likelihood method are asymptotic and apply to large data sets only...The data set involved in estimating pairwise relatedness is extremely small, only two individual genotypes.

This statement is incorrect. The asymptotic properties of the maximum likelihood technique will apply as the number of loci approach ∞, not as the number of individuals approach ∞.

Table B.1: Mistaken Probabilities in Wang [1].

$$P_0 = 1 - \phi - \Delta$$
$$P_1 = \phi$$
$$P_2 = \Delta$$

	Weir	Wang
$\Pr(ij, ij)$	$4P_0 p_i^2 p_j^2 + P_1 p_i p_j (p_i + p_j)$	$2p_i^2 p_j^2 + \frac{1}{2}\phi p_i p_j (p_i + p_j - 4p_i p_j)$
Weir = 2(Wang)	$+2P_2 p_i p_j$	$+\Delta p_i p_j (1 - 2p_i p_j)$
$\Pr(ii, ij)$		$4p_i^3 p_j + 2\phi p_i^2 p_j (1 - 2p_i)$
Weir = 2(Wang)	$2P_0 p_i^3 p_j + P_1 p_i^2 p_j$	$-4\Delta p_i^3 p_j$
$\Pr(ij, kl)$		
Weir = 4(Wang)	$4P_0 p_i p_j p_k p_l$	$p_i p_j p_k p_l - \phi p_i p_j p_k p_l - \Delta p_i p_j p_k p_l$

99

APPENDIX C

Downhill Simplex Method C++ Code

C.1   C++ Function Obtaining 8D MLE

```cpp
void Get8DMLE(double& max,    //i-o variable containing maximum likelihood value
              double& theta, //i-o variable containing coancestry coefficient MLE
              double init[], //input variable containing 8D initial simplex
              double lambda, //input variable contianing scaling factor
              int loci,      //input variable containing number of loci
              double d[])    //i-o variable containing Jacquard's 8D MLE
//global variable
//LikeClass like[NUM_LOCI];  //One likelihood for each locus
{
    SimplexClass simplex;
    double iter_delta[N+1][N];
    double like_values[N+1];
    int n_eval=0;
    int j, k;
    double sum;
    double new_inits[N];
    int iter=5;
    simplex.InitP(iter_delta, init, lambda, 1);
    simplex.InitL_Values(iter_delta, like_values, 1, loci, like);
    n_eval=0;
    simplex.Amoeba(iter_delta, like_values, n_eval, 1, loci, like);
    //restarting simplex at found point
    lambda=0.001;
    for(j=0; j<iter; j++)
    {
        for(k=0; k<N; k++)
            new_inits[k]=iter_delta[0][k];
        simplex.InitP(iter_delta, new_inits, lambda, 1);
        simplex.InitL_Values(iter_delta, like_values, 1, loci, like);
        n_eval=0;
        simplex.Amoeba(iter_delta, like_values, n_eval, 1, loci, like);
    }
    sum=0.0;
    for(k=0; k<N; k++)
```

Appendix C. Downhill Simplex Method C++ Code

```
    {
        d[k]=iter_delta[0][k];
        sum+=d[k];
    }
    d[8]=1.0-sum;
    theta=ThetaFct(d);
    max=exp(-like_values[0]);
}
```

C.2   Simplex Class C++ Header File

```
const int N=8;
const int MAX_NEVAL=100000;
const double TINY = 1.0e-10;
const double FTOL = 1.0e-10;
#include "like_class.h"
class SimplexClass
{
    public:
        SimplexClass();
        void   Swap(double &a, double &b);
        void   Get_psum(double[][N], double[], int);
        double Function(const double[], int, int, LikeClass[]);
        void   InitP(double[][N], const double[], const double, int);
        void   InitL_Values(double[][N], double[], int, int, LikeClass[]);
        double Amotry(double p[][N], double y[], double psum[], const int ihi,
                       const double fac, int rel, int loci, LikeClass[]);
        void   Amoeba(double[][N], double[], int &n_eval, int, int, LikeClass[]);
    private:
};
```

C.3   Simplex Class C++ Implementation File

```
#include "simplex_class.h"
#include <iostream.h>
#include <stdlib.h>
#include <math.h>
#include <iomanip.h>

void SimplexClass::Swap(double &a, double &b)
{
    double temp=a;
    a=b;
    b=temp;
}
```

Appendix C. Downhill Simplex Method C++ Code

```cpp
void SimplexClass::Get_psum(double p[N+1][N], double psum[], int rel)
{
    int i,j;
    double sum;
    int mpts;
    int ndim;
    if (rel==0)
    {
        mpts=3;
        ndim=2;
    }
    else
    {
        mpts=N+1;
        ndim=N;
    }
    for(j=0; j<ndim; j++)
    {
        for(sum=0.0, i=0; i<mpts; i++)
            sum+=p[i][j];
        psum[j]=sum;
    }
}

void SimplexClass::InitP(double p[N+1][N], const double p_0[N],
                         const double lambda, int rel)
{
    int mpts, ndim, i, j, k, index;
    double val[8+1];
    if (rel==0)
    {
        mpts = 3;
        ndim = 2;
        int e[2][2]={{1, 0}, {0, 1}};
        for(j=0; j<ndim; j++)
            p[0][j] = p_0[j];
        for(i=1; i<mpts; i++)
        {
            for(j=0; j<ndim; j++)
            {
                val[j]=p_0[j]+lambda*e[i-1][j];
                if (fabs(1.0-val[j])<TINY)
                    val[j]=1.0;
                else if (fabs(0.0-val[j])<TINY)
                    val[j]=0.0;
            }
```

Appendix C. Downhill Simplex Method C++ Code

```
        val[2]=1.0-val[0]-val[1];
        for(k=0; k<=ndim; k++)
        {
            if(val[k]<0.0)
            {
                index=(int)(((double)rand()/(double)(RAND_MAX+1))*2);
                while(val[index]<=fabs(val[k]))
                    index=(int)(((double)rand()/(double)(RAND_MAX+1))*2);
                val[index]=val[index]+val[k];
                val[ndim]=1.0-val[0]-val[1];

            }
        }
        if (val[2]>1)
        {
            cout << "BADNESS IN INITP" << endl;
            val[2]=1.0;
        }
        p[i][0]=val[0];
        p[i][1]=val[1];
    }
}
else
{
    mpts = N+1;
    ndim = N;
    int e[N][N]={
                {1, 0, 0, 0, 0, 0, 0, 0},
                {0, 1, 0, 0, 0, 0, 0, 0},
                {0, 0, 1, 0, 0, 0, 0, 0},
                {0, 0, 0, 1, 0, 0, 0, 0},
                {0, 0, 0, 0, 1, 0, 0, 0},
                {0, 0, 0, 0, 0, 1, 0, 0},
                {0, 0, 0, 0, 0, 0, 1, 0},
                {0, 0, 0, 0, 0, 0, 0, 1}
                };
    for(j=0; j<ndim; j++)
        p[0][j] = p_0[j];
    for(i=1; i<mpts; i++)
    {
        for(j=0; j<ndim; j++)
        {
            val[j]=p_0[j]+lambda*e[i-1][j];
            if (fabs(1.0-val[j])<TINY)
                val[j]=1.0;
            else if (fabs(0.0-val[j])<TINY)
                val[j]=0.0;
```

Appendix C. Downhill Simplex Method C++ Code

```
            }
            val[ndim]=1.0-val[0]-val[1]-val[2]-val[3]
                          -val[4]-val[5]-val[6]-val[7];
            for(k=0; k<=ndim; k++)
            {
                if(val[k]<0.0)
                {
                    index=(int)(((double)rand()/(double)(RAND_MAX+1))*8);
                    while(val[index]<=fabs(val[k]))
                        index=(int)(((double)rand()/(double)(RAND_MAX+1))*8);
                    val[index]=val[index]+val[k];
                    val[ndim]=1.0-val[0]-val[1]-val[2]-val[3]
                                  -val[4]-val[5]-val[6]-val[7];
                    if (fabs(1.0-val[ndim])<TINY)
                        val[ndim]=1.0;
                    else if (fabs(0.0-val[ndim])<TINY)
                        val[ndim]=0.0;
                }
                if(val[k]<0.0)
                    cout << "**badness in InitP**" << endl;
            }

            if (fabs(1.0-val[ndim])<TINY)
                val[ndim]=1.0;
            else if (fabs(0.0-val[ndim])<TINY)
                val[ndim]=0.0;
            if (val[ndim]>=0 && val[ndim]<=1)
            {
                for(j=0; j<ndim; j++)
                    p[i][j]=val[j];
            }
            else
                cout << "badness in InitP" << endl;
        }
    }
}

void SimplexClass::InitL_Values(double p[N+1][N], double y[N+1], int rel, int loci,
                                LikeClass like[])
{
    int ndim;
    int mpts;
    double x[N];
    if (rel==0)
    {
        ndim = 2;
        mpts = 3;
```

Appendix C. Downhill Simplex Method C++ Code

```
    }
    else
    {
        ndim = N;
        mpts = N+1;
    }
    for(int i=0; i<mpts; i++)
    {
        for(int j=0; j<ndim; j++)
            x[j]=p[i][j];
        y[i]=Function(x, rel, loci, like);
    }
}

double SimplexClass::Amotry(double p[][N], double y[], double psum[],
                            const int ihi, const double fac, int rel,
                            int loci, LikeClass like[])
{
    int valid=1;
    int j;
    double last;
    int ndim;
    double ptry[N];
    double fac1, fac2, ytry;
    if (rel==0)
        ndim=2;
    else
        ndim=N;
    fac1=(1.0-fac)/(double)ndim;
    fac2=fac1-fac;
    for(j=0; j<ndim; j++)
        ptry[j]=psum[j]*fac1-p[ihi][j]*fac2;
    for (j=0; j<ndim; j++)
    {
        if (ptry[j]>=0.0 && ptry[j]<=1.0)
            valid*=1;
        else
            valid*=0;
    }
    if (rel==0)
    {
        last=1.0-ptry[0]-ptry[1];
        if  (valid==0 || last<0 || last>1)
            return y[ihi];
        else
        {   ytry=Function(ptry, rel, loci, like);
            double sum=0.0;
```

Appendix C. Downhill Simplex Method C++ Code

```
                for(int i=0; i<ndim; i++)
                    sum+=ptry[i];
                if (ytry < y[ihi] && ((1.0-sum)>=0.0) && ((1.0-sum)<=1.0))
                {
                    y[ihi]=ytry;
                    for(j=0; j<ndim; j++)
                    {
                        psum[j]+=ptry[j]-p[ihi][j];
                        p[ihi][j]=ptry[j];
                    }
                }
                return ytry;
            }
        }
        else
        {
            last=1.0-ptry[0]-ptry[1]-ptry[2]-ptry[3]-ptry[4]-ptry[5]-ptry[6]-ptry[7];
            if  (valid==0 || last<0 || last>1)
                return y[ihi];
            else
            {
                ytry=Function(ptry, rel, loci, like);
                double sum=0.0;
                for(int i=0; i<ndim; i++)
                    sum+=ptry[i];
                if (ytry < y[ihi] && ((1.0-sum)>=0.0) && ((1.0-sum)<=1.0))
                {
                    y[ihi]=ytry;
                    for(j=0; j<ndim; j++)
                    {
                        psum[j]+=ptry[j]-p[ihi][j];
                        p[ihi][j]=ptry[j];
                    }
                }
                return ytry;
            }
        }
    }
}

void SimplexClass::Amoeba(double p[][N], double y[], int &n_eval, int rel,
                          int loci, LikeClass like[])
{
    int i, ihi, ilo, inhi, j;
    double rtol, ysave, ytry;
    double small=1e-10;
    int mpts, ndim;
    double psum[N];
```

106

Appendix C. Downhill Simplex Method C++ Code

```
if (rel==0)
{
    mpts = 3;
    ndim = 2;
}
else
{
    mpts = N+1;
    ndim = N;
}
int count=0;
Get_psum(p, psum, rel);
for(;;)
{
    ilo = 0;
    ihi= y[0]>y[1] ? (inhi=1,0) : (inhi=0,1);
    for(i=0; i<mpts; i++)
    {
        if (y[i]<=y[ilo])
            ilo=i;
        if (y[i]>y[ihi])
        {
            inhi=ihi;
            ihi=i;
        }
        else if (y[i]>y[inhi] && i!=ihi)
            inhi=i;
    }
    count++;
    rtol = 2.0*fabs(y[ihi]-y[ilo])/(fabs(y[ihi])+fabs(y[ilo])+TINY);
    if(rtol<FTOL)
    {
        Swap(y[0], y[ilo]);
        for (i=0; i<ndim; i++)
            Swap(p[0][i], p[ilo][i]);
        break;
    }
    if (n_eval >= MAX_NEVAL)
    {
        Swap(y[0], y[ilo]);
        for (i=0; i<ndim; i++)
            Swap(p[0][i], p[ilo][i]);
        cout << "MAX_NEVAL Exceeded " << rel << endl;
        break;
    }
    n_eval+=2;
    ytry = Amotry(p, y, psum, ihi, -1.0, rel, loci, like);
```

Appendix C. Downhill Simplex Method C++ Code

```
        if(ytry<=y[ilo])
            ytry=Amotry(p, y, psum, ihi, 2.0, rel, loci, like);
        else if (ytry>=y[inhi])
        {
            ysave = y[ihi];
            ytry=Amotry(p, y, psum, ihi, 0.5, rel, loci, like);
            if (ytry>=ysave)
            {
                for(i=0; i<mpts; i++)
                {
                    if (i != ilo)
                    {
                        for(j=0; j<ndim; j++)
                            p[i][j]=psum[j]=0.5*(p[i][j]+p[ilo][j]);
                        y[i]=Function(psum, rel, loci, like);
                    }
                }
                n_eval+=ndim;
                Get_psum(p, psum, rel);
            }
        }
        else
            --n_eval;
    }
}

double SimplexClass::Function(const double delta[], int rel,
                              int loci, LikeClass like[])
{
    double fctn;
    if(like[0].Value(delta, rel, N)==0 || like[0].missing_flag==-1)
        fctn=0.0;
    else
        fctn=log(like[0].Value(delta, rel, N));
    for(int i=1; i<loci; i++)
    {
        if(like[i].Value(delta, rel, N)==0|| like[i].missing_flag==-1)
            fctn+=0.0;
        else
            fctn+=log(like[i].Value(delta, rel, N));
    }
    return -fctn;
}
```

Appendix C. Downhill Simplex Method C++ Code

C.4   Likelihood Class C++ Header File

```
class LikeClass
{
    public:
        int locus;        //gives corresponding locus number
        double prob[9];   //conditional probabilities determined by Table 2.4
        int missing_flag; //indicates whether genotype data is missing (= -1)
        LikeClass();
        double Value(const double delta[], int rel, int n);
        void InitProbs(int num, double p[], int a, int b, int c, int d, int rel);
        void ReInit();
    private:
};
```

C.5   Likelihood Class C++ Implementation File

```
#include "like_class.h"
#include <math.h>
#include <iostream.h>
#include <iomanip.h>

LikeClass::LikeClass()
{
    locus = -1;
    int i;
    for (i=0; i<9; i++)
        prob[i] = 0;
    missing_flag=0;
}
double LikeClass::Value(const double delta[], //input vector of Jacquard's MLEs
                        int dim)              //input variable: =0 if 2D, =1 if 8D
{
    int ndim;
    double d9;
    double small=1e-10;
    double fctn=0.0;
    if (dim==0)
    {
        ndim=2;
        d9=1.0-delta[0]-delta[1];
        if (fabs(1.0-d9)<small)
            d9=1.0;
        else if (fabs(0.0-d9)<small)
            d9=0.0;
    }
```

Appendix C. Downhill Simplex Method C++ Code

```
    else
    {
        ndim=8;
        d9=1.0-delta[0]-delta[1]-delta[2]-delta[3]
              -delta[4]-delta[5]-delta[6]-delta[7];
        if (fabs(1.0-d9)<small)
            d9=1.0;
        else if (fabs(0.0-d9)<small)
            d9=0.0;
    }
    if(d9>=0 && d9<=1)
    {
        for(int i=0; i<ndim; i++)
        {
            fctn+=prob[i]*delta[i];
        }
        fctn+=prob[ndim]*d9;
        return fctn;
    }
    else
    {
        cout << "badness in value" << endl;
        return 0.0;
    }
}

void LikeClass::InitProbs(int num,  //in variable giving row number, see Table 2.4
                          double p[], //in variable giving allele frequencies
                          int i, int j, int k, int l, //in variables, see Table 2.4
                          int dim) //in variable: =0 if 2D, =1 if 8D
{
    if (dim==0)
    {
        switch(num){
            case 0:
                prob[0]=pow(p[i],2);
                prob[1]=pow(p[i],3);
                prob[2]=pow(p[i],4);
                break;
            case 1:
                prob[0]=0.0;
                prob[1]=0.0;
                prob[2]=pow(p[i],2)*pow(p[j],2);
                break;
            case 2:
                prob[0]=0.0;
                prob[1]=pow(p[i],2)*p[j];
```

Appendix C. Downhill Simplex Method C++ Code

```
            prob[2]=2*pow(p[i],3)*p[j];
            break;
        case 3:
            prob[0]=0.0;
            prob[1]=0.0;
            prob[2]=2*pow(p[i],2)*p[j]*p[k];
            break;
        case 4:
            prob[0]=0.0;
            prob[1]=pow(p[i],2)*p[j];
            prob[2]=2*pow(p[i],3)*p[j];
            break;
        case 5:
            prob[0]=0.0;
            prob[1]=0.0;
            prob[2]=2*pow(p[i],2)*p[j]*p[k];
            break;
        case 6:
            prob[0]=2*p[i]*p[j];
            prob[1]=p[i]*p[j]*(p[i]+p[j]);
            prob[2]=4*pow(p[i],2)*pow(p[j],2);
            break;
        case 7:
            prob[0]=0.0;
            prob[1]=p[i]*p[j]*p[k];
            prob[2]=4*pow(p[i],2)*p[j]*p[k];
            break;
        case 8:
            prob[0]=0.0;
            prob[1]=0.0;
            prob[2]=4*p[i]*p[j]*p[k]*p[l];
            break;
        default:
            cout << "badness in InitProbs" << endl;
    }
}
else
{
    switch(num){
        case 0:
            prob[0]=p[i];
            prob[1]=pow(p[i],2);
            prob[2]=pow(p[i],2);
            prob[3]=pow(p[i],3);
            prob[4]=pow(p[i],2);
            prob[5]=pow(p[i],3);
            prob[6]=pow(p[i],2);
```

111

Appendix C. Downhill Simplex Method C++ Code

```
            prob[7]=pow(p[i],3);
            prob[8]=pow(p[i],4);
            break;
        case 1:
            prob[0]=0.0;
            prob[1]=p[i]*p[j];
            prob[2]=0.0;
            prob[3]=p[i]*pow(p[j],2);
            prob[4]=0.0;
            prob[5]=pow(p[i],2)*p[j];
            prob[6]=0.0;
            prob[7]=0.0;
            prob[8]=pow(p[i],2)*pow(p[j],2);
            break;
        case 2:
            prob[0]=0.0;
            prob[1]=0.0;
            prob[2]=p[i]*p[j];
            prob[3]=2.0*pow(p[i],2)*p[j];
            prob[4]=0.0;
            prob[5]=0.0;
            prob[6]=0.0;
            prob[7]=pow(p[i],2)*p[j];
            prob[8]=2*pow(p[i],3)*p[j];
            break;
        case 3:
            prob[0]=0.0;
            prob[1]=0.0;
            prob[2]=0.0;
            prob[3]=2*p[i]*p[j]*p[k];
            prob[4]=0.0;
            prob[5]=0.0;
            prob[6]=0.0;
            prob[7]=0.0;
            prob[8]=2*pow(p[i],2)*p[j]*p[k];
            break;
        case 4:
            prob[0]=0.0;
            prob[1]=0.0;
            prob[2]=0.0;
            prob[3]=0.0;
            prob[4]=p[i]*p[j];
            prob[5]=2*pow(p[i],2)*p[j];
            prob[6]=0.0;
            prob[7]=pow(p[i],2)*p[j];
            prob[8]=2*pow(p[i],3)*p[j];
            break;
```

112

Appendix C. Downhill Simplex Method C++ Code

```
            case 5:
                prob[0]=0.0;
                prob[1]=0.0;
                prob[2]=0.0;
                prob[3]=0.0;
                prob[4]=0.0;
                prob[5]=2*p[i]*p[j]*p[k];
                prob[6]=0.0;
                prob[7]=0.0;
                prob[8]=2*pow(p[i],2)*p[j]*p[k];
                break;
            case 6:
                prob[0]=0.0;
                prob[1]=0.0;
                prob[2]=0.0;
                prob[3]=0.0;
                prob[4]=0.0;
                prob[5]=0.0;
                prob[6]=2*p[i]*p[j];
                prob[7]=p[i]*p[j]*(p[i]+p[j]);
                prob[8]=4*pow(p[i],2)*pow(p[j],2);
                break;
            case 7:
                prob[0]=0.0;
                prob[1]=0.0;
                prob[2]=0.0;
                prob[3]=0.0;
                prob[4]=0.0;
                prob[5]=0.0;
                prob[6]=0.0;
                prob[7]=p[i]*p[j]*p[k];
                prob[8]=4*pow(p[i],2)*p[j]*p[k];
                break;
            case 8:
                prob[0]=0.0;
                prob[1]=0.0;
                prob[2]=0.0;
                prob[3]=0.0;
                prob[4]=0.0;
                prob[5]=0.0;
                prob[6]=0.0;
                prob[7]=0.0;
                prob[8]=4*p[i]*p[j]*p[k]*p[l];
                break;
            default:
                cout << "badness in InitProbs" << endl;
        }
```

Appendix C. Downhill Simplex Method C++ Code

```
    }
}

void LikeClass::ReInit()
{
    locus = -1;
    int i;
    for (i=0; i<9; i++)
        prob[i] = 0;
    missing_flag=0;
}
```

APPENDIX D

Summary of Loci from CEPH Families

Table D.1: CEPH Family Locus Numbers, Names, and Chromosome Locations.

Locus	Name	Chromosome	Locus	Name	Chromosome
1	ACT1A01	18	26	T66—PvuII	4
2	afm123ya1	18	27	cCI6-24—PvuII	4
3	ATA1G10	8	28	pEFD6—BglII	4
4	ATA1H06	18	29	1346—(AC)n	6
5	CEB42	8	30	5-22—PvuII	6
6	CYP2DP8	22	31	CRI-R117—MspI	6
7	FB12B7	8	32	D1S57—TaqI	6
8	GATA23C09	8	33	LMYC—EcoRI	6
9	GATA27G11	12	34	MFD3—pcr	6
10	GATA28D12	18	35	Mfd126—(AC)n	6
11	GATA30C02	18	36	R6-2-3—BglII	6
12	GATA41A01	8	37	SL1—(GT)n	6
13	GCT10C10	22	38	SnRNP—MspI	6
14	IL2RB	22	39	HG2A—(GATA)n	10
15	LMS43	12	40	Mfd150—(AC)n	10
16	Mfd159A	8	41	Mfd28—(AC)n	10
17	Mfd302	18	42	RBP3-Bg—BglII	10
18	Mfd84	12	43	RBP3-H4—MspI	10
19	pH41A	22	44	VNTR—TaqI	10
20	pTHIZ53	12	45	ZNF22—(AC)n	10
21	CO91100—enz	4	46	afm066xa1—(AC)n	10
22	HLA—A	4	47	Mfd164-2—(AC)n	10
23	HLA—B	4	48	CYP19—(TTTA)8	15
24	HLA—DR	4	49	ZI-280—(AC)n	15
25	PLG—SacI	4	50	afm016yg1-2—(AC)n	15

Appendix D. Summary of Loci from CEPH Families

Table D.2: Allele Frequencies for CEPH Loci Defined in Table D.1.

Locus Number	1	2	3	4	5	6	7	8
Allele
1	0.0806	0.1916	0.0726	0.0189	0.2458	0.4958	0.1746	0.1667
2	0.1532	0.3879	0.5726	0.0283	0.2500	0.2941	0.3254	0.4286
3	0.3065	0.1028	0.3145	0.1415	0.2627	0.2101	0.0556	0.3175
4	0.3387	0.0374	0.0403	0.0849	0.2415		0.0238	0.0556
5	0.1210	0.2056		0.2547			0.2619	0.0317
6		0.0654		0.3585			0.1270	
7		0.0093		0.1132			0.0317	
8		0.0000						

Locus Number	9	10	11	12	13	14	15	16
Allele
1	0.2937	0.0081	0.0079	0.0242	0.4670	0.3621	0.1955	0.0812
2	0.3254	0.1290	0.1587	0.2097	0.3077	0.3836	0.1864	0.1453
3	0.3571	0.3226	0.5238	0.2016	0.0055	0.1724	0.1818	0.1923
4	0.0159	0.2903	0.2063	0.4274	0.2033	0.0647	0.1545	0.1966
5	0.0079	0.2419	0.0952	0.1129	0.0165	0.0129	0.0955	0.0983
6		0.0081	0.0079	0.0242		0.0043	0.0955	0.1923
7						0.0000	0.0636	0.0940
8							0.0273	

Locus Number	17	18	19	20	21	22	23	24
Allele
1	0.2419	0.0413	0.0091	0.1657	0.0280	0.3679	0.3459	0.3522
2	0.2500	0.0207	0.6707	0.8283	0.0000	0.2453	0.2547	0.3585
3	0.1452	0.2851	0.0183	0.0060	0.0807	0.3428	0.2736	0.2484
4	0.1210	0.0950	0.1860		0.0528	0.0440	0.1258	0.0409
5	0.1935	0.2810	0.1159		0.1491			
6	0.0403	0.0537			0.2795			
7	0.0081	0.2231			0.2267			
8					0.0342			
9					0.0839			
10					0.0062			
11					0.0373			
12					0.0000			
13					0.0000			
14					0.0186			
15					0.0000			
16					0.0000			
17					0.0031			

Appendix D. Summary of Loci from CEPH Families

Locus Number	25	26	27	28	29	30	31	32
Allele								
1	0.7610	0.4704	0.0123	0.0220	0.4469	0.5682	0.8217	0.3875
2	0.2390	0.1776	0.1481	0.9780	0.2063	0.4318	0.1783	0.4344
3		0.3520	0.4444		0.2063			0.1781
4			0.3951		0.1031			
5					0.0313			
6					0.0063			

Locus Number	33	34	35	36	37	38	39	40
Allele								
1	0.5395	0.2065	0.2421	0.8141	0.3250	0.0350	0.0216	0.0000
2	0.4605	0.2645	0.1604	0.1859	0.0094	0.9650	0.0031	0.0798
3		0.3419	0.2642		0.0375		0.1142	0.3558
4		0.1871	0.2107		0.0719		0.2500	0.2055
5			0.1006		0.0500		0.4660	0.0583
6			0.0031		0.1375		0.0586	0.1258
7			0.0189		0.2688		0.0864	0.0399
8					0.0438			0.0429
9					0.0000			0.0920
10					0.0219			
11					0.0281			
12					0.0063			

Locus Number	41	42	43	44	45	46	47	48
Allele								
1	0.0248	0.8500	0.6875	0.0062	0.0342	0.0932	0.0309	0.0154
2	0.3354	0.1500	0.3125	0.1429	0.0590	0.0031	0.1821	0.4012
3	0.0280			0.5093	0.5000	0.0901	0.3827	0.0185
4	0.0994			0.0559	0.1491	0.3665	0.3148	0.0000
5	0.4037			0.0000	0.0000	0.0186	0.0895	0.1358
6	0.1025			0.0031	0.0559	0.0745		0.0556
7	0.0062			0.0031	0.1180	0.1087		0.3735
8				0.0342	0.0373	0.1708		
9				0.2174	0.0000	0.0559		
10				0.0280	0.0000	0.0186		
11					0.0031			
12					0.0124			
13					0.0031			
14					0.0280			

Appendix D. Summary of Loci from CEPH Families

Locus Number	49	50
Allele		
1	0.0535	0.0000
2	0.0283	0.0854
3	0.1635	0.5443
4	0.1006	0.0728
5	0.1289	0.0000
6	0.1604	0.0285
7	0.0503	0.2690
8	0.2075	
9	0.1069	

118